

**Investigation of Factors that Influence Coloration  
in Polycarbonate based Compounded Plastics**

by

Shahid Ahmed

A Thesis Submitted in Partial Fulfillment  
of the Requirements for the Degree of

**DOCTOR OF PHILOSOPHY**

In

The Faculty of Engineering and Applied Science

**Mechanical Engineering**

University of Ontario Institute of Technology

August, 2015

©, Shahid Ahmed, 2015

This research is part of:

**Fundamental Studies into Causes that Influence  
Colour Quality of Compounded Plastics**

A Collaborative Project of  
University of Ontario Institute of Technology &  
SABIC Innovative Plastics Cobourg

Supported by: SABIC IP and NSERC - CRD

Principal Investigator:  
Associate Prof. Dr. Ghaus M. Rizvi

Faculty of Engineering and Applied Science  
University of Ontario Institute of Technology  
Copyright © University of Ontario Institute of Technology. All rights reserved.

I hereby declare that I am the sole author of this thesis. This is a true copy of the thesis, including any required final revisions, as accepted by my examiners.

I understand that my thesis may be made electronically available to the public.

## Abstract

Consistently producing compounded plastics in the correct colour without making adjustments of the colour formulation or the processing conditions is very challenging for coloured plastics manufacturers. Conversely, the principal objective of the present research was to identify the scientific and engineering factors that directly or indirectly cause deviation and inconsistency in the output colour of compounded plastics grades and suggest viable solutions to prevent these colour variations.

The current study mainly focused on investigating and analysing the individual and/or combined effect of the processing conditions on the colour and appearance of resulting compounded plastic grades. This study highlights individual and combined influences on the output colour, of three process parameters: temperature, screw speed and feed rate. Typical plastic grades and associated colour formulations were selected for experimentation and analysis in consultation with the innovation team of SABIC IP at their Cobourg plant. Included among the selection criteria was the frequency of colour variation encountered by a plastic grade during regular production. A wide variety of research tools and techniques were employed in this study, these include, for example, statistical methods such as Box-Behnken design (BBD); characterization techniques such as thermogravimetric analysis (TGA); imaging and image analysis using scanning electron microscopy (SEM); numerical analysis of the kneading discs zone to evaluate the mixing efficiency under varying processing conditions in a co-rotating intermeshing twin screw extruder.

Past production data of two low Chroma opaque polycarbonate (PC) plastic grades - PC1 and PC2, were statistically analysed with the aim to quantify the influence on output colour caused by small adjustments in colour formulation made during production. This study revealed that the output colour is quite sensitive to minute changes in the amount of white, black, and yellow pigments in units of PPH – parts per hundred parts of polymeric resin. A Design of Experiments (DoE) approach was applied to develop a better understanding of the relationship between process variables and output colour. Such a relationship and optimal processing conditions were investigated using Box-Behnken design of response surface for three polycarbonate resin-based plastic grades: a low Chroma translucent grade (G1), a high Chroma opaque grade (G2), and a high luminous opaque grade (G3). The obtained experimental results verify the fitness of the statistical model employed and suggests processing conditions that ensure consistency in output colour of the plastic grades examined.

To further investigate the relationship explained by statistical analysis, a novel technique was introduced to quantify dispersion of colour pigments in polymeric matrix under varying processing conditions, it is based on scanning electron micrography and image analysis. A correlation between the processing conditions and distribution graphs for pigments particle size and inter-particle distance was established and compared with the colorimetric data. The results obtained through these investigations could help plastics compounders achieve consistency in plastics coloration. To visualize the flow behaviour of kneading discs zone in a co-rotating intermeshing twin screw extruder used in experimentation, a 3D numerical analysis was carried out using OpenFOAM® software. This study evaluates the dispersive mixing parameter  $\lambda$  for a high Chroma opaque polycarbonate grade (G2) by simulating a 3-D isothermal flow pattern in the kneading discs region of the twin screw extruder. A quasi-steady state finite element method was implemented to avoid time dependent moving boundaries. The values of the mixing parameter  $\lambda$  obtained compare the flow behaviour of the kneading discs zone under varying processing conditions. Simulation results correlate well the input process variables with the dispersive mixing in the zone of the kneading discs and compare well with experimental colorimetric data.

The research work presented in this thesis significantly contributes to understanding the influence of process variables to the extrusion process, especially of temperature, screw speed and feed rate, on the output colour of polycarbonate resin grades.

## **Acknowledgements**

First of all, I 'm greatly indebted to my wife- Nayyer, my son- Usama, and my lovely daughter- Momina, for providing me the peace of mind necessary to focus on my work.

Secondly, I express my deepest respect to my upright parents, for their all-time love, prayers, support and encouragement.

I would like to extend my profound and sincere gratitude and appreciation to my supervisors, Dr. Ghaus M. Rizvi, and Dr. Remon Pop-Iliev, for the years of guidance, insightful advice, support, and continuous encouragement in the development and writing of this thesis.

My special thanks and appreciation to SABIC Innovative Plastics Cobourg Plant, ON, Canada, for providing material and financial support, and their staff members in the experimentation and data collection.

I also express my sincere gratitude to the National Science and Engineering Research Council for their all the years financial support.

My special thanks are also extended to my colleagues at advanced materials lab, for their moral support, particularly to my friend, Ali Goger, for his kind help in installing and running OpenFOAM® software.

## Table of Contents

Declaration .....	iii
Abstract.....	iv
Acknowledgements.....	vi
List of Publications.....	ix
List of Tables.....	x
List of Fig.s .....	xii
Chapter 1 Introduction.....	1
1.1 Mixing of polycarbonate blends in twin screw extruders.....	3
1.2 Polymeric materials .....	6
1.3 Colorants / additives for polymeric materials.....	7
1.4 Colour science and the basis of colour sensation .....	9
1.5 3D colour space – CIE lab model .....	15
1.6 Statistical methods and response surface methodology.....	16
1.7 Characterization techniques .....	19
1.8 Modelling and computer simulation .....	21
1.9 Problem Statement – Inconsistency in Plastics Coloration.....	24
1.10 Objectives.....	25
1.11 Overview of the Thesis.....	25
Chapter 2 Influence of Small Perturbations in Colour Formulation on Output Colour of Polycarbonate-based Compounded Plastics .....	27
2.1 Introduction.....	27
2.2 Experimentation .....	28
2.3 Results and discussion.....	30
2.4 Conclusions .....	41
2.5 Summary .....	42
Chapter 3 Process Optimization through Designed Experiments to achieve Consistent Output Color in Compounded Plastics .....	43
3.1 Introduction.....	43
3.2 Experimentation .....	46
3.3 Results and discussion.....	49

3.4	Conclusions .....	82
3.5	Summary.....	83
Chapter 4	Evaluation of Pigments Dispersion Level in Compounded Plastics using Image Analysis Technique .....	84
4.1	Introduction .....	84
4.2	Materials, equipment and process .....	86
4.3	Results and discussion.....	89
4.4	Conclusions .....	94
4.5	Summary.....	95
Chapter 5	Numerical Analysis of Mixing Efficiency under Varying Process Conditions in Intermeshing Co-rotating Twin Screw Extruder.....	96
5.1	Introduction.....	96
5.2	Geometry, Material and Process Considerations.....	99
5.3	Simulation with OpenFOAM®.....	101
5.4	Results and discussion.....	104
5.5	Conclusions .....	107
5.6	Summary.....	107
Chapter 6	Contribution and Recommendations.....	109
6.1	Contribution .....	109
6.2	Recommendations .....	110
Bibliography	.....	xv



## List of Publications

1. S. Ahmed, J. AlSadi, U. Saeed, G. Rizvi, D. Ross, R. Clarke and J. Price, "Process optimization through designed experiments to achieve consistency in output color of a compounded plastic grade" *Quality Engineering*, 27 (2), pp. 144-160, April 29, 2015.
2. S. Ahmed, J. AlSadi, U. Saeed, G. Rizvi, D. Ross, R. Clarke and J. Price, "Implementation of Box-Behnken design for optimizing compounding process ensuring consistent output colour of a polycarbonate grade" *Quality Engineering*, 2015 (submitted; Rev1 under review).
3. S. Ahmed, R. Pop-Iliev, G. Rizvi, "Effect of process variables on pigments dispersion in compounded plastics" *SPE Antec2015*, Orlando, 2015.
4. S. Ahmed, R. Pop-Iliev, G. Rizvi, "Experimental study to investigate optimal process conditions for consistency in coloration of a compounded plastic grade" *SPE Antec2015*, Orlando, 2015.
5. S. Ahmed, R. Pop-Iliev, G. Rizvi, "Evaluating pigment dispersion for better color in plastics" *Plastics Research Online*, SPEPRO, April 13, 2015.  
<http://www.4spepro.org/view.php?article=005884-2015-04-07&category=Injection+Molding>
6. J. AlSadi, U. Saeed, S. Ahmad, G. Rizvi, and D. Ross, "Processing issues of color mismatch: rheological characterization of polycarbonate blends" *Polymer Engineering and Science*, Dec 2014. <http://onlinelibrary.wiley.com/doi/10.1002/pen.24041/abstract>
7. U. Saeed, J. AlSadi, S. Ahmad, G. Rizvi, and D. Ross, "Neural Network: a potential approach for error reduction in color values of polycarbonate" *Adv In Poly Tech*, 33 (2), 2014.
8. S. Ahmed, J. AlSadi, U. Saeed, G. Rizvi, and D. Ross, "Effect of small perturbations in colour formulation on output colour of a plastic grade compounded with two polycarbonate resins" *SPE Antec2013*, Cincinnati, 2013.
9. S. Ahmed, J. AlSadi, U. Saeed, G. Rizvi, D. Ross, R. Clarke and J. Price, "Effect of small perturbations in colour formulation on output colour of a plastic grade compounded with two polycarbonate resins" *SPE Antec2013*, Cincinnati, 2013.
10. S. Ahmed, J. AlSadi, U. Saeed, G. Rizvi, and D. Ross, "A study on effect of small perturbations in colour formulation on output colour of a plastic grade compounded with a single polycarbonate resin" *SPE Antec2012*, Orlando, 2012.

## List of Tables

- Table 1.1: Requirements for colorants
- Table 1.2: A comparison between organic and inorganic pigments
- Table 2.1: Reference Colour Formulation – PC1
- Table 2.2: Percent adjustments made in reference formulation during production – PC1
- Table 2.3: Reference Colour Formulation – PC2
- Table 2.4: Percent adjustments made in reference formulation during production – PC2
- Table 2.5: ANOVA for  $\Delta L^*$ ,  $\Delta a^*$  and  $\Delta b^*$
- Table 2.6: ANOVA Results of  $\Delta L^*$ ,  $\Delta a^*$  and  $\Delta b^*$
- Table 3.1: Designed Experimental Runs and Colour Data – Grade G1
- Table 3.2: Designed Experimental Runs and Colour Data – Grade G2
- Table 3.3: Designed experimental runs and colour data – Grade G3
- Table 3.4: Colour Formulation – Grade G1
- Table 3.5: Colour Formulation – Grade G2
- Table 3.6: Colour Formulation – Grade G3
- Table 3.7: ANOVA Results for  $L^*$ ,  $a^*$  and  $b^*$
- Table 3.8: Final equations in terms of actual factors
- Table 3.9: Predicted Mean vs. Experimental Colour Data - Confirmatory Test
- Table 3.10: Predicted Mean vs. Experimental Colour Data - Delta Values
- Table 3.11: Criterion Set for Process Optimization
- Table 3.12: List of Optimal Solutions for Input Factors
- Table 3.13: ANOVA results for  $L^*$ ,  $a^*$  and  $b^*$
- Table 3.14: Final equations in terms of actual factors
- Table 3.15: Predicted Mean vs. Experimental Colour Data – Confirmatory Test
- Table 3.16: Criterion Set for Process Optimization
- Table 3.17: List of Optimal Solutions for Input Factors
- Table 3.18: ANOVA results for  $L^*$ ,  $a^*$  and  $b^*$
- Table 3.19: Final equations in terms of actual factors
- Table 3.20: Confirmation DoE results - predicted and experimental colour data
- Table 3.21: Optimization criteria set to reach the target
- Table 3.22: Three Solutions from Process Optimization
- Table 4.1: Colour Standard Formulation
- Table 4.2: Designed Experimental Runs and Colour Data

- Table 4.3: Pigments Particle Size Distribution
- Table 4.4: Inter-Particle Distance Distribution
- Table 5.1: Technical Data ZSK26 Twin Screw Extruder
- Table 5.2: Material Properties and Processing Conditions
- Table 5.3: Boundary Conditions for Velocity and Pressure
- Table 5.4: Mixing parameter values for simulated cases
- Table 5.5: Mixing parameter values vs measured colour coordinates

## List of Fig.s

- Fig. 1.1: A cross-sectioned view of an extruder with extrusion process flow chart [10]
- Fig. 1.2: A schematic view mixing operation in extruders and mixing elements [8]
- Fig. 1.3: Classification of twin screw extruders [7]
- Fig. 1.4: Visible spectrum of sunlight [22]
- Fig. 1.5: Cross section of human eye [19]
- Fig. 1.6: Magnified view of fovea near center of human eye retina [19]
- Fig. 1.7: Spectral power distribution of daylight [19]
- Fig. 1.8: Incident light and spectral reflectance curve of a red ball [19]
- Fig. 1.9 CIE Lab Model – (a) Cartesian Notation  $L^*a^*b^*$ , (b) Polar Notation  $L^*C^*h^\circ$  [22]
- Fig. 2.1: Desirability with yellow and black pigments
- Fig. 2.3: Perturbation graph of desirability
- Fig. 2.4: Perturbation graph of  $\Delta L^*$
- Fig. 2.5: Perturbation graph of  $\Delta a^*$
- Fig. 2.6: Perturbation graph of  $\Delta b^*$
- Fig. 2.7: Contour graph of  $\Delta L^*$
- Fig. 2.8: Contour graph of  $\Delta a^*$
- Fig. 2.9: Contour graph of  $\Delta b^*$
- Fig. 2.10: Desirability with yellow and black pigments
- Fig. 2.11: Perturbation graph of desirability
- Fig. 2.12: Perturbation graph of  $\Delta L^*$
- Fig. 2.13: Perturbation graph of  $\Delta a^*$
- Fig. 2.14: Perturbation graph of  $\Delta b^*$
- Fig. 2.15: Contour graph of  $\Delta L^*$
- Fig. 2.16: Contour graph of  $\Delta a^*$
- Fig. 2.17: Contour graph of  $\Delta b^*$
- Fig. 3.1: Evaluation of FDS and d for error type “Diff”
- Fig. 3.2: Evaluation of FDS and d for error type “Pred”
- Fig. 3.3: POE ( $a^*$ ) plot with factor B at Mid-Point
- Fig. 3.4: POE ( $b^*$ ) plot with factor B at Mid-Point
- Fig. 3.5: Perturbation plot for  $L^*$

- Fig. 3.6: 2FI graphs affecting  $L^*$  using ANOVA noise estimate (left), experimental error (right)
- Fig. 3.7: Contour plot for  $L^*$  slicing along factor B
- Fig. 3.8:  $L^*$  values of confirmatory test
- Fig. 3.9:  $a^*$  values of confirmatory test
- Fig. 3.10:  $b^*$  values of confirmatory test
- Fig. 3.11: Bar graph displaying individual and combined desirability level of variables and POEs
- Fig. 3.12: Graphical optimization and sweet spot flagged for a desired solution
- Fig. 3.13: 3D surface graph flagged with optimal desirability
- Fig. 3.14: 2D contour graph flagged with optimal desirability
- Fig. 3.15: Perturbation graph for  $L^*$
- Fig. 3.16: POE ( $L^*$ ) plot with factor B and C at Mid-Point
- Fig. 3.17: POE ( $a^*$ ) plot with factor B and C at Mid-Point
- Fig. 3.18: POE ( $b^*$ ) plot with factor B and C at Mid-Point
- Fig. 3.19: 2FI graphs affecting  $L^*$  using ANOVA noise estimate (left), experimental error (right)
- Fig. 3.20: Contour plot for  $L^*$  slicing along Factor B
- Fig. 3.21: Desirability levels for 4<sup>th</sup> optimal solution – Table 3.17
- Fig. 3.22: Graphical optimization and sweet spot flagged for selected optimal solution – Table 3.17
- Fig. 3.23:  $L^*$  values of verification test
- Fig. 3.24: Evaluation of FDS and d for error type Diff
- Fig. 3.25: Evaluation of FDS and d for error type Pred
- Fig. 3.26: Perturbation plot for  $L^*$
- Fig. 3.27: Interaction b/w factors C and B affecting  $b^*$
- Fig. 3.28: Contour plot for  $L^*$  slicing along factor B
- Fig. 3.29: (a) POE ( $L^*$ ) transmitted by temperature; (b) POE ( $a^*$ ) transmitted by temperature; (c) POE ( $b^*$ ) transmitted by temperature
- Fig. 3.30: 3<sup>rd</sup> optimal solution flagged in sweet spot
- Fig. 4.1: Schematic of moulded chip and sample for thin sections
- Fig. 4.3: ESEM image @ 5000x - Run 17 sample chip: Top layer (a); Centre layer (b)
- Fig. 4.4: Particle size distribution graph - top layers

- Fig. 4.5: Particle size distribution graph - centre layers
- Fig. 4.6: Nearest neighbour distance graph - top layers
- Fig. 4.7: Nearest neighbour distance graph - centre layers
- Fig. 4.8: Colour data of samples and the standard reference – CIE Lab colour space
- Fig. 4.9: Colour difference between samples and the standard reference
- Fig. 4.10: Spectral Curves: reflectance intensity @ full visible spectrum (a); @ red spectrum (b)
- Fig. 5.1: Kneading discs staggered at 45° in forward (right handed) configuration
- Fig. 5.2: Mesh view in z-direction with ParaFoam®
- Fig. 5.3: Sequential geometries for a complete rotation of kneading discs staggered at 45°
- Fig. 5.4: 3D Distribution graph of mixing parameter  $\lambda$  – R7
- Fig. 5.5: 3D Distribution graph of mixing parameter  $\lambda$  – R17

# Chapter 1

## Introduction

A recent industry profile provided by Canadian Plastics Industry Association-CPIA, indicates there are 95,400 employees enlisted on Canada's plastics industry payroll. Industry comprises over 3,170 companies, most of which are Canadian owned, and represents a \$29.2 billion industrial sector, which is sophisticated, multi-faceted and embraces plastic products manufacture, machinery, moulds and resins. Plastics industrial sector plays a vital role in Canada's global competitiveness, which is becoming more challenging due to increasing trend in plastic products usage both as consumer goods and in advanced applications such as telecommunication, electronics, aviation and aerospace, medicine and life sciences, building materials, automotive, and renewable energy. It also plays a significant role in reduction of greenhouse gases, for example products made from plastics are light weight that translates into less fuel consumption during transportation, their insulation, packaging and recyclability characteristics significantly add to fuel saving. Recent studies revealed if plastics were to be replaced with alternative materials across the whole Europe, it would require an additional 10% fuel or equivalently 25 million tonnes of crude oil, which corresponds to 105 million tonnes of CO<sup>2</sup> greenhouse gas emission per year. Similarly plastics packaging alone claims 582.6 million gigajoules of energy saving per year. A recent study by University of Toronto found replacing of old water pipes with plastic pipes would help Canada to achieve 10% of its Kyoto reduction targets. Industry as a whole is concentrated in Ontario, Quebec, British Columbia and Alberta, however Ontario is the largest plastics producing region in Canada and third largest in North America after California (No.1) and Ohio (No.2) [1].

North American plastic industry experienced both a substantial growth over the past decade and adverse effects imposed by recent economic recession and tight profit margins. North American compounding industry members, however, have an optimistic view of the changing paradigm and see the industry survival in providing innovative solutions for North American markets and expanding globally. They further realize mere innovative solutions would not suffice in maintaining a competitive edge as industry leader, cost effectiveness must compliment innovative solutions. Avoidance of waste is the key to cost effectiveness, which is also a driving philosophy in lean manufacturing / compounding. One key characteristics of plastics is their availability in a wide array of colours to meet aesthetic as well as functional needs. Over the time, producing plastics with consistent output colour and minimal wastage

has imposed a greater challenge to plastic compounders particularly those who manufacture coloured plastics in large quantities to feed plastic processing industry such as automotive or develop prototypes / master-batches in small lots at short lead times to cater for innovation and changing market needs. The challenge becomes even bigger under world's weak economic conditions, increasing prices of raw materials - resins, pigments and additives, and higher costs of energy, packaging, equipment parts and transportation. Such difficult times, however, should encourage plastic compounders to find new ways along with continued creativity and innovation to help their customers manage cost [2~4].

One of the many plastic compounders confronting the challenge of having inconsistency in output colour of compounded plastics, is SABIC Innovative Plastics (IP), formerly known as GE Innovative Plastics - a world recognized industry leader, at its manufacturing plant in Cobourg, Ontario. With 15 production lines and one technology line SABIC IP has developed its capability to produce about 200 batches a day with different grades and colours of compounded plastics. A core component of SABIC's Cobourg plants business is the supply of tailored plastics with customer specified colours at short order times. Companies like SABIC play a significant role in rapid development of prototypes to facilitate innovation and maintain a competitive edge in global market. Manufacturing coloured plastics with correct colour in one-go during production is critical to such operations as minute deviation from target colour could cause rejection of the entire production lot. Therefore SABIC IP decided to collaborate with University of Ontario Institute of Technology (UOIT) with the aim to investigate scientific reasons that cause colour deviation in compounded plastics and then develop methods to prevent or reduce it [5].

Present research undertakes fundamental studies of compounding process and associated auxiliary processes such as preparing colour formulation, and injection molding of test samples (rectangular plaques) as practiced at SABIC IP Cobourg plant for manufacture of coloured plastics. Aim was to identify factors involved directly or indirectly causing deviation and inconsistency in output colour during compounding, and suggest viable solutions to prevent these colour variations. Various factors were short listed for a detailed and comprehensive investigation of their individual and/or combined effect on colour and appearance of compounded plastic grades. However current study mainly focused on processing conditions to see their impact on output colour. Various techniques employed in this study include statistical methods such as Box-Behnken design (BBD) [6], characterization techniques such



as thermogravimetric analysis (TGA), and imaging and image analysis using scanning electron microscopy (SEM), and numerical analysis of the kneading discs zone to evaluate mixing efficiency under varying processing conditions in a co-rotating intermeshing twin screw extruder. Typical plastic grades and associated colour formulations were selected for experimentation and analysis in consultation with innovation team of SABIC IP at their Cobourg plant. Included among the selection criteria was the frequency a colour variation encountered by a plastic grade during regular production.

Polymer blending has been extensively studied and numerous publications are available to address various aspects of these systems. The literature on plastics coloration however, is not frequently available particularly about compounding. One of the main objectives of this research was to develop basic understanding of the entire compounding process, and investigate factors behind colour deviation implementing various statistical and characterization techniques. Therefore, fundamental ideas about colour and its measurement, compounding process and equipment, and colour pigments are discussed in following sections.

### **1.1 Mixing of polycarbonate blends in twin screw extruders**

Constantly increasing demands on plastic products need constant refinement in their properties, therefore, deliberate modification in properties of a base polymer by blending with additives and/or with other polymers is becoming increasingly important. The process of blending polymer resins with colorants and additives in specific proportions using extruders to produce plastics with desired properties is recognized as compounding, and the plastics produced as compounded plastics. The word “compounding” is used because a compound distinguishes from a mixture in that its constituents lose their individual characteristics adding new characteristics such as colour, surface appearance, impact strength, flexural stiffness, dielectric strength, conductivity, and flame retardancy [7 ~ 9]. In a broader sense, mixing is a process of reducing non-uniformity of a composition, however basic mechanism is to induce physical relative movement of ingredients. Types of motion that can happen in mixing include molecular diffusion, turbulent motion and convective motion. First two types essentially are limited to gases and low viscosity liquids. Convective motion is specific to high viscosity liquids such as polymer melts. Because of their high viscosity polymer melts are capable of only laminar flow. Convective mixing by laminar flow is termed as laminar mixing and this is the type of mixing that occurs in polymer melt extrusion. Mixing action is generally described by shear flow and elongational flow. Now if the ingredients to be mixed are compatible fluids

and exhibit no yield point, the mixing is distributive, however if a component of the mixture exhibits a yield stress then actual stresses involved in the process become very important. Now if one or more components in a polymer melt showing up yield point are solid, then this type of mixing is referred to as dispersive mixing, sometimes as intensive mixing. Dispersive mixing involves breakdown of solid component but that could happen only when yield stress exceeds a certain limit. If the component exhibiting yield point is a liquid, the process of mixing is termed as homogenization. Manufacture of colour concentrate can be taken as an example of dispersive mixing, where breakdown of colour pigment agglomerates below a certain critical size is of great significance. An example of distributive mixing is the manufacture of polymer blend, where two or more compatible polymers of different melt flow index (MFI) are mixed in molten state and none of the component exhibits yield point. Physically, the distributive and the dispersive mixings are not separated from each other, in fact dispersive mixing is always followed by distributive mixing, however reverse is not always true. Dispersive mixing can occur after distributive mixing only if a solid component has a yield point and the applied stress exceeds the yield limit [10]. Compounding today is predominantly carried out with co-rotating twin screw extruders with constantly increasing available drive powers, torques, and screw speeds. A brief description of the compounding process in a twin screw extruder is shown below in Fig. 1.1, and a schematic differentiating between dispersive and distributive mixing of solid colour pigments and corresponding screw elements are shown in Fig. 1.2.

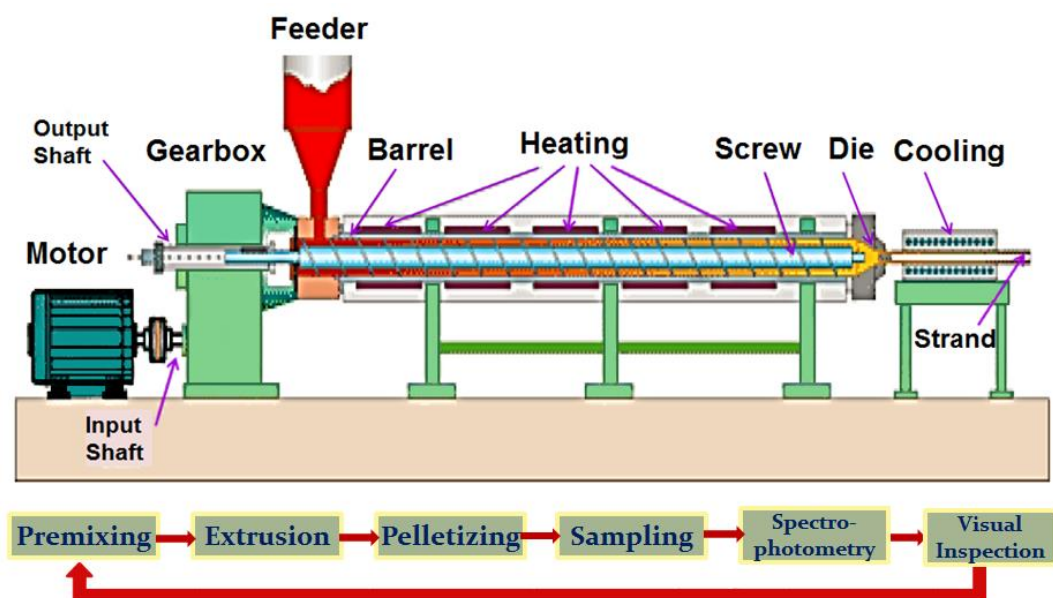


Fig. 1.1: A cross-sectioned view of an extruder with extrusion process flow chart [10]

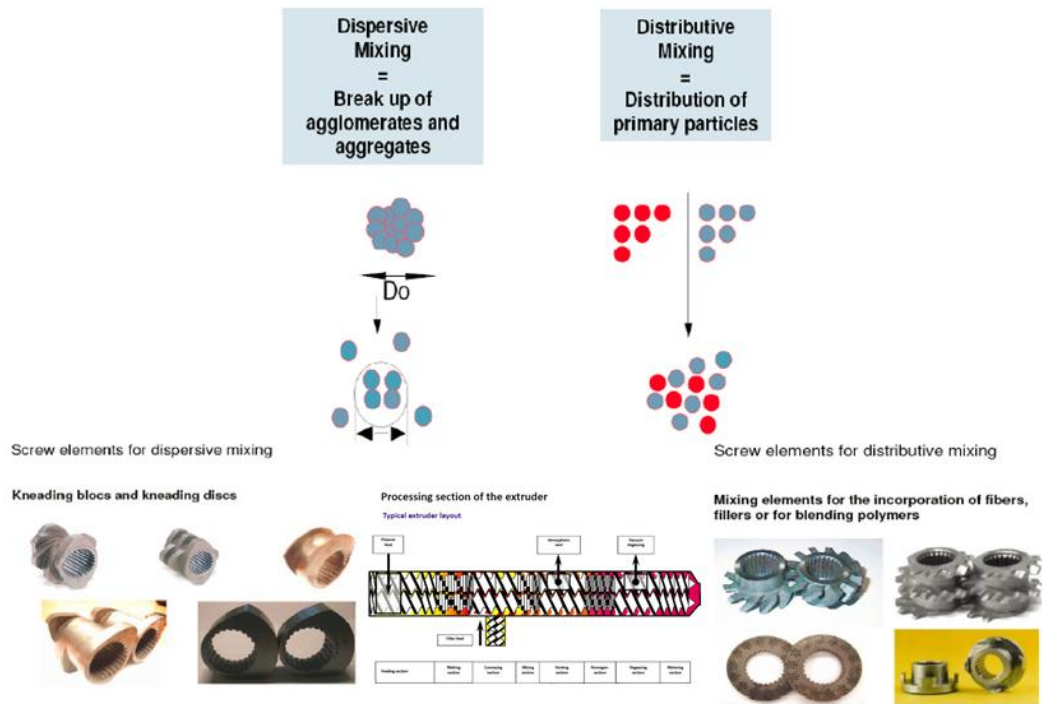


Fig. 1.2: A schematic view of mixing operation in extruders and mixing elements [8]

Extruders are widely used not only in plastics industry, but also in petrochemical and food industries for melting, mixing, blending, reacting, devolatilizing and numerous other tasks. Based on number of screws they are classified into two types: single screw and twin screw extruders (TSEs). In single screw extruders, extrusion process and conveying mechanism are highly dependent on frictional and viscous properties of material. In TSEs however, these properties play a lesser role on conveying behaviour.

TSEs can be designed in various configurations, however main classification is made if the screws are intermeshing or non-intermeshing, and whether co-rotating or counter-rotating. A description of the classification is shown below in Fig. 1.3. The non-intermeshing TSEs do not have the benefit of positive conveying characteristics as no protrusion exists between the flights of one screw and the channels of the other screw. In intermeshing TSEs, flights of one screw protrude into the channels of other screw and their positive conveying characteristics depends upon the degree of intermeshing that ranges from fully intermeshing to partially intermeshing (in some cases near to non-intermeshing).

As regards classification due to direction of screw rotation, in counter-rotating extruders, material is sheared and pressurized in a mechanism quite similar to calendaring where a material is effectively squeezed between two counter rotating rolls [11], and are preferred for

shear sensitive materials. In co-rotating screws, material transfer from one screw to other screw takes place in a Fig.-of-eight pattern and are preferred for temperature sensitive materials as the material is conveyed through the extruder quickly with little possibility of entrapment. The intermeshing co-rotating extruders can further be classified as low and high speed machines. The low speed extruders have high degree of positive conveying characteristics because of closely fitting flight and channel profile, and are preferred in profile extrusion applications. The high speed machines are characterized by their self-wiping feature. Because of the openness of the channels, material transfer takes place easily from one screw to another. They are primarily used in compounding operations [12].






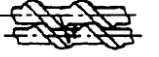
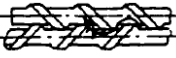

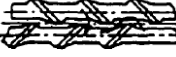
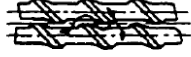
SCREW ENGAGEMENT		SYSTEM	COUNTER-ROTATING	CO-ROTATING
INTERMESHING	FULLY INTERMESHING	LENGTHWISE AND CROSSWISE CLOSED	1 	2 THEORETICALLY NOT POSSIBLE
		LENGTHWISE OPEN AND CROSSWISE CLOSED	3 THEORETICALLY NOT POSSIBLE	4 
		LENGTHWISE AND CROSSWISE OPEN	5 THEORETICALLY POSSIBLE BUT PRACTICALLY NOT REALIZED	6 
	PARTIALLY INTERMESHING	LENGTHWISE OPEN AND CROSSWISE CLOSED	7 	8 THEORETICALLY NOT POSSIBLE
		LENGTHWISE AND CROSSWISE OPEN	9A 	10A 
			9B 	10B 
			11 	12 
		NOT INTERMESHING	LENGTHWISE AND CROSSWISE OPEN	

Fig. 1.3: Classification of twin screw extruders [7]

## 1.2 Polymeric Materials

Plastics are carbon-based materials made up of very long chain molecules and are manufactured by modifying natural products as well as by synthesis from intermediates. In their pure form i.e. without any fillers or additives mixed, plastics are called polymers. Polymers can be divided based on their properties into three main groups: thermoplastics, thermosets, and elastomers or according to their production method in polymerization products, polycondensation products, and polyaddition products. Thermoplastics become soft when heated and solidify on cooling. They do not exhibit any significant change in their basic chemical nature under processing such as extrusion, hence are recyclable. Examples of

thermoplastics materials include polystyrene (PS), polyethylene (PE), polypropylene (PP) and polycarbonate (PC) – the one studied in this research. Thermosets on the other hand become hard when heated above a certain temperature. This hardening happens because of a curing or crosslinking reaction that bonds individual polymer molecules together causing the formation of a three dimensional network. This network remains intact upon cooling because crosslinking is irreversible and that is why thermosets cannot be recycled like thermoplastic materials. Thermosets usually are shaped by processing them below curing or crosslinking temperatures. Elastomers or rubbers are materials that exhibit very large deformations under applied force while behaving in a largely elastic manner. They regain their shape and size completely or mostly when the applied force is removed. Thermoplastics can further be classified as amorphous and semi-crystalline plastics. Amorphous materials are designated by their random, irregular molecular structure without any crystalline regions. Examples are PC, PS, acrylic (PMMA), acrylonitrile butadiene styrene (ABS), and polyvinylchloride (PVC). Semi-crystalline thermoplastics can form highly regular regions called crystallites where molecules come together to form crystals. Formation of crystals depends upon shape of the polymer molecules. Plastics having linear molecular structure without large side-groups can form crystallites e.g. high density polyethylene (HDPE). HDPE can achieve as high a level of crystallinity as 90%. Polystyrene on the other hand cannot form crystallites due to having bulky side-groups [13~15].

### **1.3 Colorants / Additives for Polymeric Materials**

Principally all substances that can be used in polymers coloration, are defined as colorant. The colorants can be divided based on their chemical nature into two groups: inorganic colorants and organic colorants. They can further be classified as pigments and dyes; if a colorant is insoluble in polymer it is defined as a pigment and if it is soluble in polymer it is a dye. However definition of a colorant as pigment is not always true because there are some organic pigments such as Pigment red 254 (DPP-Red) that dissolve in some polymers but are insoluble in most of the polymers. Pigment red 254 dissolves in PC at temperatures above approx. 330°C behaving like a dye. A colorant can be used as a colorant for polymers if it meets the requirements as listed below in Table 1.1. However depending on the intended use of coloured polymer a compromise is possible and quite normal in meeting the requirements. Because, practically only few colorants can fulfil all the requirements and on the other hand experience shows that not every coloured polymer requires the colorant to fulfil all the

requirements. Inorganic and organic pigments can be used to colour all types of polymers. Inorganic and organic pigments can be used in all types of polymers, however heat stability should be good enough in the polymer to be coloured. Use of dyes on the other hand is limited to amorphous polymers with high glass transition temperature such as PS, PC, and PMMA etc. A comparison of properties between inorganic and organic pigments is also presented in Table 1.2.

Inorganic pigments are available in numerous variations even though have only a few basic chemical formulas. They can be classified by either their chemical composition or by colour. Broad categories include pigments consisting of pure elements, oxide pigments, hydroxide pigments and complex inorganic pigments consisting of mixed phase metal oxides etc. Worldwide discussion on “heavy metals in our environment” has restricted the use of pigments to only those that are free from lead and cadmium [13, 16, 17]

Table 1.1: Requirements for colorants

S.No.	Requirements for pigments	Requirements for dyes
1	High hiding power	-
2	Good dispersibility	Good solubility
3	High heat stability	High heat stability
4	High tinting strength	High tinting strength
5	Good fastness properties (light/weather)	Good fastness properties (light/weather)
6	No migration	No migration
7	No warpage	No sublimation
8	Toxicologically safe	Toxicologically safe

Table 1.2: A comparison between organic and inorganic pigments

Property	Organic pigments	Inorganic pigments
Density	Low, mostly < 2.5 g/cm <sup>3</sup>	High, mostly > 2.5 g/cm <sup>3</sup>
Particle size	Mostly < 1µm, thereby high specific surface area	Mostly >1µm, thereby low specific surface area
Tendency to form agglomerates	High	Low
Dispersibility	Not very good	Much better
Solubility	Partial solubility, depends on concentration	Totally insoluble
Transparency	High, thereby low hiding power	Low, thereby high hiding power
Tinting strength	High, good brilliance	Low, mostly not brilliant
Heat fastness	Limited, sometimes low	Very high
Light fastness	Limited, sometimes low	Very good
Warpage	Sometimes very strong	None

Other than colorants, additives are most commonly used materials in plastics blends to improve various properties. The selection and use of additives are determined by the property to be improved. Most important additives are listed below with their names reflecting against specific function [14, 15, 18].

- Antistatic Agent
- Flame retardant
- Filler
- Dispersing agents / lubricant / release agent
- Nucleating agent
- Stabilizer
- Blowing agent
- Plasticizer

All these additives neither are chemically inert nor can their interactions with colorants be excluded. To predict the effect whether positive or negative on colorants caused by these interactions is almost impossible.

#### **1.4 Colour Science and the Basis of Colour Sensation**

Colour can be seen as an essential part of our life that influences our bodies, our minds and our souls. Our response to colour whether physiological, psychological or emotional has been studied in great detail. Over time the appeal of various colours changes, which leads to new colour trends in market place. In the presence of new colorant and special effect technologies, our colour choices and preferences continually evolve. Studying colour perception and trends provides us a better understanding of the market place. Basically a colour results from an interaction between light, object, and the viewer. It is in fact the light that is modified by an object in a manner that the viewer i.e. human eye perceives the modified light as a distinct colour. All three elements must be present for a colour to exist [13, 19~22].

To understand what exactly a colour means, first we need to know the basis of colour sensation by human eye. Daylights both natural and artificial are composed of wide range of electromagnetic waves such as radio waves, ultraviolet, X-rays etc. By nature they all are same, differing solely in their wavelength and frequency. From this very wide spectrum of wavelengths, only a small fraction between 400 and 700 nm is visible. Visible white sunlight

as shown below in Fig. 1.4, consists of a mixture of colours ranging from red to violet as discovered first time by Sir Isaac Newton with his famous prism experiment.

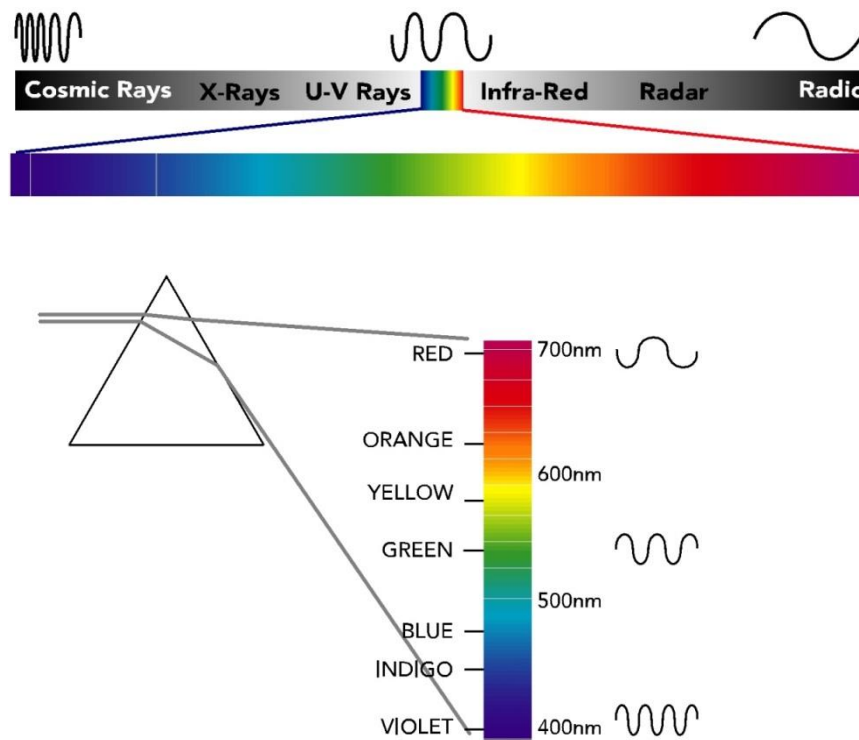


Fig. 1.4: Visible Spectrum of Sunlight [22]

When sunlight is incident on an object, a portion of it is absorbed by the object and rest is reflected back. The absorbed portion is transformed into heat and practically speaking is lost for sensation of colour. The reflected part however is detected by the human eye and after passing through pupil and lens impinges on the retina, where an inverted image of the object is formed. The retina contains two different types of cells, the so-called rods and cones as shown in the Fig. 1.5. Rods are not sensitive to colour i.e. hue and can only differentiate between light and dark. Cones however are pretty sensitive to colour and found in three types differing in their maximum spectral sensitivity to colours. One group of cones is sensitive to reds, another to greens, and third to blues as can be seen in the Fig. 1.6. At this point it is pertinent to mention that all colorimetric measurement methods find their basis in these three colours - RGB plus a light-dark differentiation. These sensors i.e. cones and rods send electrical signals in unique patterns to the brain, which processes the signals into sensation of sight i.e. of light as well as of colour. This means colour is the brain's interpretation of a mixture of these stimuli i.e. red, green and blue. Reflected part of sunlight is just a fraction of the whole spectrum, and based upon the wavelengths and intensity the reflected part owns, we see a definite colour. The object



that reflects 100% of the light is seen as white and the one that absorbs 100% of the light appears black. There is a small pit named fovea located almost in middle of the retina. Fovea is the portion of retina that has only cones in it, so maximum information about the colour i.e. hue is sensed here and sent to the brain. Angle of view that it forms with the lens is 2 degree that is where 2 degree observer is originated from. However later on a 10 degree observer was introduced by CIE and is considered more accurate. Reason being that if we stare at our thumbnail located at arm's length, it's almost impossible to see it alone, you also see some of the surrounding that makes your angle of view obviously bigger than that you are trying to focus on [13].

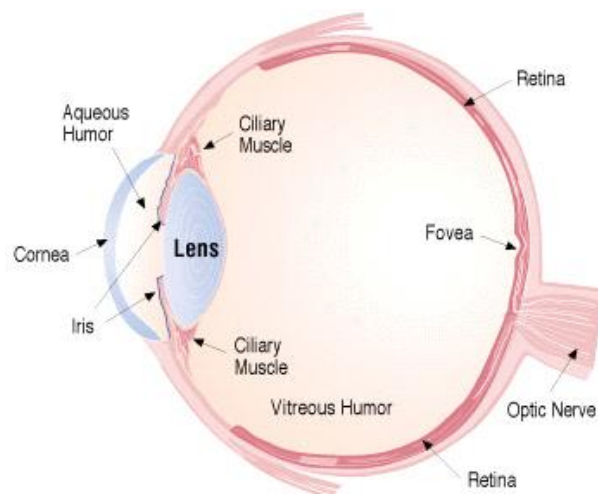


Fig. 1.5: Cross Section of Human Eye [19]

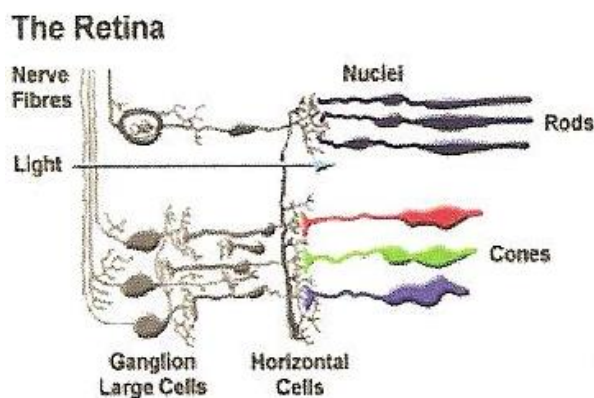


Fig. 1.6: Magnified View of Fovea near Center of Human Eye Retina [19]

Like other senses such as hearing or taste, our colour vision varies individual to individual, in some cases more obviously such as colour blindness. Capability to perceive a

colour is closely associated to individual differences in sensitivity of human eyes. This important fact, when final plastic specimen of matched colour is inspected only visually, has been a point of long discussions not only between customer and supplier but also among the experts within supplier's own quality assurance wing. That is why having same person involved in final visual inspection is highly recommended. Such controversies eventually led to development of different colorimetric systems involving instruments such as spectrophotometers. The most often used system is CIE Lab; others are Munsell and Hunter Lab. These systems are valuable tools to measure a colour, however are not able to perfectly describe what we see and cannot be a substitute to visual judgment. However in order to fully understand the scientific basis to derive a colour measuring system being used by instruments, one needs to understand the three components - elements of colour, necessary to see a colour: the light source, the object interacting with light, and the receiver that views and interprets colour of the object. If any of the elements is missing we will not be able to see any colour [13, 19~22].

#### **1.4.1 Light Source**

Colour is light and the light is energy that travels in straight lines at a speed of 299,792458 meters per second. Various physical light sources such as sunlight, incandescent lamp, candle etc. have specific spectral power distribution (SPD) i.e. energy levels associated to individual wavelengths on their emission spectrum of light. Mathematical description of the relative spectral power distribution of physical light source is termed as illuminant. Various standard illuminants such as A, C, D65, D55, D75, F2 etc. to simulate physical light sources have been described by global standards committee comprising mainly of CIE, ASTM and DIN. A careful and proper implementation of these standard illuminants in software application or in instrument firmware has allowed companies to build today's modern colour measuring devices, which are used for an accurate and standard evaluation of the object colour. A brief description of the relative spectral power distribution of various light sources is given below:

Spectral power distribution of daylight is biased towards blue as shown in the Fig. 1.7, which is a measurement of light energy on a clear day. This bias is caused by selective absorption and scattering of high energy shorter wavelength violet and blue light in the upper atmosphere, which makes our sky a clear blue canopy. Daylight varies in three different ways as illustrated in Fig. 1.7. The Daylight near sunrise or sunset contains comparatively less blue energy than red because the light has to pass through a longer slice of atmosphere causing more

absorption of blue light. It's relative spectral power distribution that can be represented by a blackbox illuminant at 5500K (D55). The daylight close to noon is represented by 6500K (D65) and illustrates a SPD of noon when both the sky and sun together light us resulting into a higher blue energy than that near sunrise or sunset. Near noon SPD designated with 7500K (D75), represents the day time near noon with the sun may have gone out of sight and only blue canopy of the sky is illuminating us. In conclusion, the SPD denoted by a low temperature i.e. D55, will have deep red, however apparent red shifts to yellow, then whiteness, and finally blues for SPDs designated by D65 and D75 respectively. Therefore, it is of great importance to know various light conditions under which an object is expected to be viewed and how it would respond to various light conditions. Light booths are the tools that can simulate various light conditions and can be used to analyse the apparent colour of an object [19, 22].

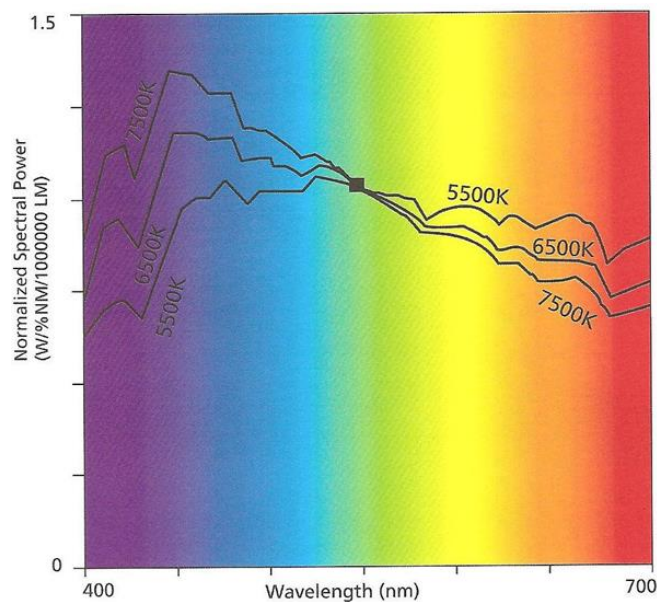


Fig. 1.7: Spectral power distribution of daylight [19]

One more point, which is worth-mentioning, is CRI – colour rendering index. CRI ranges from 0 to 100. CRI is used to compare two lights that have same temperature, e.g. for the same temperature, Xenon source light has a CRI of approx. 100 whereas that of a mercury vapour lamp goes below 20. Manufacturers of fluorescent, metal halide and other non-incandescent lighting equipment mostly use CRI to describe visual effects of light on coloured surfaces. Again the bottom line is while analysing or predicting apparent colour of an object to have standard lighting conditions is important [13, 19].

## 1.4.2 Object

Second element of colour is the object, which actually interacts with the incident light and modifies it. So colour of an object is closely related to the wavelengths of light that either reflects from or transmits through that object. For example a red ball as shown below in Fig. 1.8, will absorb all wavelengths except red component of the incident light. However if the incident light source is richer in red light energy such as D55, more long red wavelengths would be available to bounce off. That means a light source enriched with more red will make the red objects look even redder. So viewing a colour one should carefully control the viewing environment making use of a standard light source [19, 22].

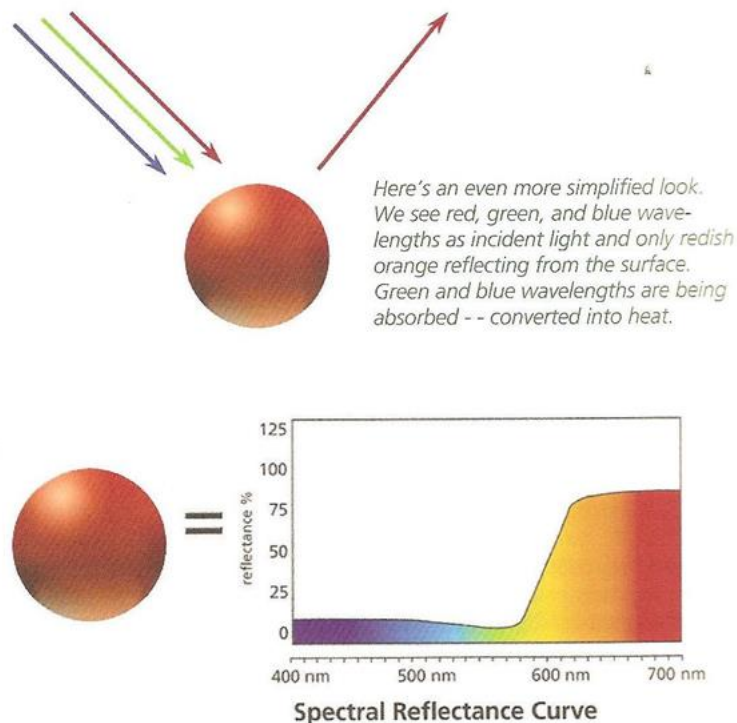


Fig. 1.8: Incident light and spectral reflectance curve of a red ball [22]

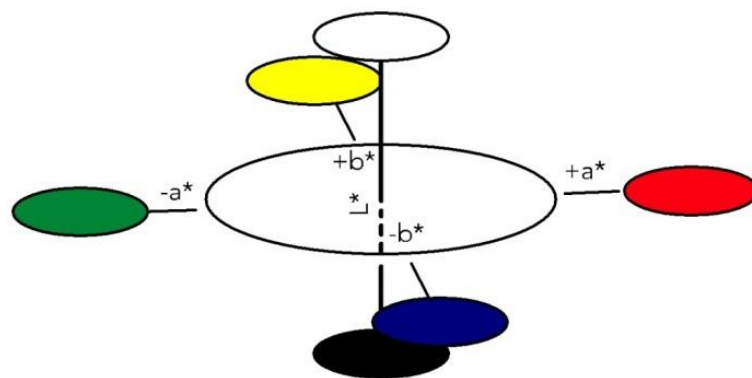
## 1.4.3 Receiver

Receiver is the third element of colour, which in visual sense is a combination of human eye and brain. Many factors such as genetics, environment, experience and education to interpret and understand colour can influence our eye and brain combination. In colour measuring instrument, the receiver is a detector used in combination with a microprocessor

programmed to understand and interpret the colour viewed by detector. In other words, eye/brain combination is replaced with a colorimeter or spectrophotometer. For an instrument to be effective, it must see in a manner similar to the human eye so the colour data produced makes good sense to the operator [19, 22].

### 1.5 3D Colour Space - CIE Lab Model

Colour of an object can be characterized by its tri-stimulus data i.e.  $L^*$ ,  $a^*$  and  $b^*$  - the three responses that are investigated in this study. The tri-stimulus colour data corresponds to a point in 3D colour space of CIE Lab model shown in Fig. 1.9 (a), which was introduced in 1976 by the international commission on light (CIE - Commission Internationale de l'Eclairage). In this model,  $L^*$  is the lightness axis whose values range from 0 (black) to 100 (white), whereas  $a^*$  and  $b^*$  represent red-green and yellow-blue axes respectively [23]. The overall colour of an object however, can be expressed as  $E^*$  - Euclidean distance in 3D colour space. A polar notation  $L^*C^*h^\circ$  of the model was also released as shown in Fig. 1.9(b) where  $L^*$  defines exactly the same axis i.e. lightness, whereas  $C^*$  denotes Chroma ( $C^* = \sqrt{a^{*2} + b^{*2}}$ ) - the saturation of the colour and  $h^\circ$  represents Hue - the basic colour described in degrees rotating counter clockwise from zero degree (red) to 90 degree (yellow), 180 degree (green), 270 degree (blue), and 360 degree back to red [23]. Any deviation of object colour from the target, exceeding permissible limits, is reported as colour mismatch and usually expressed in delta values as  $\Delta L^*$ ,  $\Delta a^*$ ,  $\Delta b^*$  and  $\Delta E^* = \sqrt{(\Delta L^*)^2 + (\Delta a^*)^2 + (\Delta b^*)^2}$  [23~25]. It is the customer needs that usually determine the threshold for these delta values, which for the plastic grades studied, were set out as  $\leq 0.6$  for  $\Delta L^*$ ,  $\Delta a^*$ ,  $\Delta b^*$  and  $\leq 1.0$  for  $\Delta E^*$ . One significant aspect in colour matching is to prepare a reference colour plaque representative of reference colour formulation, and measure its colour coordinates on a spectrophotometer. Spectrophotometers are useful quality control tools that help numerically measure colour and colour deviation [26].



(a)

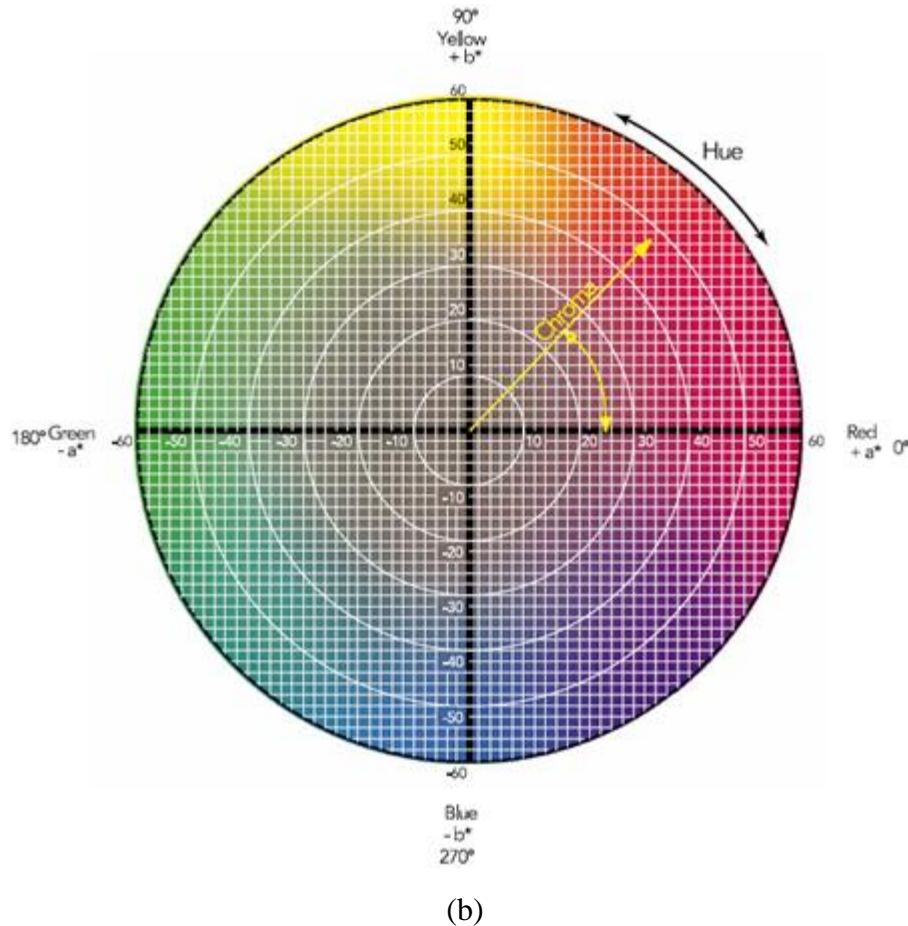


Fig. 1.9: CIE Lab Model - (a) Cartesian Notation  $L^*a^*b^*$  (b) Polar Notation  $L^*C^*h^\circ$  [22]

## 1.6 Statistical Methods and Response Surface Methodology (RSM)

Understanding the relationship between input process variables and final output colour of compounded / moulded plastic part is critical for consistency and reproducibility of response attributes of a process. Statistical methods are frequently used by researchers, to investigate and optimize the effect of process variables on responses such as colour and appearance of compounded plastics. For this purpose, they employ various statistical designs and models to fit in the response data obtained through designed experiments or past production data. Effertz [27] investigated a PVC sheet for the effect of processing conditions on its gloss and surface appearance using modified general factorial model. Bender [28] investigated the process variables causing high viscosity variability in wood-fiber compounds by executing Box-Behnken design (BBD). With Statistica®, Eric et al [29] executed a design of experiments (DoE) for 1/8th fractional factorial design to investigate the effect of seven process variables including barrel and mould temperature, injection speed, screw speed, pack and hold pressure, on five output parameters: tri-stimulus colour data, gloss and part weight.

Response surface methodology (RSM) however, is a collection of mathematical and statistical techniques, which are extremely useful in modelling and analysis of problems where a response/outcome of interest is influenced by independent variables, and the objective is to optimize the response [30]. For example in plastics coloration, the colour ( $L^*$ ) of a compounded plastic grade is influenced by levels of temperature (T), screw speed (N) and feed rate (Q), colour formulation (F) thus, the response  $L^*$  can be expressed as a function of T, N, and Q as given in equation (1.1).

$$L^* = f(T, N, Q, F) + \varepsilon \quad (1.1)$$

where  $\varepsilon$  represents noise or error in the response and if  $f(T, N, Q, F)$  is the expected response i.e.  $E(L^*)$ , then it is called response surface. In most RSM cases, it is not known what type of relationship exists between independent variables and the response. Therefore, as a first step, true functional relationship is approximated usually with a polynomial model. The general polynomial model used in this study is quadratic as expressed in equation (1.2).

$$y = \beta_0 + \sum_{i=1}^k \beta_i x_i + \sum_{i=1}^k \beta_{ii} x_i^2 + \sum_{i < j} \beta_{ij} x_i x_j + \varepsilon \quad (1.2)$$

where  $y$  is the response,  $x$  is the independent variable, and  $\beta_0, \beta_i, \beta_{ii}, \beta_{ij}$  represent a constant, linear, quadratic and interaction coefficients respectively,  $\varepsilon$  is the noise.

Along with the polynomial model, a proper choice of design is crucial for fitting and analysis of the response surface as it should provide not only sufficient amount of information to test the model fitness, but also be economical in terms of number of experimental runs. BBD [31], in this regards, is most efficient design and requires only three levels of each variable in order to generate a quadratic model [31, 32]. To capture non-linearity of the relationship, other designs need higher levels of each factor such as five in a central composite design (CCD) or more experimental runs such as in a three level factorial design. A DoE based on BBD for three independent variables, comprises only 17 experimental runs including 12 factorial and 5 center points. BBD, as a combined array design, requires lesser runs than Taguchi's crossed array designs and allows estimation for significant interactions [32, 33]. A design that combines both the controllable and the noise factors into a single design is called combined array. Whereas in Taguchi's crossed array approach, the controllable factors are placed in one design (called the inner array) and the noise factors in a second design (called the outer array), and then Cartesian product of the two designs determine the number of experimental runs. Moreover, BBD is

rotatable and spherical with a radius  $\sqrt{2}$  where all design points are located. However, the sphere it forms, does not contain vertices of cuboid region that represent extremes of each input variable [30].

### 1.6.1 Optimization of Multiple Responses

Many RSM problems involve analysis of several responses, such as in this study we measured three responses i.e.  $L^*$ ,  $a^*$  and  $b^*$  that together represent the colour of the compounded plastic grades. However, in simultaneous consideration of multiple responses, first step is to build an appropriate response surface model for each response, and then look for a set of operating conditions that optimizes all responses, or at least keep them within the desired ranges [31].

For optimizing several responses, a relatively straight forward approach (also called graphical optimization) is to overlay contour plots for each response, however, it works well only when there are three or fewer design variables involved. The most popular technique however, is the numerical optimization technique by Derringer and Suich [34]. The technique involves use of desirability functions. The procedure is to first convert each response  $y_i$  into an individual desirability function  $d_i$  that varies from 0 to 1. A  $d_i = 1$  tells the response is at its target, whereas a  $d_i = 0$ , means the response lies outside the desired region. Then the overall desirability is maximized by choosing the design variables as expressed in equation (1.3).

$$D = (d_1 d_2 \dots d_m)^{1/m} \quad (1.3)$$

where  $m$  is the number of responses to be optimized. Individual desirability functions can be expressed based upon the target value  $T$  as given in equations (1.4) to (1.6):

$$d = \begin{cases} 0 & y < L \\ \left(\frac{y-L}{T-L}\right)^r & L \leq y \leq T \\ 1 & y > T \end{cases} \quad \text{if target } T \text{ is a maximum value} \quad (1.4)$$



$$d = \begin{cases} 1 & y < T \\ \left(\frac{U-y}{U-T}\right)^r & T \leq y \leq U \\ 0, & y > U \end{cases} \quad \text{if target T is a minimum value} \quad (1.5)$$

$$d = \begin{cases} 0 & y < L \\ \left(\frac{y-L}{T-L}\right)^r & L \leq y \leq T \\ \left(\frac{U-y}{U-T}\right)^r & T \leq y \leq U \\ 0 & y > U \end{cases} \quad \text{if target T is located between L and U} \quad (1.6)$$

where  $r$  is the weight, when  $r = 1$  the desirability function is linear, however choosing  $r > 1$  put greater emphasis on to be closer to target, whereas  $0 < r < 1$  makes it less important. In present study Design-Expert® is used to implement this optimization technique.

## 1.7 Characterization Techniques

Characterization of a mixture is quite an important aspect in the study of mixing. A comprehensive characterization requires specification of the size, shape, orientation and spatial location of every discrete element of the minor component, which of course is almost impossible. However various qualitative and quantitative theories and techniques have been developed to measure and describe the mixing wellness such as thermo-gravimetric analysis (TGA), differential scanning calorimetry (DSC), X-ray Diffraction (XRD), X-ray Fluorescence (XRF), light microscopy, scanning electron microscope (SEM), energy dispersive X-ray spectroscopy (EDX), and ash content [35~37]. Recent development in X-ray imaging technique available with micro CT scanners (computed tomography) has offered significant improvement in mixing characterization [14, 15].

Various researchers have employed thermo-gravimetric analysis (TGA) for colorants quantification in a compounded plastic part. TGA can further be followed by FT-IR or mass spectrometry for identification of elements. In 2008, a supplier of automotive body panels encountered an issue with a customer – an automotive manufacturer that rejected a big lot of products delivered in year 2007 due to slight variation in colour compared with lot delivered in 2006. The issue was investigated by D. Grewell et al [37] and making use of various techniques including TGA, they concluded two reasons associated with the raw material - thermoplastic composite sheets comprising two ABS substrates (white) over-coated with clear

acrylic forming a three layer composite. One reason they identified was significant variation in outer layers thickness of the two lots and another was variation in colorant loading in the middle layers of the two lots. M. Kosrzycki et al [35] in 2008 made use of three different techniques including TGA for determination of colour concentrate in moulded Polyacetal components. I. Groves et al [36] of TA Instrument Ltd. of UK carried out a quantification analysis for making determination of Carbon black pigment content in Nylon 66. Purpose was to ensure consistency in level and dispersion of the pigments in the plastic material.

None of the above referred techniques quantified pigments dispersion level in compounded plastics. This research however, successfully employs response surface methodology, scanning electron microscopy (SEM) and image analysis, modelling mixing zone of twin screw extruders, to analyse pigment dispersion in polycarbonate grades. Evaluating pigments dispersion level within a polymer matrix determines the mixing efficiency of a compounding process, which can be correlated with processing conditions employed. Contrary to paints and coatings, compounding of plastics involves high shear rates, elevated temperatures, and high pressures. To date, only a few studies are reported in literature about effect of process variables on plastics coloration. In 2005, D. Colquhoun et al [38] investigated that control of Pigment Yellow 62 (PY62) particle size and dispersion directly affected the properties of extruded polyethylene film (1 mil thick), such as film transparency, colour development, extruder pressure build and processing time. Using that knowledge they developed and successfully tested a new PY 62 for polyethylene film. This study investigates distributive mixing in the flow direction for a single-screw extruder. S. P. Rwei [39] in 2001 carried out an investigation of the distributive mixing in the flow direction for a single-screw extruder under varying processing conditions. Experiment involved blending of a fine grade of poly(dimethyl siloxane) (PDMS, 99.6% purity) with red ink representing a single concentrate chip and results showed improved longitudinal distribution with an increasing RPM, a longer metering section, or a decreasing diameter of the die.

### **1.7.1 Scanning Electron Microscopy (SEM) and Image Analysis**

In scanning electron microscopy (SEM), an electron beam scans the surface of a specimen to be examined, and the reflected (or back-scattered) beam of electrons is collected, then displayed at the same scanning rate on a cathode ray tube (similar to a CRT television screen). The image displayed on the screen, which may be photographed, replicates the specimen surface features. The surface may or may not be polished and etched, but it must be

electrically conductive; a very thin metallic surface coating must be applied to nonconductive materials such as polymers [40]. This condition however, is no more needed in ESEM, where to eliminate electrostatic charge build-up during examination, a bridge between specimen edges and conductive tape underneath is formed by applying a conductive adhesive. Magnifications over 200,000 times, are possible, and great depths of field are possible. Qualitative and semi-quantitative analysis of the elemental composition for quite localized surface areas, are also possible when equipped with accessories such as energy dispersive X-ray spectroscopy (EDX).

Various commercially available image analysis software such as Image-Pro can be used for image processing and analysis, but they are expensive. ImageJ however, is a public domain software [41], which is available as an online applet as well as in downloadable application format, for Windows, Mac OSX and Linux. The software is enriched with quite powerful features such as spatial calibration, stacking, filtering and geometric transformations to name a few.

## **1.8 Modelling and Computer Simulation of Extrusion Process**

Many researchers have made use of numerical methods to simulate the mixing of particles in a base resin via extrusion process both for single screw extruders (SSEs) and twin screw extruders (TSEs). In 1999, Eduardo of PolyTech discussed various characteristics of a practical successful process simulator and detailed the functions of a one dimensional (1D) simulator for plastics compounding operations in modular co-rotating intermeshing twin screw extruders [42].

J. Markarian in 2005 reviewed various software available in the market for plastic compounders to simulate extrusion process on extruders. Software she compared included Win TXS of PolyTech USA – a 1D model, Akro-Co-Twin-Screw of Temarex Corporation USA – a 1D model, Ludovic of CEMEF (Centre for Material Forming) France – a 3D model, Morex of Institute of Plastics Processing (IKV) Germany – a 1D model, Polyflow of Ansys Inc. USA – a 3D model, and Sigma of Institute of Plastics Engineering (KTP) of University of Paderborn and ten industrial companies including raw material suppliers and extruder manufacturers – a 1D model. She indicated an increasing trend in plastic compounders of utilizing sophisticated computer software for simulating various process parameters [43]. Surprisingly she didn't

mention OpenFOAM® - a public domain software, probably because it was developed and released in 2004 by Open CFD Ltd, after she wrote her article.

In 2005, Kirill carried out numerical simulation of mixing of two coloured particles population in acrylonitrile-butadiene-styrene copolymer (ABS) resin by extrusion in an industrial conventional SSE and evaluated degree of mixing and colour homogeneity. Results were found consistent with experimental data [44]. Robin et al, in 2006, evaluated the mixing in single screw and co-rotating twin screw dough mixers by simulating 2D model using Polyflow® software. They concluded that overall mixing effectiveness and efficiency of twin screw mixer was much better than that in single screw mixer [45].

In 2008, Chantal et al developed a full 3D finite element code called Ximex® and simulated mixing processes of complex fluids; as a case study, flow within a TSE and flow in a batch mixer were presented [46]. Then in 2009 they employed full 3D simulation software Ximex® for characterizing flow conditions in mixing processes such as SSE, TSE and analysing the influence of geometrical parameters such as staggering angle and disc thickness of kneaders on flow conditions [47].

In 2009 and 2010, Estanislao et al carried out three dimensional (3D) simulation of reactive flow in fully-filled screw elements of co-rotating closely intermeshing twin screw extruders (COTSEs) with the aim to analyse peroxide-initiated degradation of polypropylene (PP). To achieve that end, they modelled special designs of screw elements and simulated mixing process using Polyflow® software to see their effect on the process output. However they have suggested that both 1D and 3D models should complement each other [48, 49]. Later in 2010, Wang et al carried out numerical investigation to analyse the role of screw geometry on mixing of a viscous polymer melt, they successfully modelled four geometries of cooling screws being used by extrusion industry and made use of finite element solvers for 3D non-Newtonian fluid flow and advection-diffusion heat transfer [50].

Modelling techniques that have been presented by various authors include: analytical modelling; flow analysis network (FAN); quasi steady state approximation; moving reference frame (MRF) method; mesh superimposition technique. Each approach has its own pros and cons as discussed below. Analytical modelling provides the simplest way to understand the pumping behaviour of extruders, however is valid only for Newtonian fluids, furthermore mere throughput behaviour would not suffice to understand the flow mechanism in extruders, but

rather shear stress and velocity distributions are more important to know for an insight of the flow behaviour, which require numerical solution of the problem. The most common simplified numerical approach is FAN method, which works based on dividing flow region into control volumes and then carrying out flux balance on each volume. However because of geometric and information limitations restrict its use to simple geometries only.

Quasi-steady state approximation was introduced by Lee and Castro [51]. They mentioned that the transient part in the continuum equation could be considered negligible if the Reynolds number was very small as usually the case in polymer processing. With this approximation, the resulting solution is dependent only on instantaneous material properties and boundary conditions, and screws relative positions within the barrel i.e. sequential geometries at defined angles of rotor position, can be selected and simulated under a steady state condition. Each screws relative position however, requires new meshes to be generated for a solution to run, results are then compiled together for those relative positions to understand the flow behaviour over a complete rotation cycle. Transient nature and complexity of flow geometry in twin screw extruders do not allow to reach a truly steady state condition. Many researchers therefore successfully employed quasi-steady state approximation in simulating dispersive mixing behaviour of twin screw extruders.

Yang and Manas-Zloczower [52, 53] implemented the quasi-steady technique for simulating dispersive mixing behaviour of a Banbury mixer and for an intermeshing co-rotating twin screw extruder (ICRTSE). Bravo [54] employed same approximation for obtaining flowfield solution in kneading discs region of an ICRTSE. Recently, using same approximation, Sobhani et al [55] characterized mixing flow behaviour in co-rotating twin screw extruder, and Goger [56] analysed dispersive mixing behaviour in conveying elements of a counter rotating twin screw extruder. Disadvantage of this technique is that it involves lot of meshing work, and neglecting transient term in energy equation is not justified. Moving reference frame (MRF) provides an alternate to quasi-steady state approximation, however Ortiz-Rodriquez [48] stated its limitation in predicting flow behaviour of double flighted screw as two different radial vectors were defined. Another disadvantage he mentioned was its restricted capability in describing distributive mixing behaviour in twin screw extruders. Mesh superimposition technique [57] is pretty close to quasi-steady state in nature and even more sensitive to transient effects, however geometric complexities involved in twin screw extrusion restrict it to relatively course mesh patterns causing error to the results.

In lieu of the extensive literature survey presented above, this study employs quasi-steady state approximation for simulating the flow behaviour of kneading discs zone in a twin screw extruder using OpenFOAM® software.

## **1.9 Problem Statement – Inconsistency in Plastics Coloration**

SABIC Innovative Plastics manufactures coloured plastics via compounding process using co-rotating intermeshing twin screw extruders installed on its 15 production lines at Cobourg manufacturing facility. The raw material used include resins, fillers and colour pigments, usually one or two resins with 3 to 4 fillers and 4 to 5 pigments are premixed on a super floater, in proportions specified as reference colour formulation. The premixed is then poured into hopper of twin screw extruder under pre-defined processing conditions i.e. levels of temperature, screw speed and feed rate, all the ingredients undergoing various sections of barrel and screws system, are uniformly blended under high shear and elongational stresses. The homogenized blend of materials is then pushed to exit through a die hole located at tail end of the extruder forming a strand of compounded plastic. The extruded strand, immediately after exiting from die hole, is water quenched in a water bath, air-dried under an air-knife and cut by a pelletizer into small pellets of size 2mm x 2mm. The pellets are then moulded into rectangular plaques of size 70mm x 50mm x 2.6mm on injection moulding machine, these sample chips along with a reference chip are colour evaluated on a spectrophotometer, and visually inspected by a colour expert as well. Any colour deviation, exceeding permissible tolerance limits, between the reference and the sample chips raises colour inconsistency issue, and the whole production lot may go scrapped. New production lot with minute adjustments in pigments reference formulation under the advice of a colour expert, is loaded and the colour evaluation process is repeated until the colour deviation comes out to be within tolerance limits. Frequency of such adjustments in standard formulation varies with different plastic grades and associated output colours. These colour mismatch issues cause delay in delivery schedules, wastage of materials, man-hours and most importantly loss of competitive edge in global market. Each step in the entire compounding and colour evaluation process is critical and needs particular attention to study for identifying all possible factors causing colour mismatch [9].

## 1.10 Objectives

Main objectives of this study include following:

- Develop basic understanding of the compounding process used for plastics coloration. This is achieved by going through intensive literature review, executing experimentation and analysing 3D simulation results.
- Analyse the effect of small adjustments in colour formulation on colour of the PC grades. This is done by statistically analysing past production data of the PC grades using Design-Expert® software.
- Analyse the process variables and two factor interactions that affect colour of the PC grades, and thus optimize levels of the process variables to ensure consistency in colour. This has accomplished by implementing Box-Behnken design (BBD) using Design-Expert® software.
- Evaluate pigments dispersion level in terms of particles size and spatial distribution in PC grades. This is achieved using SEM for imaging and ImageJ® for image analysis.
- Undertake 3D simulation of the dispersive mixing behaviour in the kneading discs zone (staggered at 45°) under varying processing conditions, and correlate with experimental colorimetric data of the PC grades. This is achieved by 3D simulation of the kneading discs zone in a twin screw extruder system.

## 1.11 Overview of the Thesis

The entire thesis is divided into 6 chapters including introduction and background. Chapter 2 presents statistical analysis of the past production data respecting effect of small adjustments in colour formulation on output colour of two PC grades, PC1 and PC2. Technique involves implementation of historical data design using Design-Expert® software. Results identify pigments most responsive to colour variation under small adjustments in formulation, and suggests optimal adjustments to avoid repetition. Chapter 3 is devoted to implementation of Box-Behnken design (BBD) through designed experiments and investigate the effect of processing conditions on output colour of three PC grades, G1, G2, and G3. Technique involves two step methodology: first step is to select an appropriate design of experiments (DoE) such as BBD, and then to choose a polynomial model to fit in the data at hand. Optimization of multiple responses is also covered in chapter 3. Chapter 4 presents a novel technique, which characterizes solid structure samples using ESEM for imaging and for image analysis, the

ImageJ® - a public domain software; aim was to evaluate pigments dispersion level in PC grade G2 and correlate it to colour deviation. In chapter 5, 3D simulation of mixing zone in a twin screw extruder is presented using processing condition employed in compounding of PC grade G2. Results evaluate mixing efficiency of the kneading discs zone in terms of a flow parameter called lamda,  $\lambda$ . Finally in chapter 6, main conclusions and thesis contributions are summarized. Some future recommendations are also included in chapter 6.



## Chapter 2

### Influence of Minute Adjustments in Colour Formulation on output Colour of Compounded PC Grades

#### 2.1 Introduction

To develop various operational and aesthetic attributes in plastics / products, such as ultraviolet stability, thermal and mechanical properties, plastics compounders blend polymer resins with different additives, modifiers and fillers. However, the colour and special appearance effects in plastics offer them countless possibilities for innovation and marketing of their products in a fast growing and highly competitive global market. Successful addition of a desired colour to a plastic grade requires adequate mixing of colour pigments in base polymeric resin. The mixing involves wetting the pigment surface with the polymer, breaking up of agglomerates into primary particles, and uniformly distributing the pigment particles within the polymer matrix. While plastic compounders, to ensure better dispersion, typically use twin-screw extruders, internal lubricants or slip additives, and optimized processing conditions, the suppliers of pigments however, focus on balancing the particle size, shape and surface treatments [16, 20, 40].

Each target colour is associated with a reference recipe of colour formulation that reflects pigments type, and their concentration level in base resin(s), usually expressed in units of PPH - parts per hundred parts of base resin(s). Associated with the colour formulation is a reference colour described by tri-stimulus colour data such as  $L^*$ ,  $a^*$  and  $b^*$ . Any deviation from reference colour of the output colour of a compounded plastic, is declared as colour mismatch - a key issue confronted by plastics compounders and described in delta values i.e.  $\Delta L^*$ ,  $\Delta a^*$ ,  $\Delta b^*$ ,  $\Delta E^*$ . Such colour deviations call for small adjustments in colour formulation during production so the desired target colour can be achieved [10, 25, 40, 41, 61]. Present study addresses this issue by investigating the response of output colour to minute changes made in reference colour formulation.

Statistical methods are frequently used by researchers, to investigate and optimize the effect of process variables on responses such as colour and appearance of compounded plastics. For this purpose, they employ various statistical designs and models to fit in the response data obtained through designed experiments or past production data. Effertz [27] investigated a PVC sheet for the effect of processing conditions on its gloss and surface appearance using modified general factorial model. Bender [28] investigated the process variables causing high viscosity variability in wood-fiber compounds by executing Box-Behnken design (BBD). Present study

however, employs historical data design with the aim to investigate influence of small adjustments made in colour formulation, on the output colour of two PC grades assuming other factors are invariant. Historical data design is a response surface method, and to execute such a design present study uses Design-Expert® software.

Main objectives of this study include: 1) statistically analyze the effect of minute changes in colour formulation on output colour of two PC grades i.e. PC1 and PC2 using past production data collected at SABIC IP Cobourg Plant; 2) identify the colour pigments that significantly influence the output colour under minute adjustments; 3) optimize the process so the adjustments in colour formulation are precisely made and multiple adjustments can be avoided.

## 2.2 Experimentation

Experimental set up used was a 40 mm, 112 kW twin- screw intermeshing co-rotational extruder with L/D ratio of 37 having 9 zones barrel and a 4 zone die, representing a production line at SABIC IP Cobourg plant. Processing conditions i.e. the barrel and die zones temperatures, screw speed and feed rate were kept constant. The reference colour formulation and the past data of various adjustments made were collected from SABIC IP Cobourg plant and is presented in tables 2.1 to 2.4, for the two PC grades: PC1 and PC2. As mentioned earlier, both grades low Chroma opaque compounded PC grades, the only difference between the two formulations is that, PC1 was a blend of single PC resin and colour pigments, whereas PC2 represented a blend of two PC resins and colour pigments. The target colour coordinates were  $L^*=67.29$ ,  $a^*=1.47$ , and  $b^*=4.89$  for both PC grades. For brevity the delta values representing each adjustment are shown in tables 2.2 and 2.4.

Table 2.1: Reference Colour Formulation – PC1

S-No	Type	PPH	gram
1	Polycarbonate Resin (MFI=6.5g/10min)	100	6000
2	White Pigment	1.76	105.6
3	Black Pigment	0.00968	0.5808
4	Red Pigment	0.01602	0.9612
5	Yellow Pigment	0.1084	6.504

Table 2.2: Percent adjustments made in reference formulation during production – PC1

Prod Run	White Pigment (%)	Black Pigment (%)	Red Pigment (%)	Yellow Pigment (%)
1	3.87	-5.09	5.36	-12.36
2	3.89	3.82	5.20	-8.21
3	3.87	3.95	5.36	-14.67
4	3.88	3.82	5.30	-8.21
5	3.87	-5.09	5.36	-12.36
6	3.87	3.95	5.36	-14.67
7	3.87	-7.67	1.46	-12.36
8	3.89	3.82	5.20	-8.21
9	3.87	-7.67	1.46	-12.36
10	3.87	-5.09	5.36	-12.36
11	3.87	-7.67	1.46	-12.36

Table 2.3: Reference Colour Formulation – PC2

S-No	Type	PPH	gram
1	Polycarbonate Resin-1 (MFI=6.5g/10min)	70	4200
2	Polycarbonate Resin-2 (MFI=25g/10min)	30	1800
2	White Pigment	1.76	105.6
3	Black Pigment	0.00968	0.5808
4	Red Pigment	0.01602	0.9612
5	Yellow Pigment	0.1084	6.504

Table 2.4: Percent adjustments made in reference formulation during production – PC2

Prod Run	White Pigment (%)	Black Pigment (%)	Red Pigment (%)	Yellow Pigment (%)
1	5.82	3.31	1.46	-7.75
2	5.82	11.05	-6.34	-19.28
3	8.66	3.31	1.46	-16.97
4	5.82	6.40	1.46	-12.36
5	8.66	3.31	9.27	-19.28
6	5.82	6.40	1.46	-19.28
7	5.82	6.40	1.46	-15.82
8	5.82	3.31	1.46	-7.75
9	5.82	6.40	1.46	-12.36
10	5.82	3.31	1.46	-7.75
11	5.82	6.40	1.46	-14.67
12	8.66	7.18	1.46	-26.20
13	8.66	3.31	1.46	-21.59
14	8.66	3.31	9.27	-19.28
15	8.66	3.31	1.46	-21.59

## 2.3 Results and Discussion

Historical data design of Design-Expert® software was executed for carrying out analysis of variance (ANOVA) for the two PC grades and the results are discussed separately for each grade.

### 2.3.1 Low Chroma Opaque PC Grade (PC1) – Analysis and Optimization Results

#### A. ANOVA

Historical design of response surface method using design expert® has been employed to analyse historical data. Using backward technique all trivial model terms were eliminated from the linear regression model used to reach significant model and terms. ANOVA results are shown in Table 3 for three output responses i.e.  $\Delta L^*$ ,  $\Delta a^*$  and  $\Delta b^*$ .

Table 2.5. ANOVA for  $\Delta L^*$ ,  $\Delta a^*$  and  $\Delta b^*$

Output Response	Model p-value	Significant model term	Predicted R-Squared	Adequate Precision
$\Delta L^*$	0.0253	Black Pigment	0.1085	5.265
$\Delta a^*$	< 0.0001	Yellow Pigment	0.4558	8.509
$\Delta b^*$	< 0.0001	White Pigment	0.8437	17.383
		Black Pigment		

Numerical optimization to reach zero deviation from target colour is carried out, which suggests a slightly different pigments formulation with a desirability of 0.997 for the plastic grade under consideration. Optimal pigment formulation comprises white pigment (with 0.35% increase in standard formulation) = 106gm (1.766PPH), black pigment (with 0.19% increase in standard formulation) = 0.582gm (0.0097PPH), yellow pigment (with a reduction of 3.30% in standard formulation) = 6.285gm (0.1048PPH) and red pigment = any value within experimental variation range. Desirability 3D contour graphs shown here in Fig. 2.1 and Fig. 2.2 reveal a process window large enough to explore experimental design space for various combination of pigments formulation to reach target colour values. Based upon this optimal pigments formulation, perturbation graphs are shown in Fig. 2.3 to Fig. 2.6 for desirability,  $\Delta L^*$ ,  $\Delta a^*$  and  $\Delta b^*$  respectively. These graphs reveal how sensitive the output responses are to variation in pigments optimal formulation.

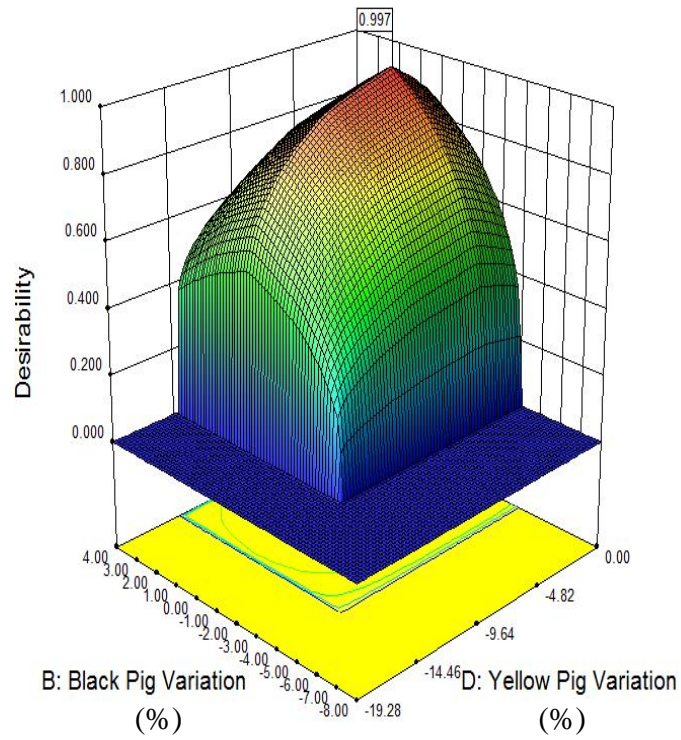


Fig. 2.1: Desirability with yellow and black pigments

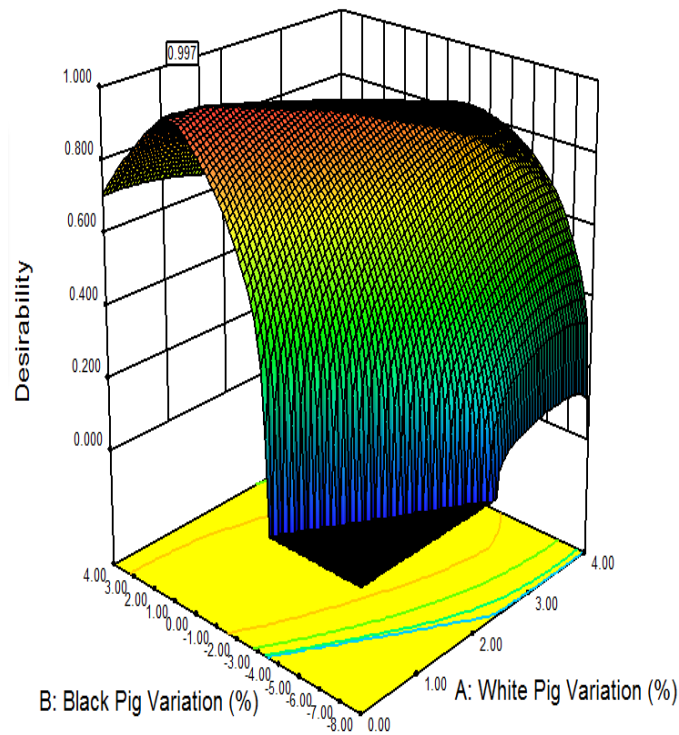


Fig. 2.2. Desirability with white and black pigments

B. Effect on desirability

Desirability perturbation graph shown here in Fig. 2.3 reveals that any change in optimal formulation of white, black and yellow pigments would significantly lower the desirability level. It further reveals that desirability is more sensitive to change in black and yellow pigments as compared to white.

C. Effect on  $\Delta L^*$ ,  $\Delta a^*$  and  $\Delta b^*$

Perturbation graphs shown in Figs 2.4, 2.5 and 2.6 tell about the sensitivity of  $\Delta L^*$ ,  $\Delta a^*$  and  $\Delta b^*$  values to variation in pigments optimal values respectively. Fig. 2.4 and Fig. 2.6 clearly indicate a significant effect on both  $\Delta L^*$  and  $\Delta b^*$  of varying black pigment optimal value and associate a change of 0.03 in  $\Delta L^*$  and 0.07 in  $\Delta b^*$  to each 1% change in black pigment optimal value. This further reveals that comparing with  $\Delta L^*$ ,  $\Delta b^*$  values are more sensitive to variation in black pigment amount. Fig. 2.6 also shows a significant effect on  $\Delta b^*$  values of changing white pigment amount and associates as an average a change of 0.1 in  $\Delta b^*$  to each 1% change in white pigment optimal amount. A significant effect on  $\Delta a^*$  of variation in yellow pigment amount could also be seen in Fig. 2.5, attributing a change of 0.0085 in  $\Delta a^*$  to each 1% variation in yellow pigment optimal value. For further clarity of these trends, contour graphs are presented in Figs 2.7, 2.8 and 2.9 for  $\Delta L^*$ ,  $\Delta a^*$  and  $\Delta b^*$  respectively.

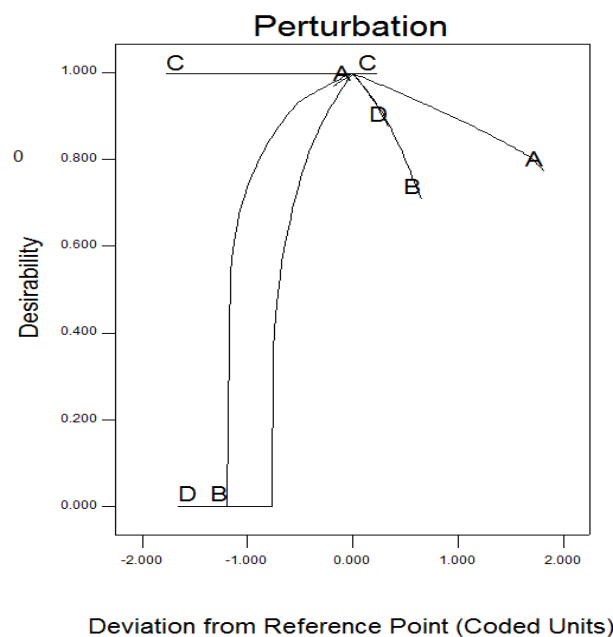


Fig. 2.3: Perturbation Graph of desirability

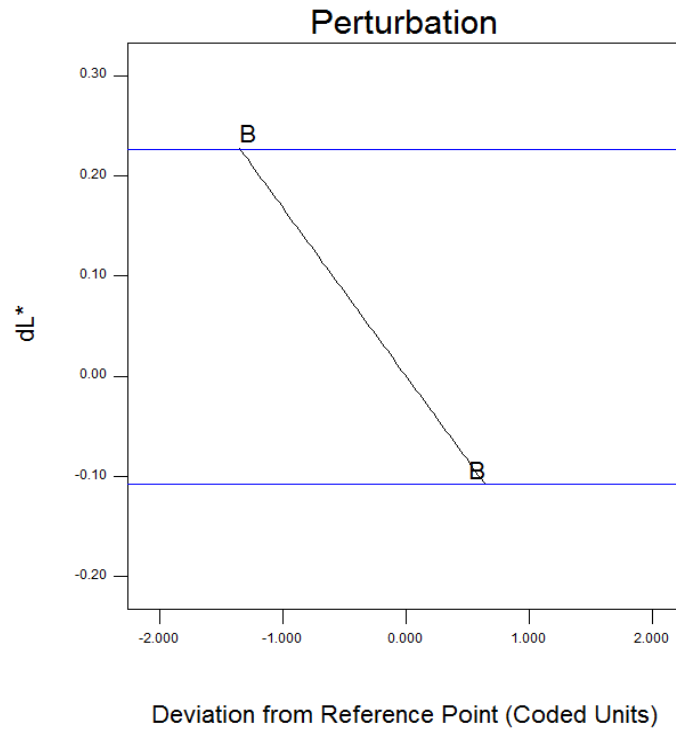


Fig. 2.4: Perturbation Graph of  $\Delta L^*$

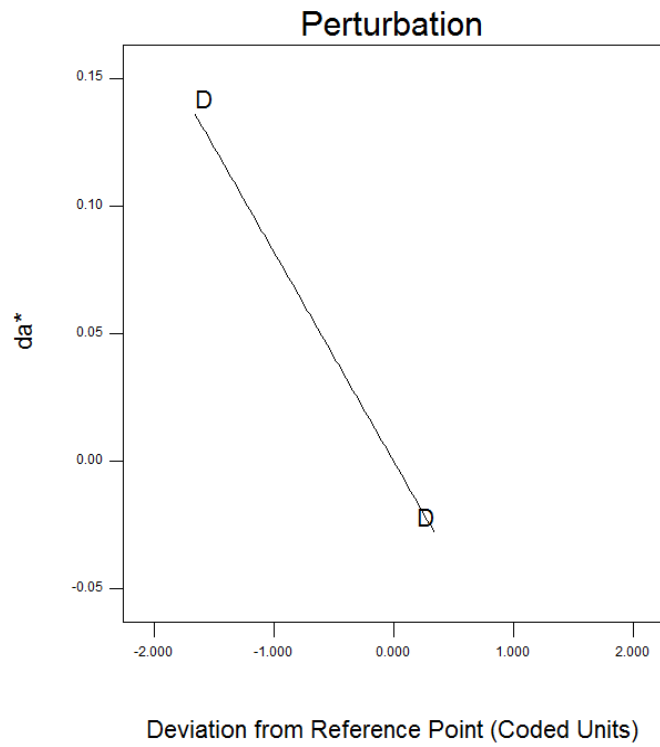
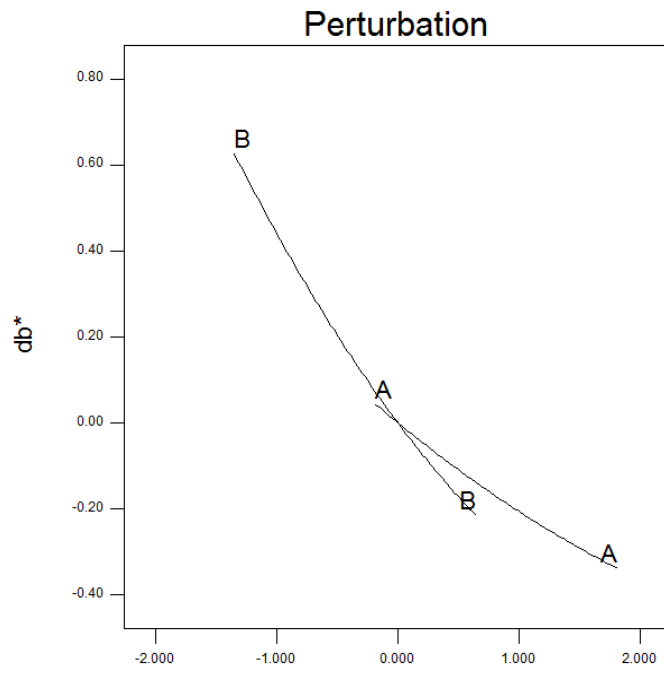
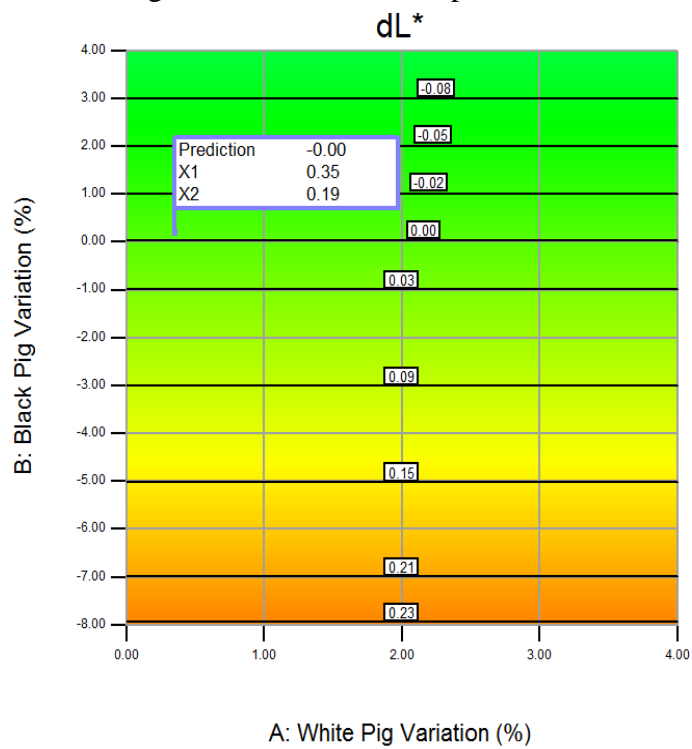


Fig. 2.5: Perturbation Graph of  $\Delta a^*$



Deviation from Reference Point (Coded Units)

Fig. 2.6: Perturbation Graph of  $\Delta b^*$



A: White Pig Variation (%)

Fig. 2.7: Contour Graph of  $\Delta L^*$



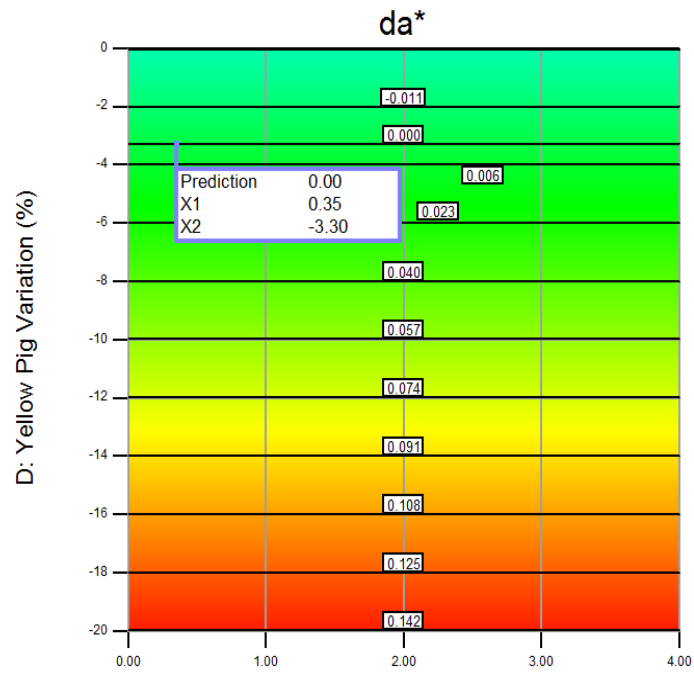


Fig. 2.8: Contour Graph of  $\Delta a^*$

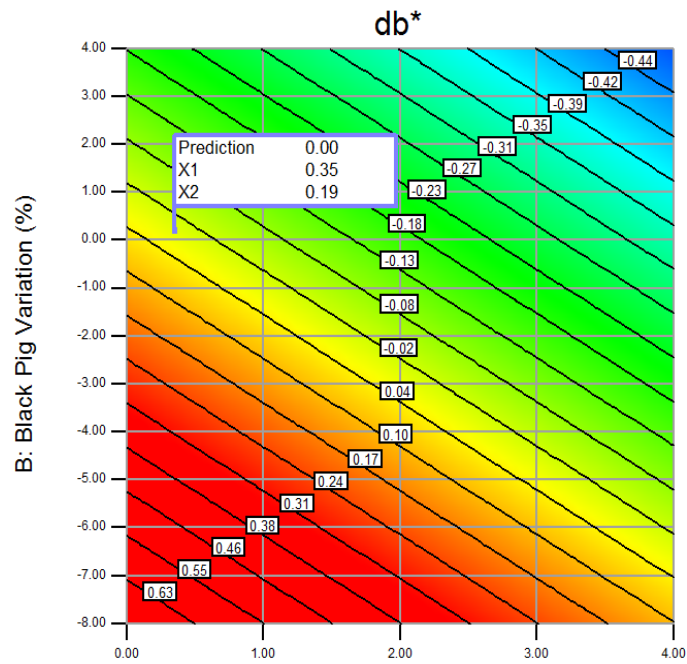


Fig. 2.9: Contour Graph of  $\Delta b^*$

### 2.3.2 Low Chroma Opaque PC Grade (PC2) – Analysis and Optimization Results

#### A. ANOVA

Historical data design of response surface method has been employed to analyse data. Using backward technique all trivial model terms were eliminated from the linear regression model used to make it significant. ANOVA results are shown in Table 2.6 for the three output responses i.e.  $\Delta L^*$ ,  $\Delta a^*$  and  $\Delta b^*$ .

Table 2.6. ANOVA Results of  $\Delta L^*$ ,  $\Delta a^*$  and  $\Delta b^*$

Output Response	Model p-value	Significant model term	Predicted R-Squared	Adequate Precision
$\Delta L^*$	0.0066	White Pig	0.1464	6.486
	0.0044	Yellow Pig		
$\Delta a^*$	0.0187	White Pig	0.0112	4.279
	0.0447	Yellow Pig		
$\Delta b^*$	0.0133	White Pig	0.3584	8.894
	0.0011	Yellow Pig		

Numerical optimization to reach zero deviation from target colour is carried out, which suggests slightly different pigments formulation compared to the standard given in Table 2.1, with desirability of 0.755 for the plastic grade under consideration. Optimal pigment formulation comprises white pigment (with 5.29% increase in standard formulation) = 111.2gm (1.853PPH), yellow pigment (with a reduction of 13.59% in standard formulation) = 5.62gm (0.0937PPH) and black and red pigment = any value within experimental variation range. Desirability 3D graph shown here in Fig. 2.10 reveals a process window large enough to explore experimental design space for various combination of pigments formulation to reach target colour values. Based upon optimal pigments formulation suggested, perturbation graphs are shown in Fig. 2.11 to Fig. 2.14 for desirability,  $\Delta L^*$ ,  $\Delta a^*$  and  $\Delta b^*$  respectively. These graphs reveal how sensitive the output responses are to variation in pigments optimal formulation.

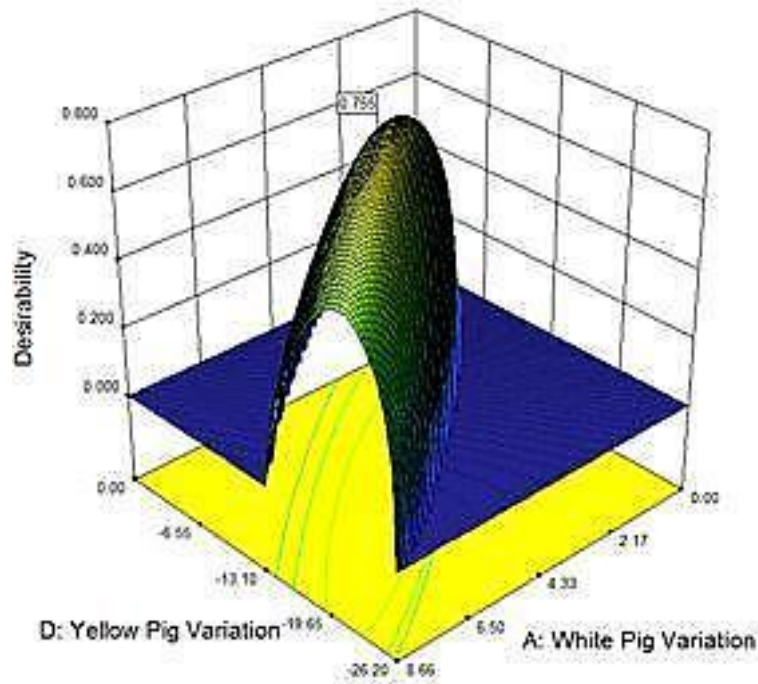


Fig. 2.10: Desirability with yellow and white pigments

B. Effect on desirability

Desirability perturbation graph shown here in Fig. 2.11 reveals that any change in optimal formulation of white and yellow pigments would significantly lower the desirability level. It further reveals that desirability is almost equally sensitive to change in white and yellow pigments.

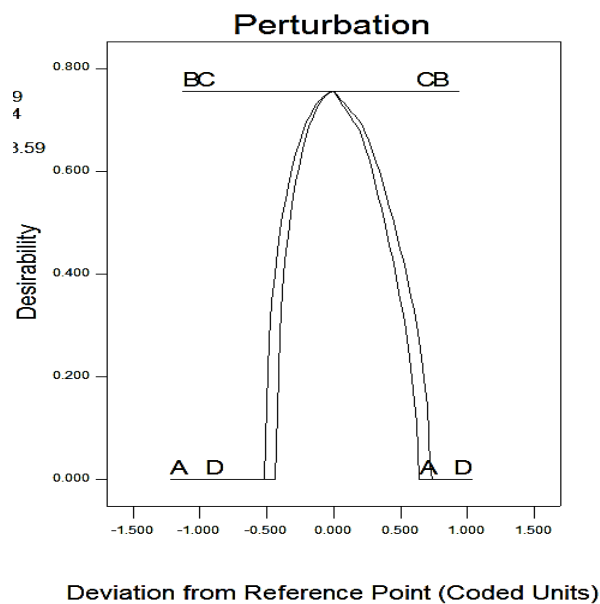


Fig. 2.11: Perturbation Graph of desirability

C. Effect on  $\Delta L^*$ ,  $\Delta a^*$  and  $\Delta b^*$

Perturbation graphs shown in Figs. 2.12, 2.13, and 2.14 depict the sensitivity of  $\Delta L^*$ ,  $\Delta a^*$  and  $\Delta b^*$  values to variation in pigments optimal values respectively. Figs. 2.12 to 2.14 clearly indicate a significant effect on  $\Delta L^*$ ,  $\Delta a^*$  and  $\Delta b^*$  of varying white and yellow pigments optimal value and associate a change of 0.17 in  $\Delta L^*$ , 0.05 in  $\Delta a^*$  and 0.13 in  $\Delta b^*$  to each 1% change in white pigment optimal value. Figs. 3 to 5 further reveal that a change of 0.07 in  $\Delta L^*$ , 0.02 in  $\Delta a^*$  and 0.07 in  $\Delta b^*$  is associated with each 1% change in yellow pigment optimal value. Comparing the variation effects in white and yellow pigments, it turns out that  $\Delta L^*$ ,  $\Delta a^*$  and  $\Delta b^*$  values are more sensitive to white pigment's percent change than yellow. Contour graphs presented in Figs. 2.15, 2.16 and 2.17 of  $\Delta L^*$ ,  $\Delta a^*$  and  $\Delta b^*$ , respectively, shed further light on the trends discussed above and are clearly discernible.

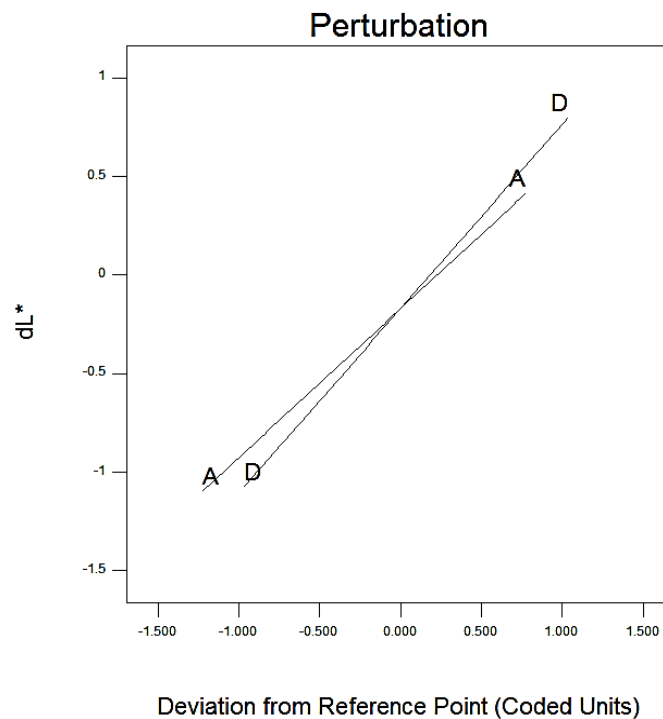
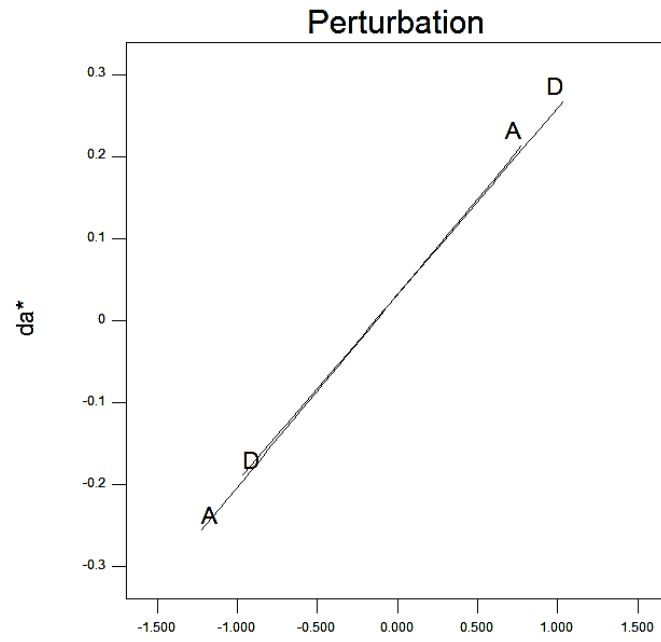
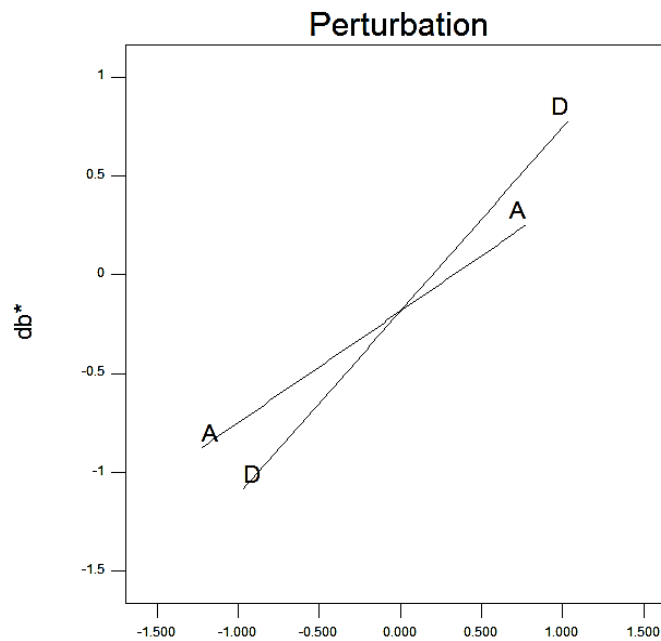


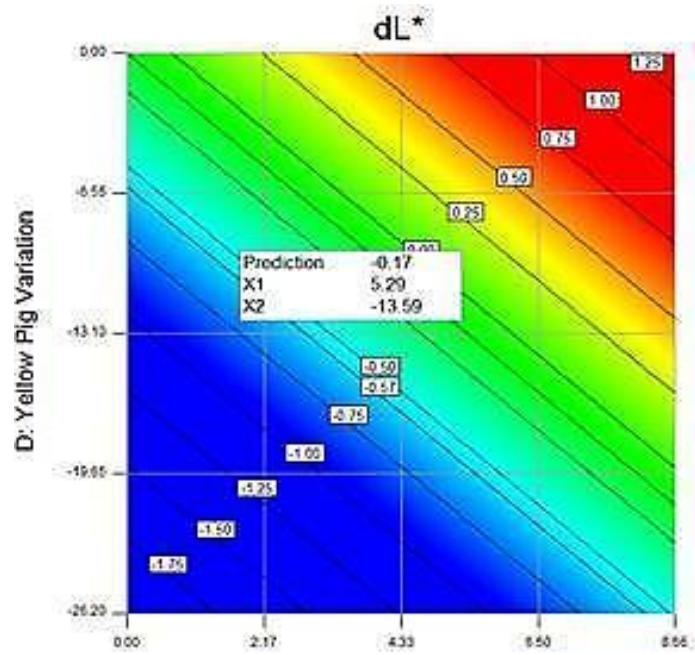
Fig. 2.12: Perturbation Graph of  $\Delta L^*$



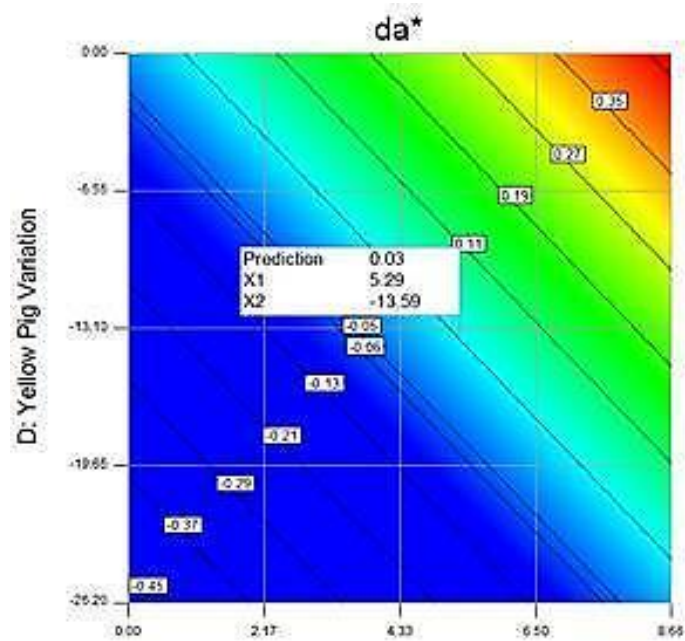
Deviation from Reference Point (Coded Units)  
 Fig. 2.13: Perturbation Graph of  $\Delta a^*$



Deviation from Reference Point (Coded Units)  
 Fig. 2.14: Perturbation Graph of  $\Delta b^*$



A: White Pig Variation  
 Fig. 2.15: Contour Graph of  $\Delta L^*$



A: White Pig Variation  
 Fig. 2.16: Contour Graph of  $\Delta a^*$

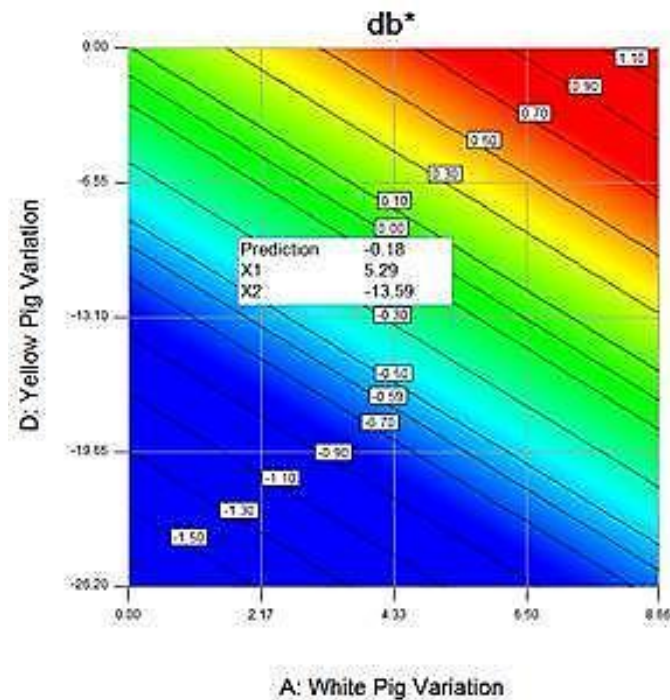


Fig. 2.17: Contour Graph of  $\Delta b^*$

## 2.4 Conclusions

### 2.4.1 Low Chroma Opaque PC Grade - PC1

This investigation identifies both the pigments type and variation in pigments formulation needed during production to tackle colour deviation of compounded plastic grade PC1. The optimization results suggest a formulation for white, black and yellow pigments slightly different from standard one minimizing colour deviation for the plastic grade. It may also be concluded that with the findings of current study in hand, a colour expert would have made more precise decision for the minute adjustments needed during production in pigments standard formulation and resulted into improved productivity. Furthermore, the study has emphasized on the need to take maximum care when preparing a pre-mixture for PC1 production batch particularly in measuring small amounts of identified pigments as the output colour is quite sensitive to minute change in pigments formulation.

### 2.4.2 Low Chroma Opaque PC Grade - PC2

Present study has identified the pigments and the adjustments needed in pigments amount during production to tackle the colour mismatch of compounded plastic grade PC2. The optimization results suggest a slightly different formulation from reference, of white and yellow pigments, to be used to minimize any colour deviation from target. It is believed that findings of this study would help colour experts in making precise and accurate adjustments in

colour formulation during production, thus improving productivity. Study further suggests that maximum care needs to be taken while preparing a colour formulation to be used in compounding. Special attention is needed in measuring small amounts of identified pigments being more responsive to variation in output colour.

## **2.5 Summary**

In this study, past production data of two low Chroma opaque polycarbonate (PC) plastic grades - PC1 and PC2, were statistically analysed with the aim to quantify the influence on output colour caused by small adjustments in colour formulation made during production. These PC grades were compounded on a co-rotating intermeshing twin screw extruder, at SABIC IP Cobourg plant. PC1 represented a blend of four colour pigments and four additives in one PC resin grade, whereas PC2 was a blend of four colour pigments and five additives in two PC resin grades. Colour mismatch caused by these adjustments is presented in terms of  $\Delta L^*$ ,  $\Delta a^*$ ,  $\Delta b^*$  and  $\Delta E^*$ . This study reveals that output colour is quite sensitive to minute changes in amount of white, black, and yellow pigments. Optimization results suggest precise adjustments in pigments amount to be made in dealing with colour deviations encountered during compounding of PC1 and PC2 plastic grades.



## Chapter 3

### Process Optimization through Designed Experiments to achieve Consistent Output Colour in Compounded Plastics

#### 3.1 Introduction

Plastic compounders use various modifiers, fillers and additives for polymeric material grades to inculcate and improve upon their desired attributes such as thermal, UV stability and mechanical properties. All parameters including processing and rheological conditions come into focus throughout developmental cycle of the plastic grades; however, in the present fast growing plastic market, adding a specific colour and appearance to plastic grades has become even more demanding. Taking into account the colourability right from onset of development cycle of a polymeric material grade is imperative [20].

Presence of three elements of light – a light source, observer and an object, is a must to see a colour. When a light beam is incident on an object, a part (<1%) of it is reflected back from the surface interface, which can be specular or diffuse reflection depending upon surface condition, whereas the rest of the light penetrates into the surface and is modified by three phenomenon; that is, selective absorption, reflection/transmission, and scattering. It is the selective absorption and reflection/transmission that determine the colour of the object, whereas the scattering takes care of the whiteness, brightness, and opacity of the object. However, scattering occurs only when the refractive index of any additives, pigments, or regions within plastic grade differ from the base resin and cause a change in both the direction and velocity of incident light. The refractive index depends on not only the type of substance itself but the wavelength of the incident light. Scattering may not be a desired phenomenon as it prevents the light from penetrating deeper into the object and therefore can hinder achievement of the desired colour; however, scattering can be a choice, where opacity is the priority. Polycarbonate resins are transparent and do not scatter light; therefore, to achieve a certain opacity level, white pigment (titanium dioxide) is added to create scattering at the cost of loss in apparent colour strength [20, 42, 61, 62].

Key factors that can cause colour mismatch to occur include: 1) inadequate mixing, both dispersive and distributive, of colour pigments; 2) incorrect formulation; 3) pigment particle size variation; 4) degradation of polymer resin and/or pigments, and 5) particles/regions of varying refractive index within the polymeric resin causing scattering. All such factors need to be studied to understand their effect on output colour [10, 20, 40, 41, 61].

Design of experiments (DoE) is a planned approach that allows an experimenter to precisely determine cause-and-effect relationships. Many researchers have employed statistical techniques to investigate / optimize the effect of input factors on desired output attributes. Design-Expert® software (Stat-Ease, Inc., Minneapolis, MN, USA) offers the use of various statistical designs and models to fit the experimental data at hand. Effertz [27] employed a modified general factorial DoE for investigating the effect of changes in compounding process variables on gloss and surface appearance of a PVC sheet. Similarly, Bender [28] successfully executed a DoE involving Box-Behnken design (BBD) to determine the relationship between processing conditions and viscosity variability for a wood-fiber compound. The present study utilized a DoE based on BBD in Design-Expert® software. The aim was to investigate the effect on output colour of three compounded plastic grades under varying processing conditions employed in an extrusion process. SABIC IP's technology line at Cobourg Plant, which comprises a twin screw extruder (TSE), was used to execute the DoEs. Assuming that previously discussed variables were well under control, the present study suggests optimal values for process variables to achieve consistency in output colour of the plastic grades.

### **3.1.1 Response Surface Methodology (RSM) and Box-Behnken Design (BBD)**

As explained in chapter 1, RSM involves use of mathematical and statistical techniques, which are extremely useful in modelling and analysis of problems where a response of interest is influenced by independent variables, and the objective is to optimize the response. In most RSM cases like ones examined in this study, type of relationship is not known between independent variables and the response. Therefore, a true functional relationship is approximated with a polynomial model as expressed in equation 1.2, followed by a proper choice of design that should provide sufficient amount of information to test the model fitness, and is economical too in terms of experimental runs. Therefore, in this study we chose BBD that requires only three levels of each variable in order to generate a quadratic model and capture two factor interactions.

### **3.1.2 Optimization of Multiple Responses**

As explained in chapter 1, most RSM problems involve simultaneous analysis of multiple responses, which was the case in this study where we measured three responses i.e.  $L^*$ ,  $a^*$  and  $b^*$  representing colour of the compounded plastic grades examined. However, in a simultaneous consideration of multiple responses, first step is to build an appropriate response surface model for each response, and then look for a set of operating conditions that optimize all responses, or at least keep them within the desired ranges.

The most popular technique however, is the numerical optimization technique by Derringer and Suich, which involves use of desirability functions. The procedure as explained in chapter 1, is to first convert each response  $y_i$  into an individual desirability function  $d_i$  that varies from 0 to 1. A  $d_i = 1$  tells the response is at its target, whereas a  $d_i = 0$  means the response lies outside the desired region. Then the overall desirability is calculated by taking geometric mean of individual desirability functions as expressed in equation (1.3).

### 3.1.3 Response and 3D Colour Space - CIE Lab Model

As mentioned earlier, the colour of an object can be characterized by its tri-stimulus data i.e.  $L^*$ ,  $a^*$  and  $b^*$  - the three responses that are investigated in this study. The tri-stimulus colour data corresponds to a point in 3D colour space of CIE Lab model, which was introduced in 1976 by the international commission on light (CIE - Commission Internationale de l'Eclairage). Any deviation from the reference target colour that exceeds permissible limits, is reported as colour mismatch and usually expressed in delta values as  $\Delta L^*$ ,  $\Delta a^*$ ,  $\Delta b^*$  and  $\Delta E^* = \sqrt{(\Delta L^*)^2 + (\Delta a^*)^2 + (\Delta b^*)^2}$ . It is the customer needs that usually decide a threshold for these delta values, which for the plastic grades studied, were set out as  $\leq 0.6$  for  $\Delta L^*$ ,  $\Delta a^*$ ,  $\Delta b^*$  and  $\leq 1.0$  for  $\Delta E^*$ . One significant aspect in colour matching is to prepare a rectangular moulded chip similar to moulded sample chips, for use as reference representing reference colour formulation. Colour coordinates of reference chip are measured and stored on a spectrophotometer. Spectrophotometers are useful quality control tools that help to numerically measure colour and colour variation.

### 3.1.4 Propagation of Error (POE) Technique and Process Robustness

Robustness of design is ensured by incorporating propagation of error (POE) technique in RSM design. POE is taken as a measure of standard deviation of transmitted variability in output response, which is caused by fluctuations in significant controllable process variables during experimentation assuming uncontrollable factors noise to zero [30]. Using POE technique with RSM design, levels of controllable input factors can be found that keep output responses close to their target values and reduce variation transmitted by lack of control over input controllable factors. In other words, POE technique makes a process insensitive to variation in input factors. However, the technique is beneficial only when RSM reveals curvilinear relationships between input factors and output responses, and transmitted variation is reduced by moving to plateaus [60]. Mathematical expression for POE is given below in equation (3.1) [61]. It takes partial derivatives of response polynomials (Y) in actual units with

respect to input variables ( $X_i$ ) and incorporates variation in input variables ( $\sigma_{X_i}$ ) and unexplained residual i.e. experimental noise ( $\sigma_{resid}$ ).

$$POE = \sqrt{\sigma_Y^2} = \sqrt{\left[\frac{\partial Y}{\partial X_i}\right]^2 \sigma_{X_i}^2 + \sigma_{resid}^2} \quad (3.1)$$

### 3.1.5 Objectives

Main objectives of this study include following:

- 1) Identify process variables and their interactions affecting colour of compounded PC grades
- 2) Optimize levels of the process variables to ensure consistency in output responses
- 3) Achieve robustness of the design by incorporating POE technique

### 3.2 Experimentation

The process equipment used in this study was a 25.4 mm, 27 kW, intermeshing, co-rotational twin-screw extruder (TSE: ZSK26 Coperion Germany), which represents a technology line of SABIC IP at Cobourg Plant. TSE with L/D ratio of 37 and  $D_o/D_i$  of 1.55 has 10 heating zones - 9 identified on the barrel and 1 on die. Three process parameters i.e. temperature, screw speed and feed rate were varied through 3 levels for 17 experimental runs as per DOE. On exiting from die, plastic strands underwent cooling through a water channel, were dried under an air knife and cut into pellets. The pellets from each experimental run were preheated isothermally in an oven at 120°C for about 2 hours and then moulded into at least three sample chips of the size: 70mm x 50mm x 2.6mm, on an injection moulding machine. These sample chips and the target colour reference chips were measured on an X-Rite spectrophotometer - Colour-Eye® 7000A. The average colour data of three sample chips representing each experimental run of DoE were used for regression analysis with Design-Expert® software. Colour data obtained as per DoE for the three PC grades: G1, G2 and G3, are presented in tables 3.1, 3.2 and 3.3 respectively. As mentioned earlier, grade G1 represents a translucent low Chroma PC compounded plastic, grade G2 is a high Chroma opaque PC compounded plastic, whereas grade G3 is a high luminous opaque PC compounded plastic. Colour formulations corresponding to G1, G2, and G3 grades are presented in tables 3.4, 3.5 and 3.6 respectively along with mention of their reference colour coordinates.

Table 3.1. Designed Experimental Runs and Colour Data – Grade G1

Run No.	Process Variable			Average Output Response		
	Temperature (°C)	Screw Speed (rpm)	Feed Rate (kg/hr)	L*	a*	b*
1	280	650	19	70.00	3.37	17.75
2	280	850	19	69.92	3.39	17.73
3	280	750	11	69.78	3.48	17.82
4	255	650	27	70.23	3.61	17.87
5	255	650	11	70.57	3.78	18.24
6	255	750	19	70.24	3.98	18.46
7	255	850	27	70.59	3.73	18.21
8	230	750	11	70.40	3.70	17.96
9	255	850	11	69.94	3.52	17.78
10	255	750	19	70.31	4.04	18.48
11	280	750	27	70.05	3.38	17.80
12	230	850	19	70.63	3.77	18.20
13	230	750	27	70.51	3.77	18.07
14	255	750	19	70.19	3.97	18.04
15	255	750	19	70.16	3.99	18.09
16	255	750	19	70.19	3.99	18.04
17	230	650	19	70.55	3.79	18.23
Reference colour coordinates				70.4	3.41	18.09

Table 3.2. Designed Experimental Runs and Colour Data – Grade G2

Run No.	Process Variable			Average Output Response		
	Temperature (°C)	Screw Speed (rpm)	Feed Rate (kg/hr)	L*	a*	b*
1	240	600	23	42.88	45.31	23.53
2	300	750	11	41.96	42.83	21.82
3	300	750	35	42.58	44.76	23.13
4	300	600	23	42.64	45.01	23.35
5	270	600	11	42.62	44.56	23.1
6	240	750	35	42.74	45.42	23.65
7	240	900	23	42.90	45.19	23.54
8	270	750	23	42.63	45.14	23.22
9	270	750	23	42.65	45.12	23.41
10	270	600	35	42.76	45.25	23.38
11	270	750	23	42.78	45.26	23.38
12	270	900	11	42.29	44.11	22.6
13	240	750	11	42.07	43.65	22.36
14	270	750	23	42.62	44.79	23.26
15	270	750	23	42.77	45.55	23.59
16	270	900	35	42.91	45.33	23.43

17	300	900	23	42.43	43.99	22.66
Reference colour coordinates				43.26	44.89	24.09

Table 3.3: Designed experimental runs and colour data – Grade G3

Run No.	Process Variable			Average Output Response		
	Temperature (°C)	Screw Speed (rpm)	Feed Rate (kg/hr)	L*	a*	b*
1	270	750	23	89.73	-0.07	6.55
2	270	750	23	89.53	-0.09	6.33
3	270	900	11	89.45	-0.10	6.35
4	270	900	35	89.69	-0.07	6.54
5	270	750	23	89.60	-0.09	6.52
6	240	900	23	89.70	-0.07	6.50
7	300	900	23	89.61	-0.06	6.66
8	300	750	35	89.74	-0.07	6.63
9	270	600	35	89.60	-0.08	6.39
10	240	750	35	89.85	-0.07	6.53
11	300	600	23	89.65	-0.04	6.80
12	270	750	23	89.59	-0.09	6.39
13	270	600	11	89.69	-0.05	6.68
14	300	750	11	89.45	-0.03	6.79
15	240	600	23	89.89	-0.08	6.51
16	270	750	23	89.67	-0.09	6.50
17	240	750	11	89.57	-0.07	6.52
Reference colour coordinates				89.39	0.02	6.67

Table 3.4. Colour Formulation – Grade G1

S.No.	Type	PPH	grams
1	PC Resin-1 (MFI=25 g/10min)	33	2640
2	PC Resin-2 (MFI=6.5 g/10min)	67	5360
3	White Pigment	0.25	15.00
4	Black Pigment	0.0004	0.032
5	Red Pigment	0.0016	0.128
6	Yellow Pigment	0.0710	5.68
7	Filler 1	0.0350	2.80
8	Filler 2	0.2000	16.00
9	Filler 3	0.0650	5.2

Table 3.5. Colour Formulation – Grade G2

S.No.	Type	PPH	grams
1	PC Resin (MFI=6.5 g/10min)	100	9000
2	White Pigment	0.422	38.00
3	Black Pigment	0.00013	0.012
4	Solvent Red 135	0.281	25.30
5	Solvent Red 207	0.070	6.30

6	Pigment Orange 107	0.202	18.20
7	Filler 1	0.050	4.50ml
8	Filler 2	0.022	2.00ml

Table 3.6: Colour Formulation – Grade G3

S-No	Type	PPH	gram
1	PC Resin (MFI=6.5 g/10min)	100	10000
2	White Pigment	2.11	211
3	Black Pigment	0.045	4.5
4	Red Pigment	0.313	31.3
5	C.I. Pigment Brown 24	2.0	200
6	Pigment Yellow 163	0.086	8.6
7	Filler 1	0.20	20
8	Filler 2	0.60	60
9	Filler 3	0.05	5ml

### 3.3 Results and Discussion

The average colour data obtained from execution of DoEs respecting three PC grades, were analysed by carrying out analysis of variance (ANOVA) using Design Expert® software. The effect of significant main factors, quadratic factors and two factor interactions on output responses are discussed. The fitness of predictive model equations is verified by further experimentation, and the optimization results are presented.

#### 3.3.1 Low Chroma Translucent PC Grade (G1) – Analysis and Optimization Results

##### A. ANOVA and Design Evaluation

Quadratic model as suggested by fit summary showing no aliases terms was employed. ANOVA for all three output responses i.e. L\*, a\* and b\* was executed and significant quadratic models with p-value < 0.05 were obtained. All trivial model terms with p-value > 0.10 were eliminated from each significant model employing backward technique. To ensure validity of model, required design evaluation and diagnostic checks were carried out and all statistics found well within threshold limits. For instance, lack of fit for the three models was insignificant with degrees of freedom (df) greater than minimum limit of 3, difference between adjusted R-squared and predicted R-squared values was below 0.2, adequate precision – a measure of signal to noise ratio, was well above its threshold of 4, standard error values associated with coefficients respecting linear, cross product and quadratic terms, were found exactly same within their specific type, variance inflation factors (VIF) of all coefficients were found at a Fig. of 1 - an ideal value that ensures design orthogonality, and all residuals behaved well, except few DFFITS (difference of fits – a statistics helpful in detecting influential runs)

values, one for L\* and two for a\*, found exceeding a threshold of ±2, this statistics however for smaller designs like BBD is overly sensitive and can be ignored [30]. A summary of some of these statistics and predicting model equations are presented in Table 3.7 and Table 3.8 respectively for each response.

Table 3.7. ANOVA Results for L\*, a\* and b\*

Output Variable	Significant Factor	p-value (<0.05)	Adjusted R-Squared	Predicted R-Squared	Adequate Precision
L*	Model	< 0.0001	0.9547	0.8694	20.261
	A	< 0.0001			
	C	0.0037			
	BC	< 0.0001			
	B <sup>2</sup>	0.0104			
a*	Model	< 0.0001	0.9731	0.8941	22.819
	A	< 0.0001			
	AC	0.0517			
	BC	0.0009			
	A <sup>2</sup>	< 0.0001			
	B <sup>2</sup>	< 0.0001			
	C <sup>2</sup>	< 0.0001			
b*	Model	0.0276	0.5246	0.4417	5.487
	A	0.0148			
	BC	0.0331			
	A <sup>2</sup>	0.0447			

Note: A – Temperature, B – Screw speed, C – Feed rate

Table 3.8. Final equations in terms of actual factors

$L^* = 83.30647 - 0.01172 * \text{Temperature} - 0.02130 * \text{Speed} - 0.22115 * \text{Feed rate} + 0.00031 * \text{Speed} * \text{Feed rate} + 0.00001 * \text{Speed}^2$
$a^* = -29.45174 + 0.19773 * \text{Temperature} + 0.02291 * \text{Speed} + 0.06395 * \text{Feed rate} - 0.00022 * \text{Temperature} * \text{Feed rate} + 0.00012 * \text{Speed} * \text{Feed rate} - 0.00039 * \text{Temperature}^2 - 0.00002 * \text{Speed}^2 - 0.00261 * \text{Feed rate}^2$
$b^* = 3.89675 + 0.14196 * \text{Temperature} - 0.00500 * \text{Speed} - 0.10565 * \text{Feed rate} + 0.00025 * \text{Speed} * \text{Feed rate} - 0.00029 * \text{Temperature}^2 - 0.00213 * \text{Feed rate}^2$

Fraction of design space (FDS) check was also carried out in order to determine if a fraction equal to 80% of design space existed with required precision. To carry out such an evaluation it is recommended to employ experimental error instead of ANOVA estimate of standard deviation, therefore a standard deviation (s) of 0.28 for L\*, 0.15 for a\* and 0.2 for b\*, estimated from past experimentation data, were used. With s=0.28 a threshold value of d = 0.59 for error type “Diff” indicates that design can detect a minimum change of 0.59 in output



response as revealed in FDS graph shown below in Fig. 3.1. Similarly for error type “Pred” a value of  $d=0.79$  reveals that design is capable enough to predict output response with prediction interval (PI)  $\pm 0.79$  as indicated in Fig. 3.2. These threshold values of  $d$  were imperative to evaluate for making an intelligent and careful guess of the system noise from past experience, so the output response can precisely be predicted.

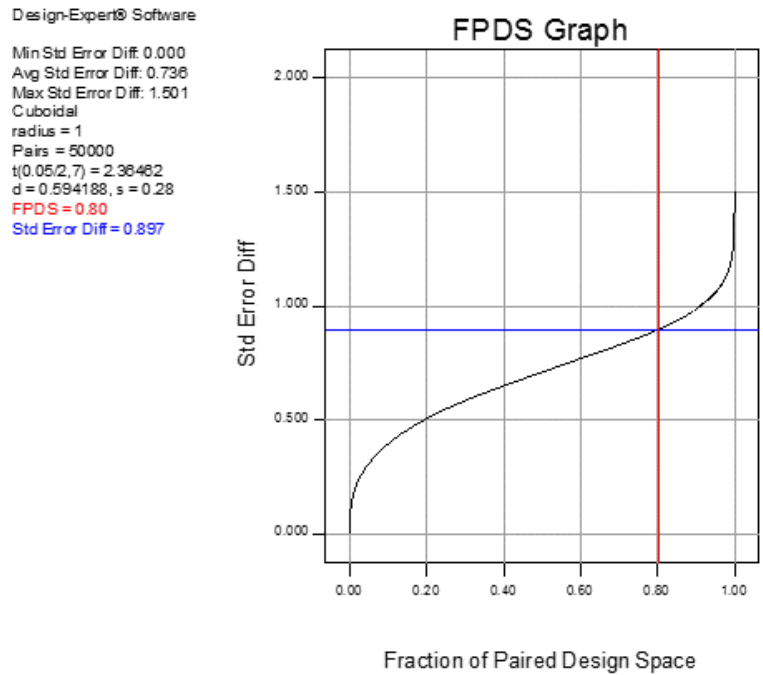


Fig. 3.1: Evaluation of FDS and  $d$  for Error Type “Diff”

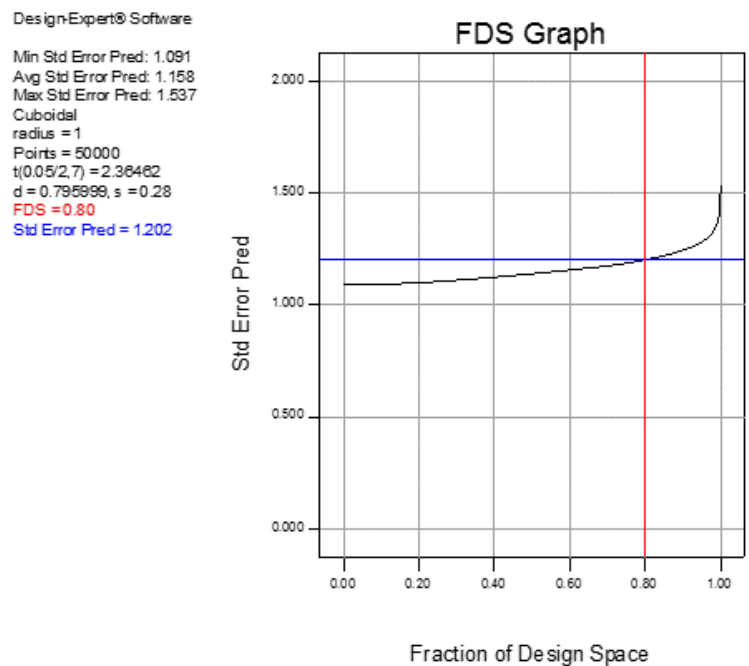


Fig. 3.2: Evaluation of FDS and  $d$  for Error Type “Pred”

## B. Evaluation of POE and Design Robustness

Robustness of design is ensured by incorporating propagation of error (POE) in RSM design. POE is taken as a measure of standard deviation of transmitted variability in output response, which is caused by fluctuations in significant controllable process variables during experimentation assuming uncontrollable factors noise to zero [30]. Using POE technique with RSM design, levels of controllable input factors can be achieved that would keep output responses close to their target values and reduce variation transmitted by lack of control over input factors. In other words, POE technique makes a process less sensitive to variation in input factors. However, POE technique is beneficial when RSM reveals curvilinear relationships between input factors and output responses, and transmitted variation is reduced by moving to plateaus [60]. Mathematical expression for POE is given in equation (3.1) [61].

The variation in process variables, observed during experimentation and incorporated in RSM design, include 10°C in temperature, approx. 1rpm in screw speed and about 0.01kg/hr in feed rate. Response polynomials, used to calculate POEs, are expressed as predictive model equations given in Table 3.8 in non-coded units.

From perturbation graphs for  $L^*$ ,  $a^*$  and  $b^*$ , not shown here except for  $L^*$  in Fig. 3.5, it's evident that response surface of  $L^*$  is slightly curvilinear in direction of B dimension, that of  $a^*$  is slightly curvilinear in directions of B and C dimensions, but along A dimension, its curviness is quite significant. Similarly looking at  $b^*$  response surface, a significant curvilinear relationship along A and C dimensions is quite visible. This indicates that a search to find out plateaus – flat regions, would be worthwhile. To achieve that objective, POE calculations were performed using Design-Expert® software of Stat-Ease, Inc., which created 3D response surfaces of  $L^*$ ,  $a^*$ ,  $b^*$  and corresponding POEs. For brevity, only plots of POE ( $a^*$ ) and POE ( $b^*$ ) are shown here in Fig.s 3.3 and 3.4 respectively. It is evident from these plots that flat regions exist around mid-range temperature: 244 for  $a^*$  and 243 for  $b^*$ .

Design-Expert® Software  
Factor Coding: Actual  
POE(a\*)

X1 = A: Temperature  
X2 = C: Feed Rate

Actual Factor  
B: Screw Speed = 750

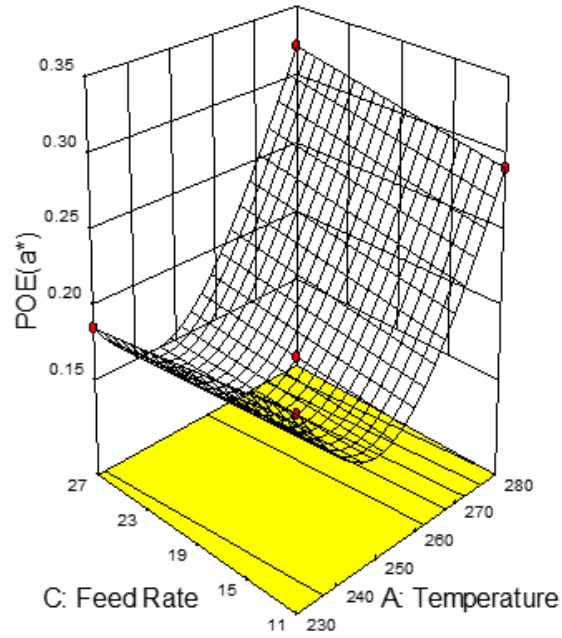


Fig. 3.3: POE (a\*) Plot with Factor B at Mid-Point

Design-Expert® Software  
Factor Coding: Actual  
POE(b\*)

X1 = A: Temperature  
X2 = C: Feed Rate

Actual Factor  
B: Screw Speed = 750

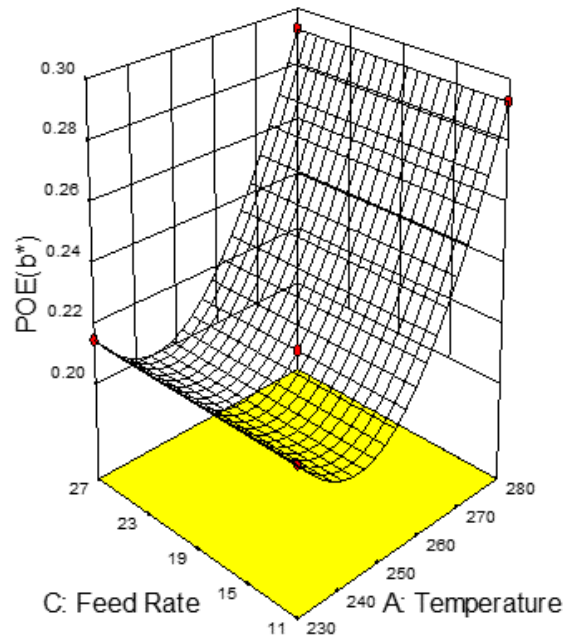


Fig. 3.4: POE (b\*) Plot with Factor B at Mid-Point

### C. Perturbation Graphs

Perturbation plots help to understand and compare the effect of all significant factors at a specific point in design space. For sake of brevity, only  $L^*$  perturbation plot is shown below in Fig. 3.5. Design-Expert® software, by default, sets the reference point at mid-level (coded 0) of all input variables. This reference point can be changed to other point of interest such as optimal point when optimization is the target. Response is plotted by changing one factor over its range while keeping other factors constant. It is evident from these plots that output responses are highly sensitive to changes in temperature, for  $L^*$  the effect is linear and of same intensity on either side of the midpoint, however for  $a^*$  and  $b^*$  effect is quadratic in nature and much stronger towards higher end of temperature range compared with lower end. Plot for  $L^*$  further reveals that shifting the temperature to lower end of range has a positive effect on  $L^*$  whereas dragging it to higher end of range imposes a reverse, but equal effect on  $L^*$ . This can be attributed to shear thinning of base resins caused by higher temperatures lowering their viscosity and resulting into poor dispersion of colour pigments. However unlike temperature effect, change in feed rate shows up a positive effect on  $L^*$  that can be explained by the fact that at constant temperature and screw speed raising feed rate would cause the viscosity of base resins a bit higher resulting into better dispersion of pigments. For  $a^*$  and  $b^*$  feed rate imposes a negative effect on either side of the midpoint that can be attributed to a strong interaction existed between these two factors.

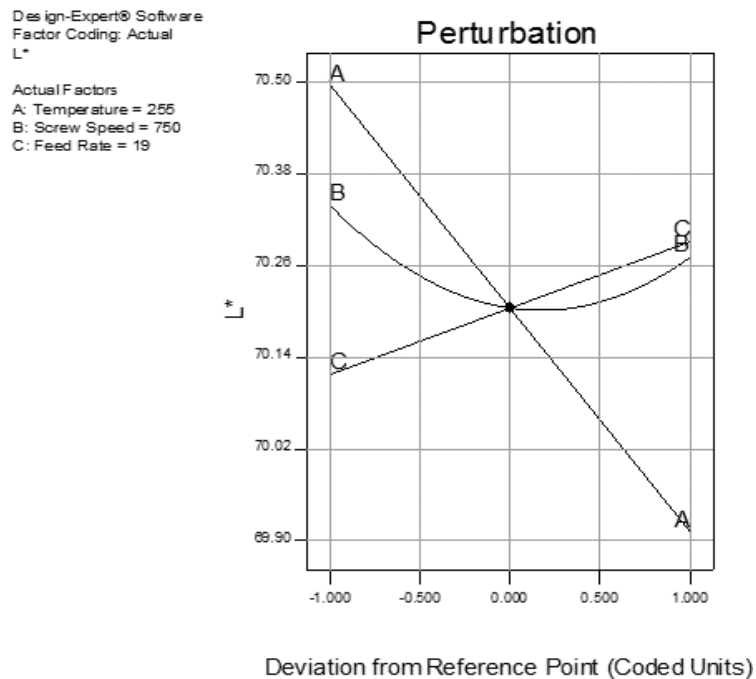


Fig. 3.5: Perturbation Plot for  $L^*$

#### D. Two Factor Interactions and Contours Graphs

Significant two factor interactions (2FI) between B and C affecting  $L^*$ ,  $a^*$  and  $b^*$ , and between A and C affecting  $a^*$  are captured by ANOVA based on their “p” values as reflected in Table 3.7. For brevity, only  $L^*$  plot of 2FI is shown in Fig. 3.6 using both the ANOVA estimate (left graph) of noise - standard deviation of 0.07, and past experimental estimate (right graph) of noise i.e. 0.28. It is evident from  $L^*$  interaction graph that positive effect on  $L^*$  caused by increase in feed rate at maximum screw speed, is reversed when speed level is set at minimum. A similar behaviour is reflected from interaction graphs of  $a^*$  and  $b^*$ . This effect can be attributed to the fact that increase in feed rate, holding screw speed at minimum level and temperature at its mid-level, would have caused poor dispersion of pigments resulting into lower response values. However, overlapping of least significant distance (LSD) error bars in right graph of Fig. 3.6 rejects the significance of these interactions.

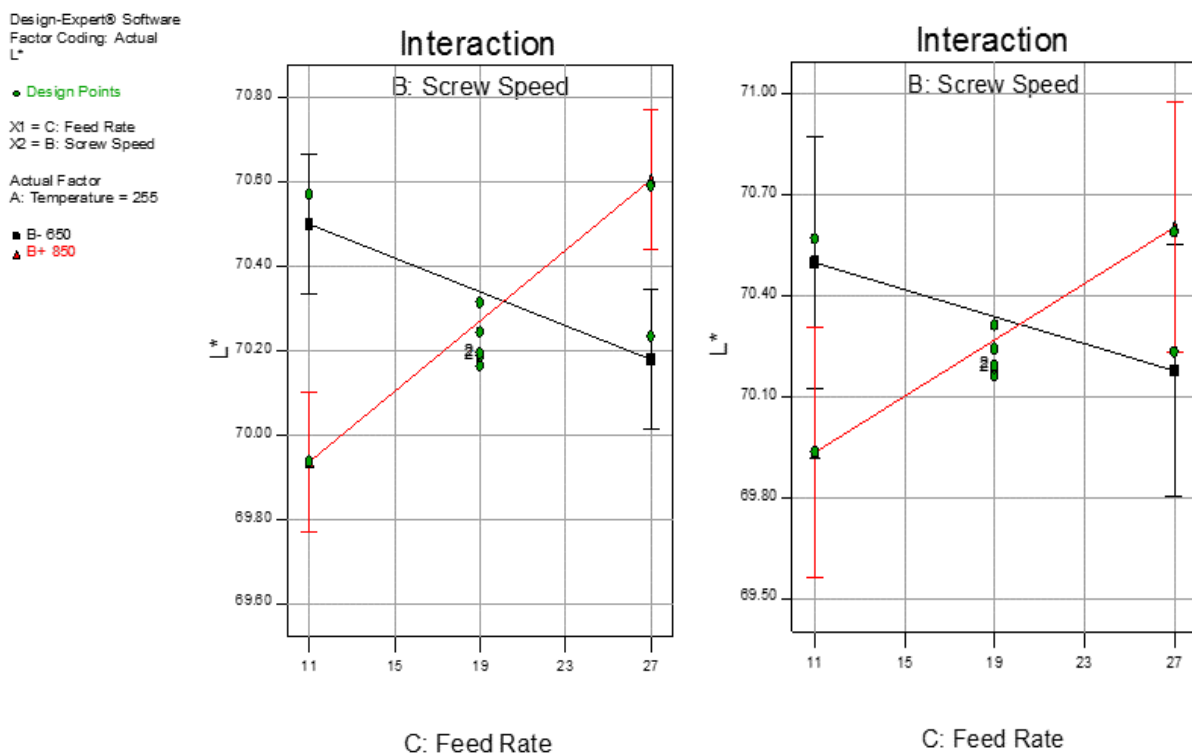


Fig. 3.6: 2FI graphs affecting  $L^*$  using ANOVA noise estimate (left), experimental error (right)

Contour plot is another representation of the effect of process variables on output response. For brevity, only  $L^*$  contour plot is shown below in Fig. 3.7 reflecting effect of temperature and feed rate on output response while holding screw speed at its midpoint. It is

evident from L\* graph that increase in temperature has a negative effect on L\*, whereas feed rate imposes a reverse effect on response.

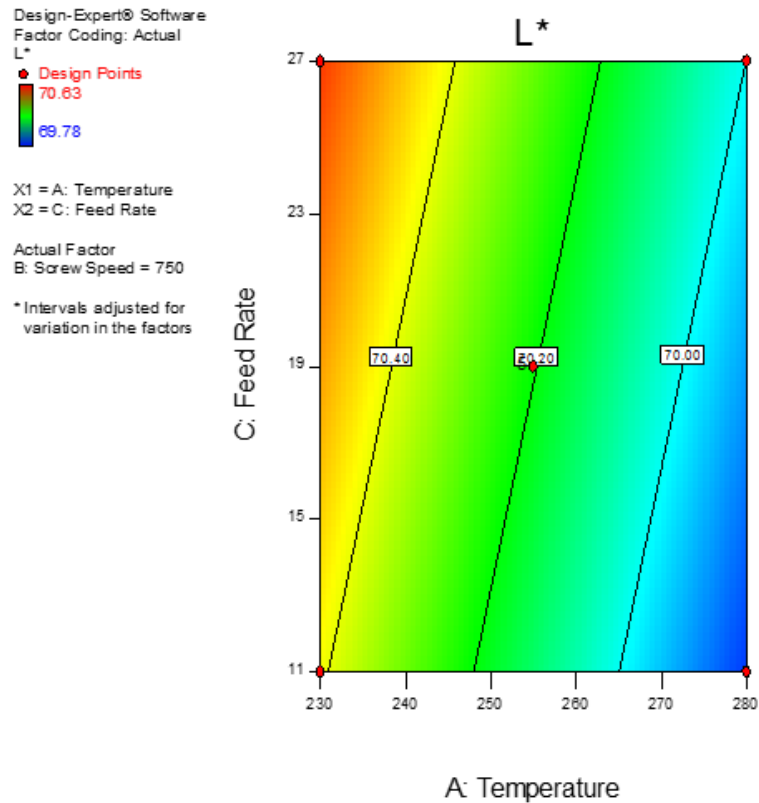


Fig. 3.7: Contour Plot for L\* Slicing along Factor B

#### E. Validity Check of Predictive Model Equations

After a careful design evaluation and analysis, three separate confirmatory DoEs were prepared using point prediction node of Design-Expert® software and executed on same technology line of SABIC IP Cobourg plant. Aim was to carry out a validity check of our predicting model before its use for process optimization. Therefore, all prediction points were carefully chosen to ensure no vertices included in DoEs. Experimental data obtained from execution of confirmatory DoEs has been compared with predicted response values and for brevity, results of first confirmatory test are shown below in tables 3.9 and 3.10. Experimental values reported in Table 3.9 for runs 1, 2, 3, 5, 6, 10 and 13 represent average data of the three confirmatory tests.

Table 3.9. Predicted Mean vs. Experimental Colour Data - Confirmatory Test

Run No.	Process Parameter			Predicted Response									Experimental Response		
	Temp (°C)	Speed (rpm)	Feed (kg/hr)	L*			a*			b*			L*	a*	b*
				Mean	PI low	PI high	Mean	PI Low	PI high	Mean	PI low	PI high			
1	230	750	11	70.41	69.63	71.19	3.71	3.08	4.35	18.03	17.45	18.6	69.93	3.70	17.98
2	230	750	27	70.58	69.81	71.36	3.81	3.24	4.37	18.07	17.49	18.64	70.05	3.78	17.95
3	230	850	11	70.23	69.35	71.11	3.43	2.73	4.13	17.8	17.16	18.45	69.80	3.82	17.88
4	250	763	11	70.14	69.4	70.89	3.83	3.42	4.23	18.04	17.52	18.56	69.60	3.69	18.04
5	255	650	11	70.5	69.65	71.35	3.77	3.29	4.26	18.26	17.65	18.87	70.17	3.68	18.20
6	255	650	27	70.18	69.33	71.03	3.58	3.05	4.11	17.9	17.29	18.51	70.06	3.58	17.98
7	255	750	25	70.27	69.54	71	3.9	3.46	4.34	18.13	17.62	18.64	69.85	3.52	18.02
8	255	750	25	70.27	69.54	71	3.9	3.46	4.34	18.13	17.62	18.64	69.75	3.57	18.19
9	255	750	25	70.27	69.54	71	3.9	3.46	4.34	18.13	17.62	18.64	69.77	3.56	17.86
10	255	850	11	69.94	69.08	70.79	3.54	3.06	4.03	17.82	17.21	18.43	69.69	3.47	17.78
11	269	745	18.6	70.04	69.32	70.76	3.82	3.23	4.41	18.04	17.45	18.64	69.49	3.46	17.60
12	274	728	22.4	70.01	69.28	70.74	3.66	2.96	4.37	17.93	17.28	18.58	69.46	3.65	17.66
13	280	750	27	70	69.22	70.78	3.37	2.38	4.35	17.73	16.94	18.51	69.76	3.50	17.69

Note: PI – 95% Prediction Interval

Table 3.10. Predicted Mean vs. Experimental Colour Data – Delta Values

Run No.	Process Parameter			Experimental - Predicted			
	Temp (°C)	Speed (rpm)	Feed (kg/hr)	$\Delta L^*$	$\Delta a^*$	$\Delta b^*$	$\Delta E^*$
1	230	750	11.00	-0.48	-0.01	-0.05	0.49
2	230	750	27.00	-0.53	-0.03	-0.12	0.54
3	230	850	11.00	-0.43	0.39	0.08	0.59
4	250	763	11.00	-0.54	-0.14	0.00	0.56
5	255	650	11.00	-0.34	-0.09	-0.07	0.35
6	255	650	27.00	-0.12	0.00	0.08	0.14
7	255	750	25	-0.42	-0.38	-0.11	0.58
8	255	750	25	-0.52	-0.33	0.06	0.62
9	255	750	25	-0.50	-0.34	-0.27	0.66
10	255	850	11.00	-0.25	-0.07	-0.04	0.26
11	269	745	18.60	-0.55	-0.36	-0.44	0.79
12	274	728	22.40	-0.55	-0.01	-0.27	0.61
13	280	750	27.00	-0.24	0.13	-0.04	0.28

A comparison between experimental and predicted values for confirmatory DoEs is further illustrated in Fig.s 3.8 to 3.10 and discussed hereunder for  $L^*$ ,  $a^*$  and  $b^*$  respectively. It is evident from these Fig.s that observed response values of confirmatory test runs are in good agreement with PIs of predicted means, thereby verify the fitness of our predicting model.  $L^*$  values of run 1 & 2 however, were slightly exceeding PI lower limit in the first confirmatory test so the runs were repeated in second confirmatory test and average values are shown in Table 3.10. This slight variation can be attributed to the possibility of having a bit pronounced experimental error at lower end of the temperature range. Confirmatory tests further reveal that the gap between experimental and predicted values, in particular for  $a^*$  and  $b^*$ , becomes narrowed for runs representing mid-range temperatures along with odd combination of speed (B) and feed rate (C) e.g. runs 6 and 10 in Table 3.10. This behaviour can be associated to the fact that mid-range temperatures and odd combinations of speed and feed rate represent the plateau with minimum POE as explained above under POE graphs. However, having experimental and predicted output response values close to each other does not guarantee they will hit the target response values as well. This clearly indicates the need to adopt for a trade-off while optimizing a process having multi-objective output responses.



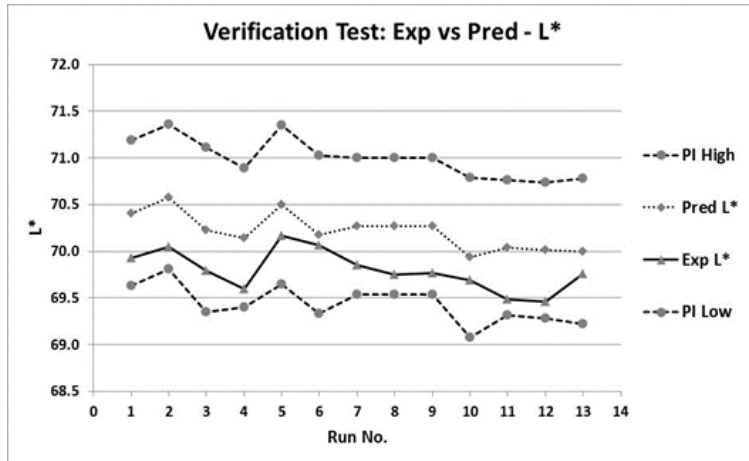


Fig. 3.8: L\* Values of Confirmatory Test

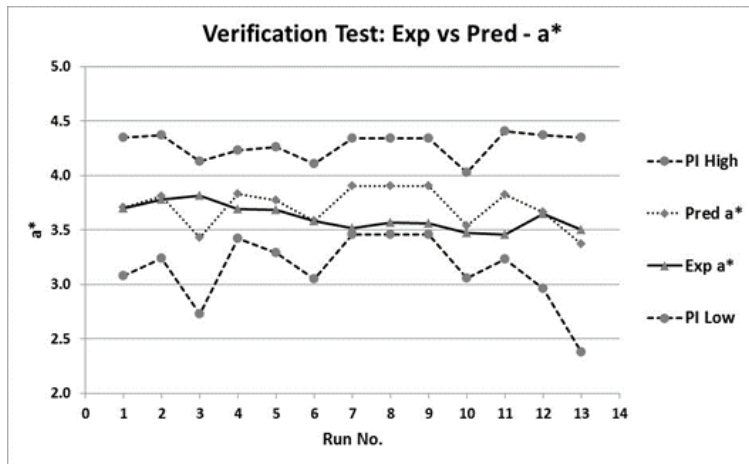


Fig. 3.9: a\* Values of Confirmatory Test

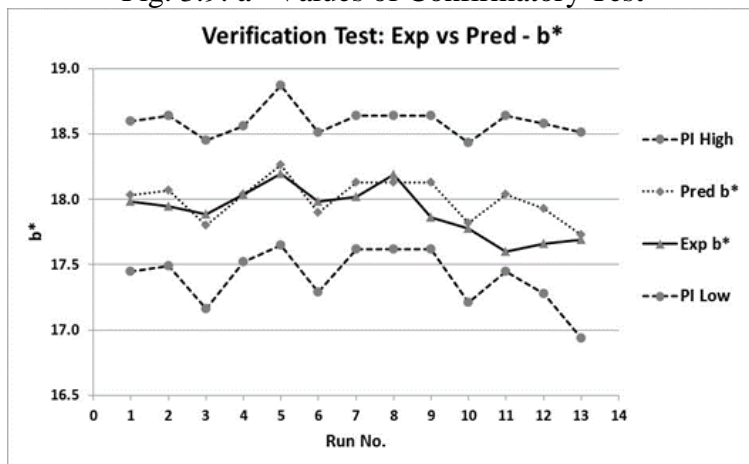


Fig. 3.10: b\* Values of Confirmatory Test

## F. Process Optimization

Once the predicting model is verified through confirmatory tests, process optimization can be confidently exercised, which allows to determine an optimal set of input process variables that could satisfy constraints imposed on multiple response output and associated errors in design. Both numerical and graphical optimization techniques are successfully employed in present study. Pasted below in Table 3.11 are constraints / criterion set out for process optimization. Five solutions with overall desirability level ranging from 0.875 to 0.809 are reported in Table 3.12. Overall desirability level reflects the extent to which output response could be achieved if optimal solution is implemented. As explained earlier, when objective is to reach multiple output targets and simultaneously reduce POE to ensure robustness of design, a trade-off is inevitable. All five solutions offer minimum overall colour deviation in terms of delta values respecting thresholds ( $\Delta L^* \leq 0.6$ ,  $\Delta a^* \leq 0.6$ ,  $\Delta b^* \leq 0.6$  and  $\Delta E^* \leq 1$ ) set by customer for the plastic grade studied and a robust design restricting the variation band of delta values to a narrow and a stable window. Bar graph, shown in Fig. 3.11, displays desirability levels achieved for individual factors as well as overall objective. It can be noticed that a\* desirability level is the lowest one compared with other factors, this can be improved by adjusting its weight and importance factors equal to those set for POEs, but at the cost of high POE. This situation is the one often come across by experimenters while dealing with multi-objective output response, where intelligent trade-offs help decide best possible solution [30].

Table 3.11. Criterion Set for Process Optimization

Name	Goal	Lower Limit	Upper Limit	Lower Weight	Upper Weight	Importance
A:Temperature	is in range	230	280	-	-	-
B:Screw Speed	is in range	650	850	-	-	-
C:Feed Rate	is in range	11	27	-	-	-
L*	is target = 70.04	69.78	70.63	1	1	3
POE(L*)	minimize	0.30	0.30	1	10	5
a*	is target = 3.41	3.37	4.04	1	1	3
POE(a*)	minimize	0.16	0.32	1	10	5
b*	is target = 18.09	17.73	18.48	1	1	3
POE(b*)	minimize	0.21	0.29	1	10	5

Table 3.12. List of Optimal Solutions for Input Factors

Factor A	Factor B	Factor C	L*	POE (L*)	a*	POE (a*)	b*	POE (b*)	Desirability	$\Delta L^*$	$\Delta a^*$	$\Delta b^*$	$\Delta E^*$
253	850	14	70.07	0.3	3.68	0.16	17.98	0.21	0.875	-0.03	-0.27	0.11	0.29
247	850	14	70.14	0.3	3.69	0.15	18	0.2	0.866	-0.1	-0.28	0.09	0.31
254	833	15	70.11	0.3	3.78	0.16	18.05	0.21	0.862	-0.07	-0.37	0.04	0.38
251	652	26	70.25	0.3	3.67	0.16	17.97	0.2	0.846	-0.21	-0.26	0.12	0.36
240	650	26	70.37	0.3	3.67	0.15	17.98	0.2	0.809	-0.33	-0.26	0.11	0.43

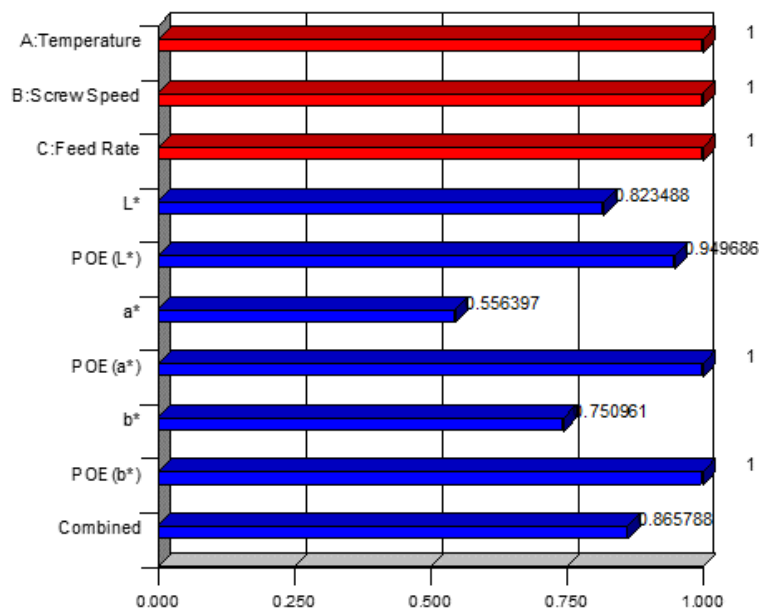


Fig. 3.11: Bar Graph Displaying Individual and Combined Desirability Level of Variables and POEs

Numerical optimization if followed by graphical analysis of set criterion provides powerful insights of optimization process [62]. This is done by overlaying contour graphs of all variables involved. Solutions suggested by numerical optimization should be located in sweet spot (bright yellow) as shown in Fig. 3.12 flagged for solution reported in second row of Table 3.12, which simultaneously satisfies all constraints. It may be noticed that sweet spot does not encompass entire experimental test range rather it reflects quite a narrow process window limiting the navigators to a much smaller region of interest truncated at extreme ends of factors. Dark gold region located in-between grey and sweet spot is the one, where response estimates meet all the required criteria, but part of an interval estimate does not. This is how graphical optimization helps numerical optimization to obtain a desired set of process conditions that truly satisfies all constraints.

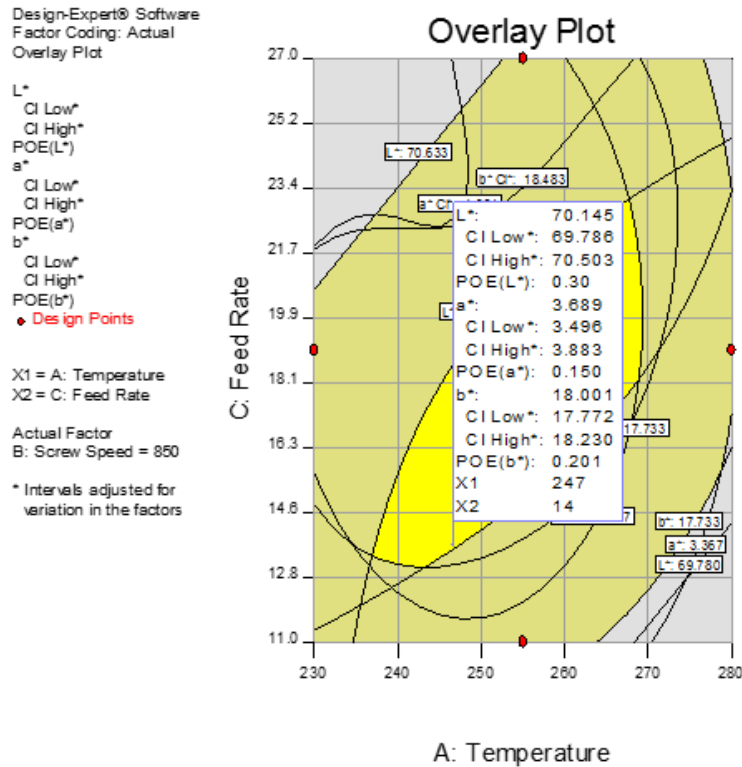


Fig. 3.12: Graphical Optimization and Sweet Spot Flagged for a desired Solution

Shown below in Fig. 3.13 is a 3D graph of combined desirability respecting solution reported second in Table 3.12. The graph displays a process window large enough for navigating process conditions that could satisfy the optimization criterion. Flagged point with a desirability level of 0.866 predicts output response values:  $L^*=70.15$ ,  $a^*=3.69$  and  $b^*=18.00$ , at 95% confidence intervals (CIs) and minimum level of POE for an optimal set of process variables i.e. temperature =247 °C, screw speed = 850 rpm and feed rate = 14 kg/hr. Contour graph shown in Fig. 3.14 reflects same optimal solution with a desirability level of 0.866. A verification test for a significance level  $\alpha=0.05$  and number of trials  $n=200$  was carried out using confirmation node of the software. It has verified the fitness of optimal solutions by showing up response mean values within 95% CIs.

Design-Expert® Software  
 Factor Coding: Actual  
 Desirability  
 ● Design points below predicted value

X1 = A: Temperature  
 X2 = C: Feed Rate

Actual Factor  
 B: Screw Speed = 850

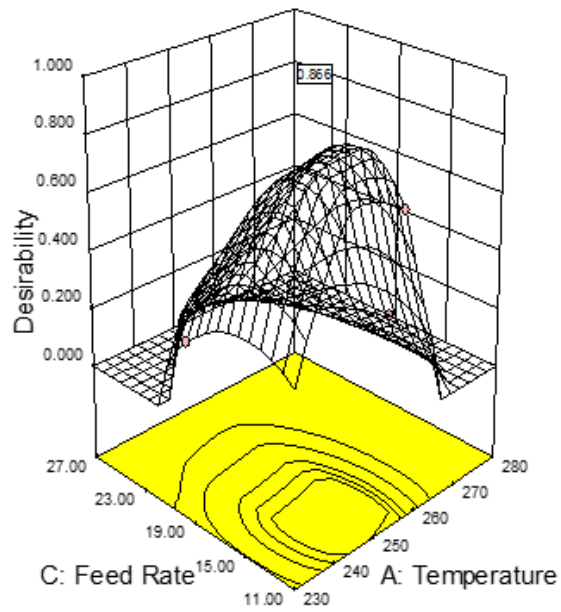


Fig. 3.13: 3D Surface Graph Flagged with Optimal Desirability

Design-Expert® Software  
 Factor Coding: Actual  
 Desirability  
 ● Design Points  
 1.000  
 0.000

X1 = A: Temperature  
 X2 = C: Feed Rate

Actual Factor  
 B: Screw Speed = 850

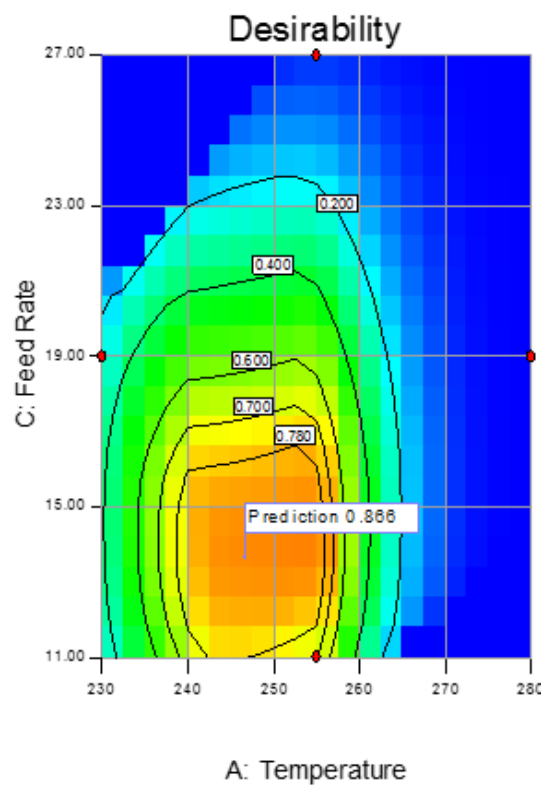


Fig. 3.14: 2D Contour Graph Flagged with Optimal Desirability

### 3.3.2 High Chroma Opaque PC Grade (G2) – Analysis and Optimization Results

#### A. ANOVA and Design Evaluation

ANOVA for the three output responses i.e.  $L^*$ ,  $a^*$  and  $b^*$ , was executed choosing quadratic model as suggested by fit summary (not shown here). Backward technique was employed to eliminate trivial model terms and to obtain only significant models / model terms having  $p$ -value  $< 0.05$ . Design evaluation and diagnostic checks carried out and all statistics were found well within stipulated threshold validating fitness of the models, for instance, lack of fit of the three models was found not-significant at a  $p$ -value = 0.208 and degree of freedom = 5. All residuals behaved well, except few DFFITS (difference of fits) – a statistics helpful in detecting influential runs, which can be ignored being overly sensitive to smaller designs like BBD [30]. The ANOVA results and predicting model equations obtained for the three output responses are summarized below in Table 3.13 and Table 3.14 respectively.

Table 3.13. ANOVA results for  $L^*$ ,  $a^*$  and  $b^*$

Output Variable	Significant Factor	p-value (<0.05)	Adjusted R-Squared	Predicted R-Squared	Adequate Precision
$L^*$	Model	< 0.0003	0.8530	0.5448	14.149
	A	< 0.0086			
	C	< 0.0001			
	BC	< 0.0499			
	$A^2$	0.0223			
	$B^2$	0.0093			
	$C^2$	0.0028			
$a^*$	Model	0.0001	0.7756	0.6446	11.816
	A	0.0110			
	C	0.0001			
	$A^2$	0.0182			
	$C^2$	0.0094			
$b^*$	Model	0.0004	0.7277	0.5476	10.320
	A	0.0140			
	C	0.0003			
	$A^2$	0.0868			
	$C^2$	0.0113			

Legend: A – Temperature, B – Screw speed, C – Feed rate

Table 3.14. Final equations in terms of actual factors

$\mathbf{L^*} = 36.73988 + 0.080125 * \text{Temperature} - 0.013020 * \text{Speed} + 0.038432 * \text{Feed rate} + 0.000066 * \text{Speed} * \text{Feed rate} - 0.000156 * \text{Temperature}^2 + 0.0000075 * \text{Speed}^2 - 0.001444 * \text{Feed rate}^2$
$\mathbf{a^*} = 7.64475 + 0.26662 * \text{Temperature} + 0.22652 * \text{Feed rate} - 0.00052 * \text{Temperature}^2 - 0.00365 * \text{Feed rate}^2$
$\mathbf{b^*} = 4.40524 + 0.13285 * \text{Temperature} + 0.15959 * \text{Feed rate} - 0.00026 * \text{Temperature}^2 - 0.00263 * \text{Feed rate}^2$

A check for 80% fraction of design space was carried out to determine precision of the model expressed in terms of a parameter “d” representing noise in the system. In this regard, we employed experimental error in output response values i.e. 0.28 for L\*, 0.15 for a\* and 0.2 for b\*. For error type “Pred” a value of d=0.79 revealed the design space was capable enough to predict output responses with prediction interval (PI) ±0.79.

#### B. Evaluation of POE and Design Robustness

To ensure the selected RSM design is robust, propagation of error (POE) technique explained earlier, was employed. The fluctuations in controllable process variables observed during experimentation, and incorporated in RSM design included: 10°C in temperature, approx. 1rpm in screw speed and about 0.01kg/hr in feed rate. Response polynomials that were used to calculate POEs, are expressed as predictive model equations in Table 3.14.

A curvilinear relationship between input and output factors that is required for usefulness of POE technique, can be identified by plotting a perturbation graph for response surface. The perturbation graphs for L\*, a\* and b\* reveal that response surface L\* is curvilinear in the direction of A, B, and C, whereas a\* and b\* are in A and C directions. Perturbation graphs also help to understand the sensitivity of output response to any changes in significant input factors at a particular point in design space. For brevity, only L\* perturbation graph is shown in Fig. 3.15, which indicates that a search for plateaus would be a worthwhile exercise. Therefore calculation for POE were performed using Design Expert® software and the POE graphs obtained for L\*, a\* and b\* in the direction of temperature, are presented in Figs 3.16 to 3.18 respectively. It is evident from these POE graphs that a temperature range from 250 °C to 265 °C reflects the plateaus, which is a bit higher compared with one identified in our previous investigation of PC grade G1. This can be associated with lower MFI of the PC resin used in present study. MFI is an inverse measure of the polymer melt viscosity and its average molecular mass.

Design-Expert® Software  
 Factor Coding: Actual  
 L\*

Actual Factors  
 A: Temp = 270  
 B: Speed = 750  
 C: Feed = 23

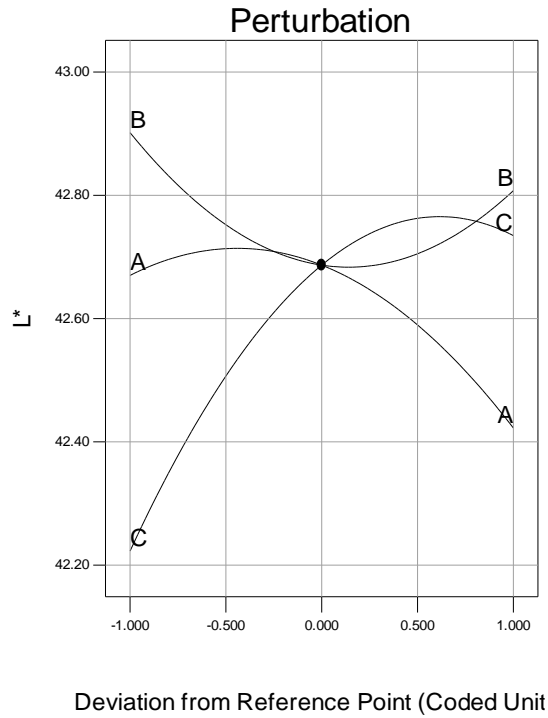


Fig. 3.15: Perturbation graph for  $L^*$

Design-Expert® Software  
 Factor Coding: Actual  
 POE( $L^*$ )

● Design Points

X1 = A: Temp

Actual Factors  
 B: Speed = 750  
 C: Feed = 23

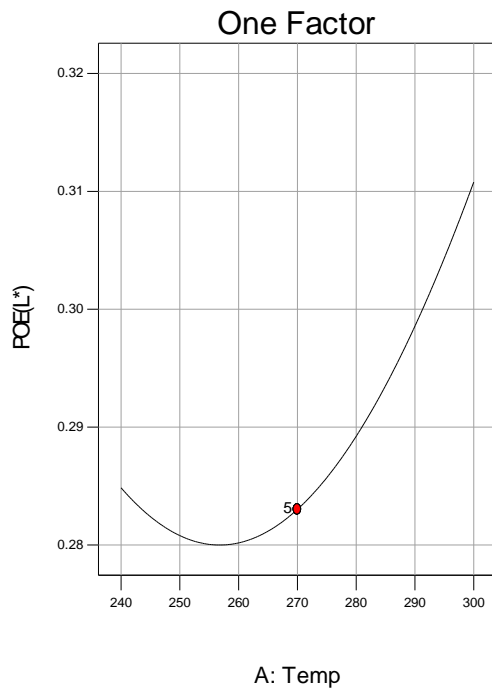


Fig. 3.16: POE ( $L^*$ ) Plot with Factor B and C at Mid-Point

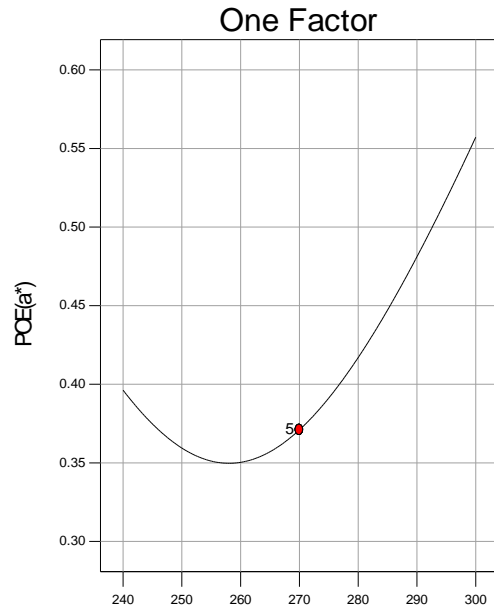


Design-Expert® Software  
Factor Coding: Actual  
POE(a\*)

● Design Points

X1 = A: Temp

Actual Factors  
B: Speed = 750  
C: Feed = 23



A: Temp

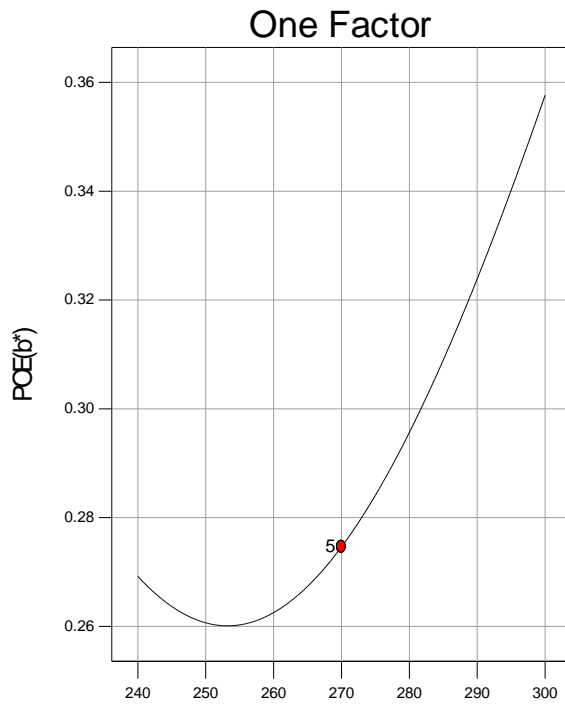
Fig. 3.17: POE (a\*) Plot with Factor B and C at Mid-Point

Design-Expert® Software  
Factor Coding: Actual  
POE(b\*)

● Design Points

X1 = A: Temp

Actual Factors  
B: Speed = 750  
C: Feed = 23



A: Temp

Fig. 3.18: POE (b\*) Plot with Factor B and C at Mid-Point

### C. Two Factor Interactions and Contours Graphs

The only significant two factor interaction (2FI) captured was “BC” i.e. the interaction between screw speed and feed rate, affecting  $L^*$ . The 2FI is shown in Fig. 3.19 for both, with ANOVA estimate of the noise i.e. 0.1 (left) and with experimental error i.e. 0.28 (right). The two graphs reveal that  $L^*$  value improves by increasing feed rate level for a fixed screw speed level until the feed rate reaches a level called critical point (highlighted blue), beyond which the effect of increasing feed rate turns into negative for minimum speed level. This can be attributed to inadequate pigments dispersion in polymeric matrix resulting into a lower  $L^*$  value. Overlapping of error bars in Fig. 3.19 (right) however, invalidates the significance of 2FI, the error bars represent least significant distance (LSD).

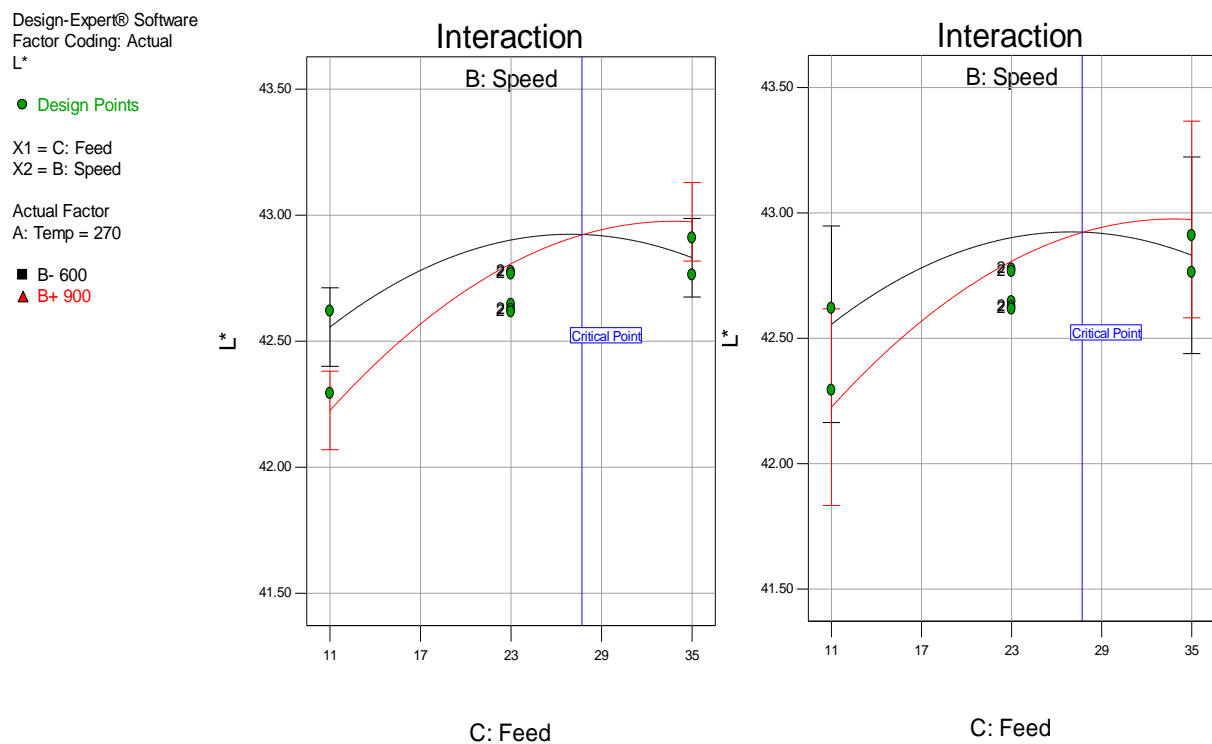


Fig. 3.19: 2FI graphs affecting  $L^*$  using ANOVA noise estimate (left), experimental error (right)

Contour plot shown in Fig. 3.20 is a two-dimensional representation of the response  $L^*$  across two input variables i.e. temperature and feed rate, and sliced along direction of 3<sup>rd</sup> variable i.e. screw speed. The contour graph sliced at a speed of 750rpm, clearly indicates that  $L^*$  responds negatively to an increase in temperature and a decrease in feed rate.

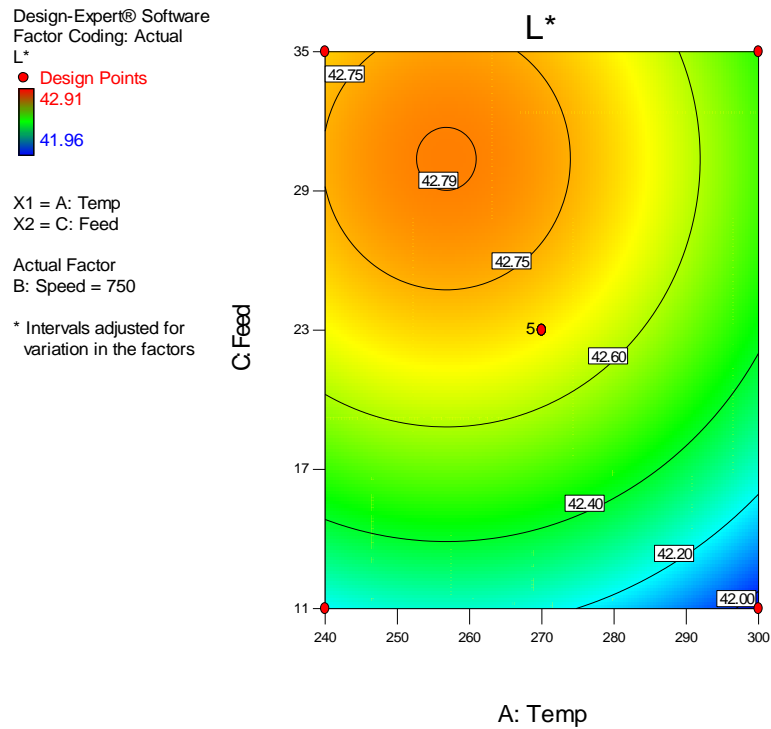


Fig. 3.20: Contour Plot for L\* Slicing along Factor B

#### D. Validity Check of Predictive Model Equations

After a careful evaluation of the design and ANOVA discussed in the preceding sections, a confirmatory DoE prepared using predicting model equations given in Table 3.14, was executed on the same technology line. Aim was to carry out a validity check of our predicting model before its use for process optimization. Therefore, all prediction points were carefully chosen to ensure no vertices included in DoE. Experimental data obtained is compared with predicted mean of response values and the difference is presented in Table 3.15 in terms of delta values i.e.  $\Delta L^*$ ,  $\Delta a^*$  and  $\Delta b^*$ . All delta values were found well within PI of  $\pm 0.79$  except  $\Delta a^*$  for run 1, which verified our predicting model.

Table 3.15: Predicted Mean vs. Experimental Colour Data – Confirmatory Test

Run No.	Process Parameter			Experimental – Predicted Mean		
	Temp (°C)	Speed (rpm)	Feed (kg/hr)	$\Delta L^*$	$\Delta a^*$	$\Delta b^*$
1	240	750	11	0.54	0.89	0.65
2	270	600	11	0.06	0.53	0.50
3	270	750	35	0.37	0.44	0.44
4	270	900	23	0.07	0.18	0.22
5	300	750	23	0.37	0.70	0.48

Confirmatory test further revealed that the delta values, in particular  $\Delta L^*$  of run 2 and run 4 in Table 3.15, were at their minimum, which indicated the processing conditions employed were close to the plateau region identified by POE analysis. However, having minimum delta values do not guarantee the experimental colour data would hit the target response values as well. Which is why a trade-off is adopted while optimizing a process for multi-objective output response.

#### E. Process Optimization

After having the design predictive power verified through confirmation DoE, numerical optimization of the extrusion process was executed with the aim to explore various combinations of input variables that would satisfy not only the constraints imposed on desirable responses but also the associated design precision. The numerical optimization was complemented by graphical optimization, ensuring that optimal solutions satisfied all the constraints. Numerical optimization if followed by graphical analysis of set criterion provides powerful insights of optimization process [62].

Optimization criterion used is shown in Table 3.16 and eight solutions are reported in Table 3.17 with overall desirability level from 0.958 to 0.784. The overall desirability level is a measure of the extent the output response variables can be optimized if an optimal set of process conditions is executed. As explained earlier, a trade-off is inevitable when objective is to simultaneously optimize multiple response variables and reduce POE to ensure design robustness. The eight solutions reported in Table 3.17, reflect that the colour deviations expressed in delta values, are well within permissible limits, however,  $\Delta b^*$  delta values representing first five solutions i.e.  $\leq 0.6$ . Same has reflected in the bar graph, shown in Fig. 3.21 for the 4<sup>th</sup> optimal solution, where the  $b^*$  desirability level is lowest compared with other response variables. The  $b^*$  desirability level can be improved by adjusting its weight and/or importance factors, but at the cost of high POE. This situation is often confronted by experimenters and demands intelligent trade-offs for best possible solution [30].

Table 3.16. Criterion Set for Process Optimization

Name	Goal	Lower Limit	Upper Limit	Lower Weight	Upper Weight	Importance
A:Temperature	is in range	240	300	-	-	-
B:Screw Speed	is in range	600	900	-	-	-
C:Feed Rate	is in range	11	35	-	-	-
L*	maximize	41.96	42.91	1	1	3
POE(L*)	minimize	0.11	0.17	1	1	5
a*	is target = 44.89	42.83	45.55	1	1	3
POE(a*)	minimize	0.37	0.56	1	1	5
b*	maximize	21.82	23.65	1	1	3
POE(b*)	minimize	0.27	0.36	1	1	5

Table 3.17. List of Optimal Solutions for Input Factors

Factor A	Factor B	Factor C	L*	POE (L*)	a*	POE (a*)	b*	POE (b*)	Desirability	$\Delta L^*$	$\Delta a^*$	$\Delta b^*$	$\Delta E^*$
246	600	18	42.83	0.11	44.89	0.37	23.25	0.26	0.958	-0.43	0	-0.84	0.94
249	600	18	42.82	0.11	44.89	0.36	23.24	0.26	0.957	-0.44	0	-0.85	0.96
252	600	18	42.82	0.11	44.89	0.35	23.23	0.26	0.956	-0.44	0	-0.86	0.97
258	600	17	42.82	0.10	44.89	0.35	23.21	0.26	0.954	-0.44	0	-0.88	0.98
246	900	18	42.64	0.11	44.89	0.37	23.25	0.26	0.929	-0.62	0	-0.84	1.04
241	897	35	42.96	0.12	45.35	0.39	23.55	0.27	0.825	-0.3	0.46	-0.54	0.77
270	879	35	42.92	0.11	45.42	0.37	23.52	0.27	0.793	-0.34	0.53	-0.57	0.85
270	600	35	42.83	0.11	45.42	0.37	23.52	0.27	0.784	-0.43	0.53	-0.57	0.89

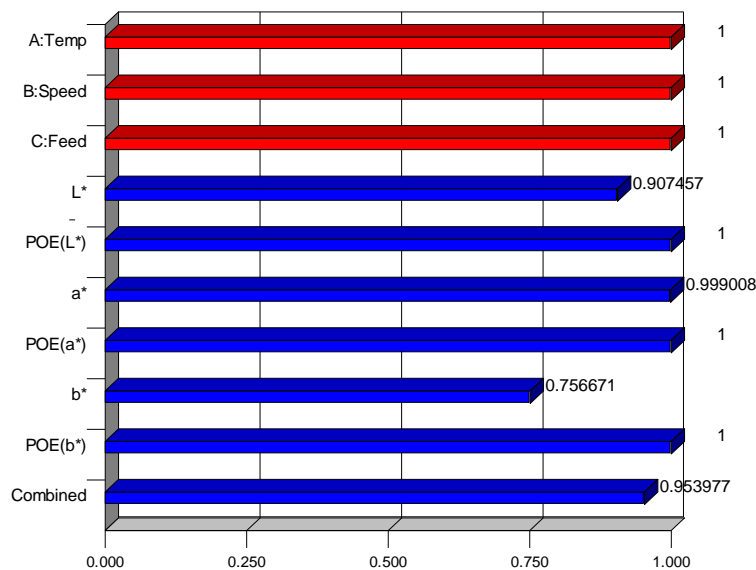


Fig. 3.21: Desirability Levels for 4<sup>th</sup> Optimal Solution – Table 3.17

An overlay plot is presented in Fig. 3.22 reflecting 4<sup>th</sup> optimal solution flagged in the sweet (yellow) spot. This yellow spot is the outcome of graphical optimization and verifies that the solution located inside, satisfies all constraints set out for optimization and robustness of the process. It may be noticed that sweet spot does not encompass the entire experimental test range rather it reflects a narrow process window limiting the navigators to a smaller region of interest. Dark gold region located in-between grey (a small circle) and sweet spot is the one, where response estimates meet all criteria except a part of an interval estimate. This is how graphical optimization helps numerical optimization to reach a solution that satisfies all constraints.

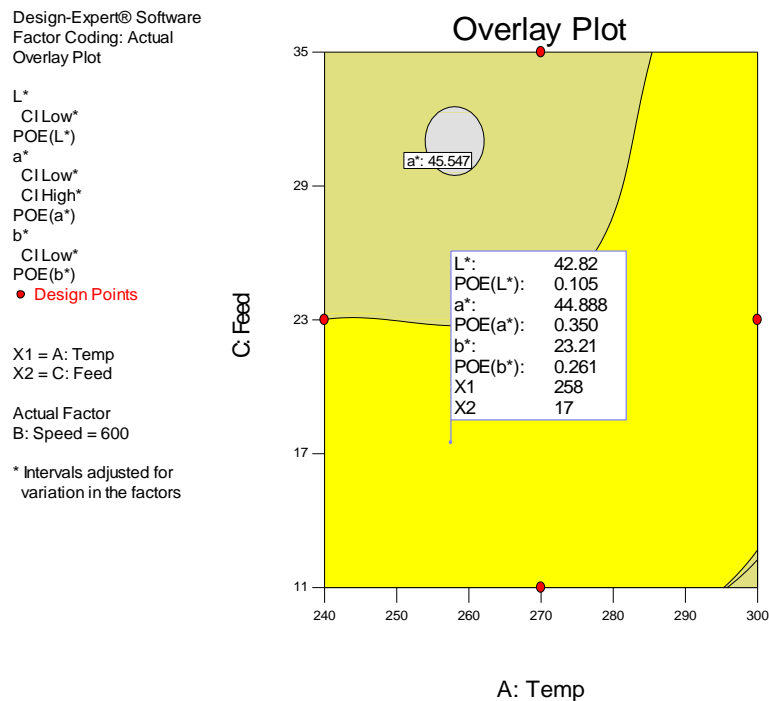


Fig. 3.22: Graphical Optimization and Sweet Spot Flagged for Optimal Solution – Table 3.17

A verification test was carried out with the help of confirmation node available in Design Expert® software. A significance level  $\alpha=0.05$  and number of trials  $n=200$  were used for the test, which verified the fitness of eight optimal solutions keeping response values within 95% CIs. Experimental verification of some optimal solutions listed in Table 3.17 was also conducted and the experimental response values were found well within 95% confidence intervals. For brevity verification results for L\* only are shown in Fig. 3.23.

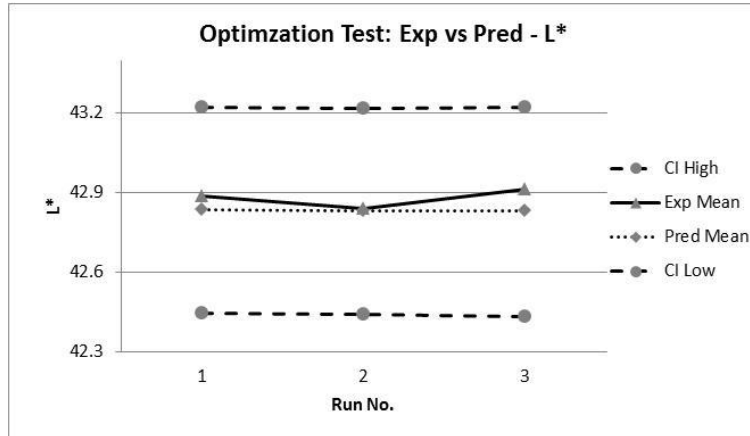


Fig. 3.23: L\* Values of Verification Test

### 3.3.3 High Luminous Opaque PC Grade (G3) – Analysis and Optimization Results

#### A. ANOVA and Design Evaluation

Quadratic model as suggested by fit summary showing no aliases terms was employed. ANOVA for all three output responses i.e. L\*, a\* and b\* was executed and significant quadratic models with p-value < 0.05 were obtained. All trivial model terms with p-value > 0.10 were eliminated from each significant model employing backward technique. To ensure validity of model, required design evaluation and diagnostic checks were carried out and all statistics found well within threshold limits. For instance, lack of fit for the three models was insignificant with degrees of freedom (df) greater than minimum limit of 3, difference between adjusted R-squared and predicted R-squared values was below 0.2, adequate precision – a measure of signal to noise ratio, was well above its threshold of 4, standard error data values associated with coefficients respecting linear, cross product and quadratic terms, were found exactly same within their specific type, variance inflation factors (VIF) of all coefficients were found at a Fig. of 1 - an ideal value that ensures design orthogonality, and all residuals behaved well, except few DFFITS (difference of fits – a statistics helpful in detecting influential runs) values, one for L\* and two for a\*, found exceeding the threshold of  $\pm 2$ , this statistics however for smaller designs like BBD is overly sensitive and can be ignored [16]. A summary of some of these statistics and predicting model equations are presented in Table 3.18 and Table 3.19 respectively for each response.

Table 3.18. ANOVA results for L\*, a\* and b\*

Output Response	Significant Factor	p-value <0.05	Adjusted R-Squared	Predicted R-Squared	Adequate Precision
L*	Model	0.0016	0.6854	0.5689	10.775
	A	0.0163			
	C	0.0007			
	A <sup>2</sup>	0.0164			
	C <sup>2</sup>	0.0666			
a*	Model	0.0013	0.5852	0.4289	6.801
	A	0.0214			
	A <sup>2</sup>	0.0014			
b*	Model	0.0012	0.7517	0.6865	9.741
	A	0.0016			
	B	0.2307			
	C	0.3451			
	BC	0.0307			
	A <sup>2</sup>	0.0017			

Legend: A – temperature, B – screw speed, C – feed rate

Table 3.19. Final equations in terms of actual factors

$L^* = +97.76248 - 0.061734 * A + 0.033287 * C + 1.10053E-004 * A^2 - 4.99339E-004 * C^2$
$a^* = +1.80583 - 0.014375 * A + 2.73148E-005 * A^2$
$b^* = +18.97167 - 0.086577 * A - 1.64119E-003 * B - 0.048111 * C + 6.10946E-005 * B * C + 1.66733E-004 * A^2$

Legend: A – temperature, B – screw speed, C – feed rate

Fraction of design space (FDS) check was also carried out in order to determine if a fraction greater than 80% of design space existed with required precision. To carry out such an evaluation it is recommended to employ experimental error instead of ANOVA estimate of standard deviation, therefore a standard deviation i.e.  $s = 0.28$  for L\*,  $= 0.15$  for a\* and  $= 0.2$  for b\*, determined from past experience of experimentation were used. With  $s=0.28$  a threshold value of  $d = 0.59$  for error type “Diff” indicates that design can detect a minimum change of 0.59 in output response as revealed in FDS graph shown in Fig. 3.24. Similarly for



error type “Pred” a value of  $d=0.85$  reveals that design is capable to predict output response with prediction interval (PI)  $\pm 0.85$  as shown in Fig. 3.25. These threshold values of  $d$  were imperative to evaluate making an intelligent and careful guess of system noise from past experience so the output response can precisely be predicted.

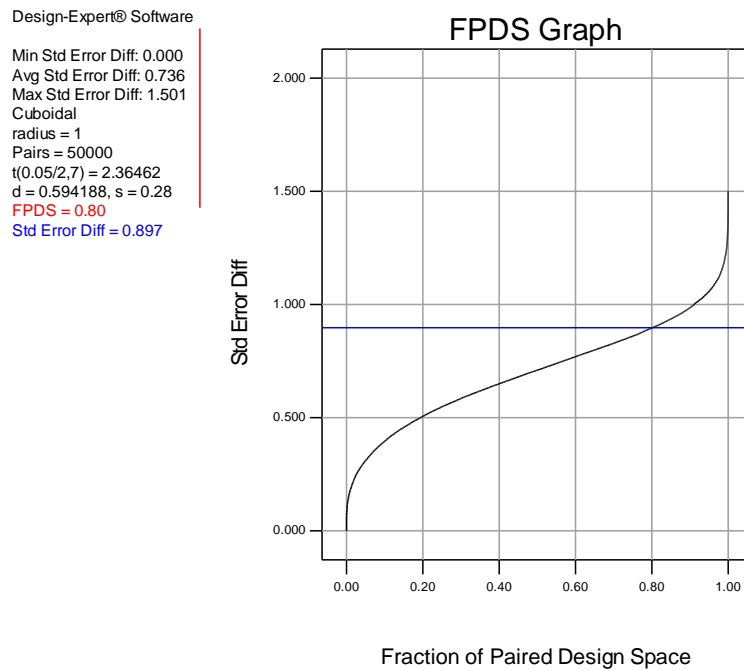


Fig. 3.24: Evaluation of FDS and  $d$  for error type Diff

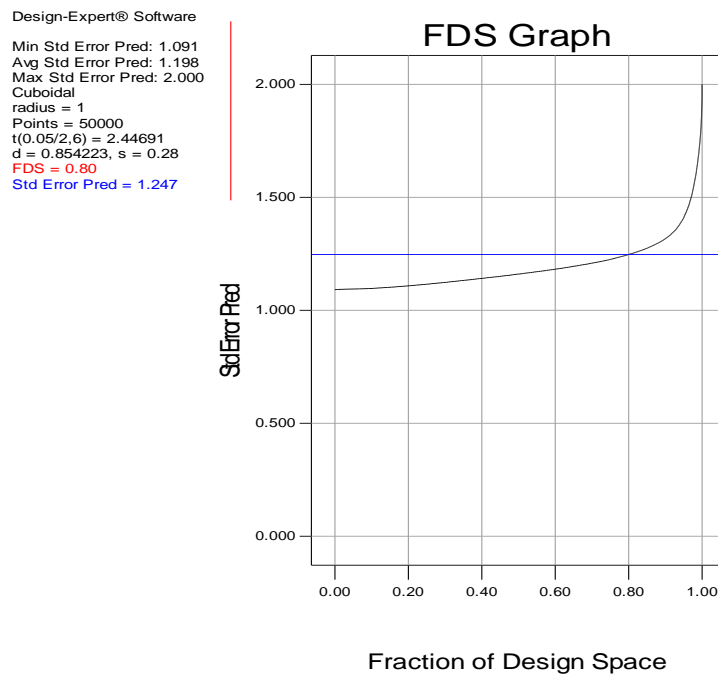


Fig. 3.25: Evaluation of FDS and  $d$  for error type Pred

Therefore, a confirmation DoE was prepared using predictive model equations obtained from ANOVA with Design Expert®. The aim was to verify the design's power to predict output responses. All prediction points were carefully chosen ensuring no vertices included. Experimental data obtained from confirmation DoE is compared with predicted points and results are presented in Table 3.20. It is evident from comparison given in Table 3.20 that experimental response values of each confirmation run are within prediction intervals i.e.  $\pm 0.85$ , which verifies fitness of the design.

Table 3.20: Confirmation DoE results - predicted and experimental colour data

Run No.	Process Parameter			Predicted Data			Experimental Data			Difference ( $\leq 0.85$ ) (Exp - Pred)		
	Temp (°C)	Speed (rpm)	Feed (kg/hr)	L*	a*	b*	L*	a*	b*	dL*	da*	db*
1	240	750	23	89.24	-0.07	6.51	89.72	-0.06	6.68	0.49	0.01	0.17
2	270	600	11	88.73	-0.08	6.64	89.69	-0.05	6.68	0.96	0.03	0.04
3	270	750	35	88.98	-0.08	6.44	89.71	-0.08	6.67	0.73	0.01	0.23
4	270	900	23	88.92	-0.08	6.43	89.66	-0.08	6.69	0.74	0.01	0.26
5	300	750	23	88.79	-0.05	6.72	89.56	-0.04	6.62	0.77	0.01	-0.10

#### B. Perturbation Graphs

Perturbation plots help to understand and compare the effect of all significant factors at a specific point in design space. For sake of brevity only L\* perturbation plot is presented below in Fig. 3.26. It is evident from these plots that output responses are highly sensitive to changes in temperature and feed rate, and the relationship is not linear.

#### C. Two Factor Interactions and Contours Graphs

Significant interaction identified by analysis of variance is also reflected in interaction plot for b\*, shown in Fig. 3.27. The plot reveals a strong interaction that exists between feed rate and screw speed. It is evident from interaction graph for b\* that lower end of screw speed reverses the effect on output response caused by increase in feed rate. This effect can be attributed to the fact that the increase in feed rate while holding screw speed at its lower end and temperature at its midpoint has caused inadequate pigments dispersion.

Design-Expert® Software  
 Factor Coding: Actual  
 L\*

Actual Factors  
 A: Temp = 270  
 \*B: Speed = 750  
 C: Feed = 23

Factors not in Model  
 B

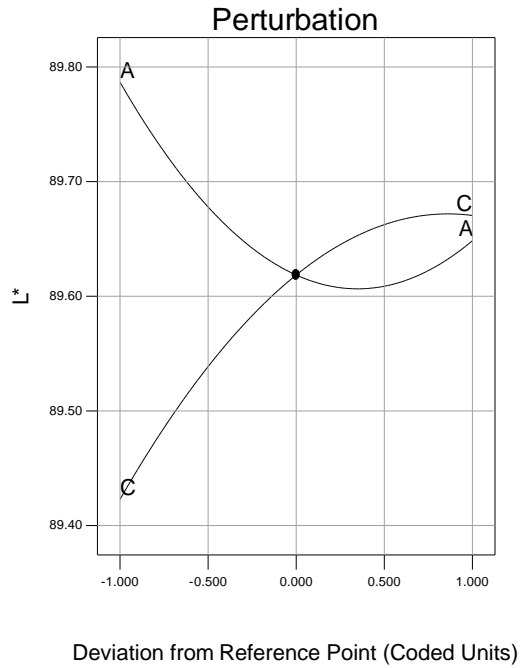


Fig. 3.26: Perturbation Plot for L\*

Design-Expert® Software  
 Factor Coding: Actual  
 b\*

● Design Points

X1 = C: Feed  
 X2 = B: Speed

Actual Factor  
 A: Temp = 270

■ B- 600  
 ▲ B+ 900

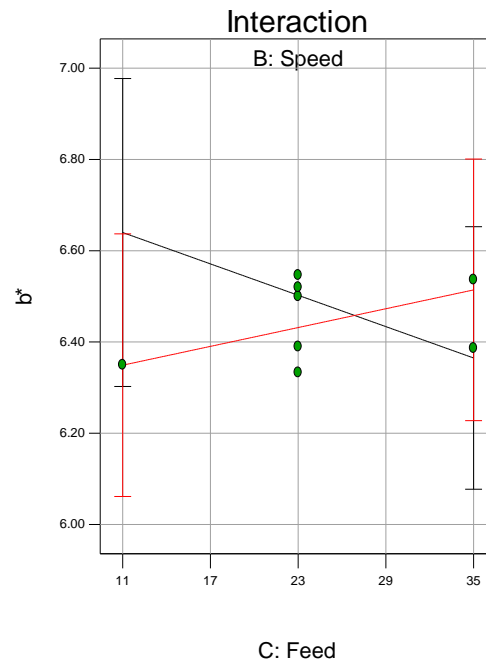


Fig. 3.27: Interaction b/w factors C and B affecting b\*

Contour plot is another representation of the effect of process variables on output response. For brevity only L\* contour plot is shown in Fig. 3.28 reflecting effect of temperature and feed rate on output response while holding screw speed at its midpoint. It is evident from L\* contour graph that increase in temperature has a negative effect on L\* whereas feed rate imposes a reverse effect on the response.

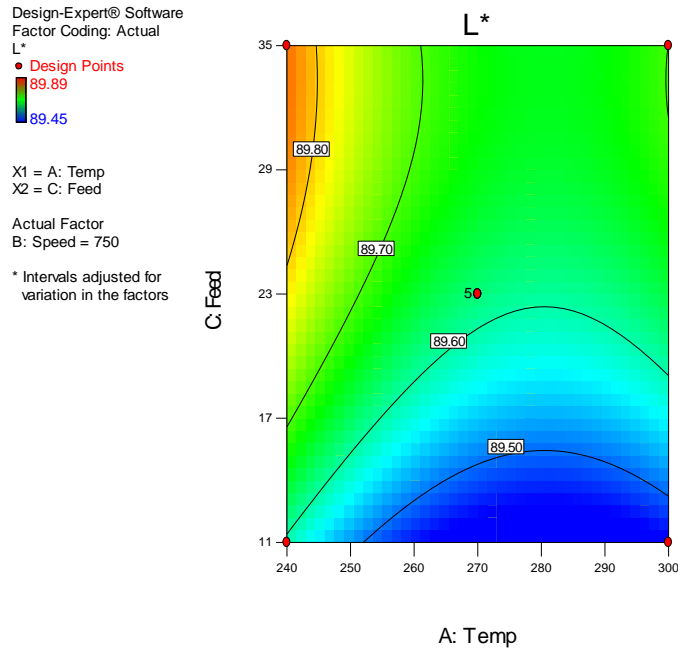


Fig. 3.28. Contour plot for L\* slicing along factor B

#### D. Process Optimization

After having the design predictive power verified through confirmation DoE, numerical optimization of the extrusion process was executed with the aim to discover various combinations of input variables that would satisfy not only the constraints imposed on output responses but also associated design precision. The numerical optimization was complemented by graphical optimization, ensuring that optimal solutions truly satisfied the constraints. Moreover, design robustness was achieved by incorporating propagation of error (POE) model during optimization process. Observed fluctuations during experimentation were: 10°C in temperature, 1rpm in screw speed and 0.01kg/hr in feed rate were incorporated in design. The POE plots for L\*, a\* and b\* showing transmitted variability due to temperature fluctuations are presented in Figs. 3.29a to 3.29c respectively. It is evident from these graphs that a temperature between 270°C and 280°C is the one where the output responses are least sensitive to POE caused by fluctuation in temperature. Therefore keeping the temperature in this range would serve the purpose to make the design robust. POE analysis further revealed that fluctuations in screw speed and feed rate caused negligible transmitted variability in response.

Design-Expert® Software  
Factor Coding: Actual  
POE(L\*)

• Design Points

X1 = A: Temp

Actual Factors  
B: Speed = 750  
C: Feed = 23

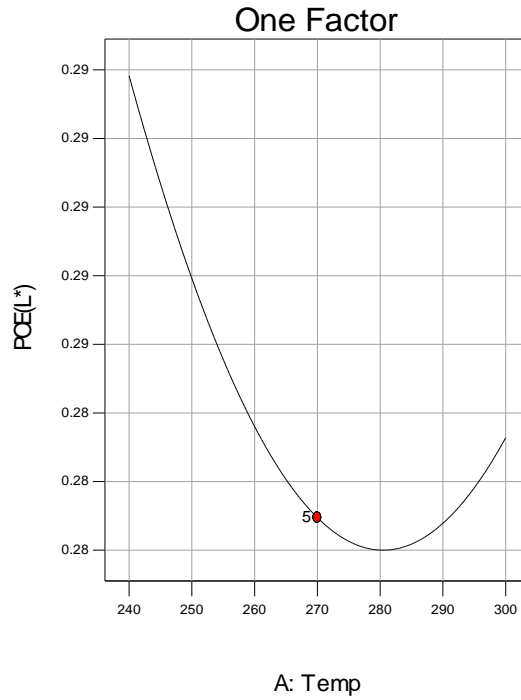


Fig. 3.29a: POE (L\*) transmitted by Temperature

Design-Expert® Software  
Factor Coding: Actual  
POE(a\*)

• Design Points

X1 = A: Temp

Actual Factors  
B: Speed = 750  
C: Feed = 23

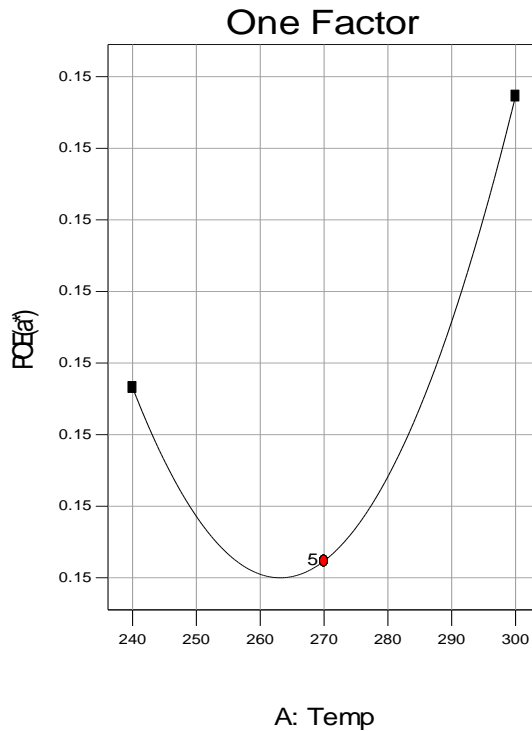


Fig. 3.29b: POE (a\*) transmitted by Temperature

Design-Expert® Software  
 Factor Coding: Actual  
 POE(b\*)

• Design Points

X1 = A: Temp

Actual Factors  
 B: Speed = 750  
 C: Feed = 23

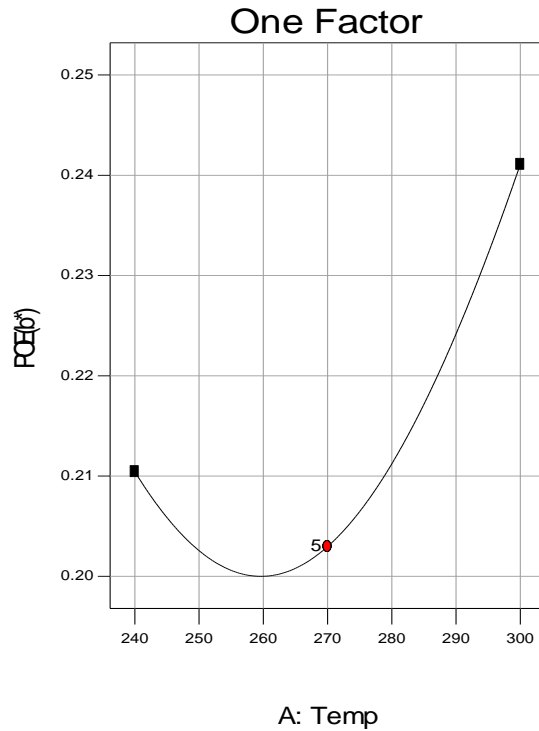


Fig. 3.29c: POE (b\*) transmitted by Temperature

Optimization criterion used is shown in Table 3.21 and three solutions out of nine, with desirability level from 0.79 to 0.71 are reported in Table 3.22. All the three solutions reflect a colour deviation in terms of delta values well within permissible limits compared with reference standard.

Table 3.21. Optimization criteria set to reach the target

Name	Goal	Lower Limit	Upper Limit
A: Temperature	is in range	240	300
B: Screw Speed	is in range	600	900
C: Feed Rate	is in range	11	35
L*	is target = 89.45	89.45	89.89
POE(L*)	minimize	0.281	0.294
a*	is target = -0.027	-0.10	-0.027
POE(a*)	minimize	0.150	0.151
b*	is target = 6.67	6.333	6.697
POE(b*)	minimize	0.21	0.29

Table 3.22. Three Solutions from Process Optimization

Factors	1 <sup>st</sup> Solution	2 <sup>nd</sup> Solution	3 <sup>rd</sup> Solution
Temperature	280	279	276
Screw Speed	600	600	600
Feed Rate	15	15	15
L*	89.49	89.49	89.49
POE(L*)	0.28	0.28	0.28
a*	-0.08	-0.08	-0.08
POE(a*)	0.15	0.15	0.15
b*	6.65	6.64	6.62
POE(b*)	0.21	0.21	0.22
$\Delta L^*$	-0.1	-0.1	-0.1
$\Delta a^*$	0.1	0.1	0.1
$\Delta b^*$	0.02	0.03	0.05
$\Delta E^*$	0.0204	0.0209	0.0225
Desirability	0.79	0.77	0.71

An overlay plot is presented in Fig. 3.30 reflecting 3<sup>rd</sup> optimal solution flagged in the sweet (yellow) spot. This yellow spot is the outcome of graphical optimization and verifies that the solution located inside, satisfies the constraints set out for optimization and process robustness.

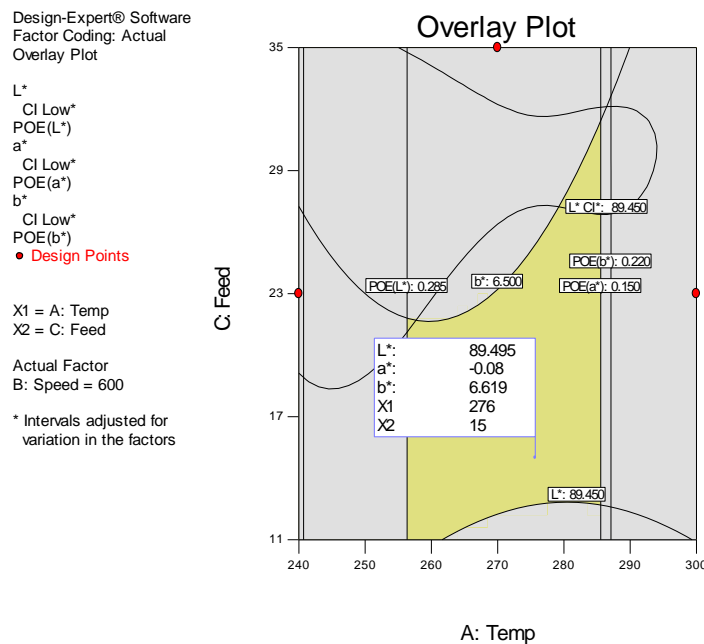


Fig. 3.30: 3<sup>rd</sup> optimal solution flagged in sweet spot

A verification test was carried out with the help of confirmation node available in Design Expert® software. A significance level  $\alpha=0.05$  and number of trials  $n=200$  were used for the test, which verified the fitness of three optimal solutions keeping response values within 95% CIs. Experimental verification of the optimal solutions listed in Table 3.22 was also conducted and the experimental response values (not shown here) were found well within 95% confidence intervals.

## **3.4 Conclusions**

### **3.4.1 Low Chroma Translucent PC Grade (G1)**

Present investigation identifies process variables that can significantly influence output colour of PC grade G1. This study suggests five sets of optimal process conditions. These optimal process conditions can be employed with greater confidence to achieve consistency in output colour while restricting POEs at minimum and overall colour deviation ( $\Delta E^*$ ) to a narrow range of 0.29 to 0.43, which lies well below the stipulated threshold of 1.0.

The experimental study offers plastic compounders a narrow but a precise process window - region of interest (sweet spot) shown yellow in overlay plot of Fig. 3.12. This study would not only help them overcome colour mismatch issue by allowing to choose a set of optimal process variables that ensures consistency in output colour, but also enable them make a right choice from available optimal solutions in order to reduce specific mechanical energy (SME), and thus improve productivity. In this perspective optimal solution reported in last row of Table 3.12 is the best choice.

### **3.4.2. High Chroma Opaque PC Grade (G2)**

Present experimental study identifies process variables that impose a significant impact on output colour of the PC grade G2 in individual capacity as well as in 2 factor interactions (2FIs). The study suggests eight optimal process conditions that can be employed to achieve consistent output colour for the plastic grade examined, with greater confidence and with least colour deviation from reference standard. The study further reveals the usefulness of POE technique to ensure the process robustness along with optimization. Moreover, higher temperature plateaus compared with grade G1, identified in POE graphs, can be associated with low MFI of the PC resin used in formulation.

### **3.4.3 High Luminous Opaque PC Grade (G3)**

Present experimental study identifies through statistical analysis, the process input variables that have a significant impact on output colour of PC grade G3, individually as well as in terms of their two factor interaction (2FI). The study suggests optimal process conditions



that can be employed to achieve consistent output colour for the plastic grade examined, with greater confidence and with least colour deviation from reference standard. The study further reveals that POE technique is quite useful in making a compounding process robust while implementing process optimization.

### **3.5 Summary**

Plastics compounders need to understand the relationship between process variables and output colour and know the optimal process conditions to achieve consistency in output. Such a relationship and optimal processing conditions are investigated using Box-Behnken design of response surface for three polycarbonate resin-based plastic grades: a translucent low Chroma grade (G1), an opaque high Chroma grade (G2), and an opaque high luminous grade (G3). This study analyses and discusses the results of designed experiments and highlights individual and combined influences on output colour, of three process parameters: temperature, screw speed and feed rate. Experimental results verify the fitness of the statistical model employed. This study suggests sets of processing conditions ensuring consistency in output colour of the plastic grades.

## Chapter 4

### Evaluation of Pigments Dispersion Level in Polycarbonate Compounded Plastic

#### 4.1 Introduction

Many colour processing mismatch issues are related to inadequate and inefficient mixing of colour pigments in a polymer matrix during compounding. During compounding both dispersive and distributive mixing processes generally take place simultaneously. The former aims at breaking of agglomerates into primary particle size, whereas the latter process increases the randomness of the spatial distribution of pigments within the polymer matrix without any further change in their size [63].

Factors that can possibly cause inadequacy of pigment mixing and eventually colour deviations, include changes in processing parameters, variation in colour formulation, degradation behaviour, variation in primary particle size distribution, and regions of variable refractive index within polymer matrix and pigments. Processing aides are frequently used, and these also affect rheological properties, and thus dispersibility of pigments in the resin [64]. All these factors need to be considered while doing an assessment of whether the mixing quality of compounding operations is adequate in regards to plastics coloration [10, 20, 25, 38, 39, 58]. However, for plastics compounders, knowing the optimal levels of process variables such as temperature, feed rate, and screw speed, is extremely important and help them achieve consistent output colour by ensuring pigments are adequately mixed and scattering of incident light is controlled. The transparency of polycarbonate resins does not allow scattering to happen, therefore in order to create scattering and achieve a certain level of opacity, brightness and whiteness, white pigments (titanium oxide) are added but at the cost of loss in apparent colour strength [20, 42, 61].

Optical theory suggests that most efficient scattering occurs when the particle size of the implemented pigments is slightly smaller than half the wavelength of incident light. The visible spectrum wavelength range (0.4–0.7 $\mu\text{m}$ ) suggests a particle size of 0.2–0.35 $\mu\text{m}$  will optimize scattering. However, pigments have tendency to stick together forming agglomerates - particles larger in size than 0.35 micron. Consequently, higher is the number and size of agglomerates in compounded plastics, lower would be the pigments scattering power [59, 65]. As the highest refractive index (about 2.7) is associated to TiO<sub>2</sub> pigment (rutile phase), it has the strongest scattering power at an optimum particle size of about 0.2 micron. As per Mie scattering theory, the angle-weighted scattering coefficient  $S$  is estimated as 12  $\mu\text{m}^{-1}$  at 550 nm

(visible spectrum mid-point) assuming a 0.22 micron diameter particles suspended in a clear binder with a refractive index of 1.5 [66~68].

Various techniques have been used to investigate factors such as pigments volume concentration, affecting plastics coloration. Included among these techniques are thermogravimetric analysis (TGA), differential scanning calorimetry (DSC), scanning electron microscopy (SEM), energy dispersive X-ray spectroscopy (EDX), and ash content [34~36]. None of the techniques were used to quantify pigments dispersion level in compounded plastics. We however, have successfully employed environmental scanning electron microscopy (ESEM) and image analysis to analyse pigment dispersion in a high-Chroma polycarbonate grade. A similar technique is reported to be used by Gunde and co-workers [69], but for powder-coated, plasma-etched samples.

Evaluating pigments dispersion level within a polymer matrix determines the mixing efficiency of a compounding process, which can be correlated with processing conditions employed. Contrary to paints and coatings, compounding of plastics involves high shear rates, elevated temperatures, and high pressures. To date, only a few studies are reported in literature about effect of process variables on plastics coloration [38, 39].

#### **4.1.1 Environmental Scanning Electron Microscopy (ESEM)**

In scanning electron microscopy (SEM), an electron beam scans the surface of a specimen to be examined, and the reflected (or back-scattered) beam of electrons is collected, then displayed at the same scanning rate on a cathode ray tube (similar to a CRT television screen). The image displayed on the screen, which may be photographed, replicates the specimen surface features. The surface may or may not be polished and etched, but it must be electrically conductive; a very thin metallic surface coating must be applied to nonconductive materials such as polymers [40]. This condition however, is no more needed in ESEM, where to eliminate electrostatic charge build-up during examination, a bridge between specimen edges and conductive tape underneath is formed by applying a conductive adhesive. Magnifications over 200,000 times, are possible, and great depths of field are possible. Qualitative and semi-quantitative analysis of the elemental composition for quite localized surface areas, are also possible when equipped with accessories such as energy dispersive X-ray spectroscopy (EDX).

#### **4.1.2 Image Analysis with ImageJ®**

Various commercially available image analysis software such as Image-Pro can be used for image processing and analysis, but they are expensive. ImageJ however, is a public domain

software [41], which is available as an online applet as well as in downloadable application format, for Windows, Mac OSX and Linux. The software is enriched with quite powerful features such as spatial calibration, stacking, filtering and geometric transformations to name a few.

### **4.1.3 Objectives**

Main objectives to carry out this study include following:

- 1) Evaluate pigments dispersion level by determining their particle size and spatial distribution in a high Chroma opaque compounded polycarbonate grade.
- 2) Correlate pigments dispersion to employed processing conditions and hence to output colour of the plastic grade.

## **4.2 Materials, equipment and process**

As explained in chapter 3, three compounded polycarbonate grades: 1) a translucent low Chroma grade, 2) opaque high lightness grade, and 3) opaque high Chroma grade, were statistically analysed using Box-Behnken design (BBD). Model equations were determined to see the effect of changing processing conditions on their output colour and optimal processing conditions proposed for achieving colour consistency in compounding. The present study, however, evaluates pigment dispersion and their spatial distribution within polymer matrix by characterizing solid structure of opaque high Chroma compounded polycarbonate grade. The characterization involves use of ESEM (FEI Quanta FEG 250) for imaging, and ImageJ® – a public domain software for image analysis [41]. A correlation between the processing parameters and the distribution graphs of particle size and inter-particle distance was established and compared with colorimetric and statistical analyses.

The plastic grade formulation used in the experimentation comprised LEXAN (105 – 111N) – a bisphenol A - polycarbonate (BPA-PC) resin, five colour pigments including Titanium dioxide, and two fillers. PC resin used is a highly viscous resin with a melt flow index (MFI) of 6.5g/10min at 300°C/1.2kg load. All ingredients were precisely weighed in proportions shown in Table 4.1 and dry -mixed on a super floater. The premix was then compounded and pelletized using a 25.4 mm, 27 kW, fully intermeshing, co-rotating twin-screw extruder (ZSK26). After being preheated in an oven isothermally at 120 °C for about 2 hours, these pellets were injection moulded into rectangular chips of the size: 75mm x 50mm x 2.6mm. These sample chips were then colour measured on Colour-Eye® 7000A - an X-Rite spectrophotometer, applying large area sample aperture, specular component included and

reflectance mode. Calculations were made for colour difference between the samples obtained by experimental runs and the standard chips using CIELAB colour space, D<sub>65</sub> illuminant and 10° observer [23]. These differences are presented in Table 4.2 as total colour difference ( $\Delta E^*$ ), and net differences in lightness ( $\Delta L^*$ ), red-green axis ( $\Delta a^*$ ), yellow-blue axis ( $\Delta b^*$ ), and Chroma ( $\Delta C^* = \sqrt{\Delta a^{*2} + \Delta b^{*2}}$ ). The target (reference) colour coordinates were: L\*=43.26, a\*=44.89 and b\*=24.09.

Table 4.1. Colour Standard Formulation

S.N	Ingredient	Chemical Name	PPH	Weight (g)
1	Resin	BPA-PC	100	9000
3	C.I. Pigment White 6	TiO <sub>2</sub>	0.422	38.00
4	Black Pigment, Amorphous	-	0.00013	0.012
5	C.I Solvent Red 135	-	0.281	25.30
6	C.I Solvent Red 207	-	0.070	6.30
7	C.I Disperse Orange 45	-	0.202	18.20
8	Filler 1 (anti-Oxidant)	Diphenyl Isodecyl Phosphite	0.050	4.50ml
9	Filler 2 (Lube)	Methyl hydrogen Siloxane	0.022	2.00ml

Legend: PPH – Parts per hundred parts of resin

Table 4.2. Designed Experimental Runs and Colour Data

Run No.	Process Variable			Colour difference				
	Temp (°C)	Speed (rpm)	Feed (kg/hr)	$\Delta L^*$	$\Delta a^*$	$\Delta b^*$	$\Delta C^*$	$\Delta E^*$
1	240	600	23	-1.01	0.42	-0.56	0.70	1.23
2	300	750	11	-1.93	-2.06	-2.27	3.07	3.62
3	300	750	35	-1.31	-0.13	-0.96	0.97	1.63
4	300	600	23	-1.25	0.12	-0.74	0.75	1.46
5	270	600	11	-1.27	-0.33	-0.99	1.04	1.64
6	240	750	35	-1.15	0.53	-0.44	0.69	1.34
7	240	900	23	-0.99	0.3	-0.55	0.63	1.17
8	270	750	23	-1.26	0.25	-0.87	0.91	1.55
9	270	750	23	-1.24	0.23	-0.68	0.72	1.43
10	270	600	35	-1.13	0.36	-0.71	0.80	1.38
11	270	750	23	-1.11	0.37	-0.71	0.80	1.37
12	270	900	11	-1.6	-0.78	-1.49	1.68	2.32
13	240	750	11	-1.82	-1.24	-1.73	2.13	2.80
14	270	750	23	-1.27	-0.1	-0.83	0.84	1.52
15	270	750	23	-1.12	0.66	-0.5	0.83	1.39
16	270	900	35	-0.98	0.44	-0.66	0.79	1.26
17	300	900	23	-1.46	-0.9	-1.43	1.69	2.23

Legend: rpm – Revolution per minute; kg/hr – Kilogram per hour

Two experimental runs i.e. Run7 and Run17 (highlighted grey in Table 4.2) were selected for evaluation of pigment dispersion, because the two runs represent low and high temperature ends, i.e. 240 °C and 300 °C, respectively. The screw speed and feed rate were fixed at 900 rpm (high shear rate end) and 23 kg/hr (middle end of the feed rate), respectively. The reason to choose these experimental runs is that polycarbonate resins are more sensitive to temperature than shear rate, although their rheology still holds a non-Newtonian characteristic, they display a very low shear-thinning behaviour compared with other thermoplastics [70]. Rectangular moulded chips of the two selected experimental runs were cut into thin sections (15 each) on a fully automatic rotary microtome (CUT 6062 of SLEE). A schematic reflecting the moulded chip and the sample for thin sections is presented in Fig. 4.1. From the outer surface to centre layer of the rectangular chips, the first six sections were cut at a thickness of 50 micron each, and then the rest nine in sequence were cut at 100 micron each. Therefore, the 15<sup>th</sup> layer of the thin sections approximately represents the centre of the rectangular chips, where viscous effects are considered at their minimum compared with top surfaces (1<sup>st</sup> layer) being in direct contact with the wall of the die cavity during melting. Each thin section was then imaged from different locations applying an ESEM and images were processed with ImageJ® software to evaluate pigments particle size distribution and their inter-particle distance. For brevity the average Image data obtained for top and centre layers are presented in Table 4.3 and Table 4.4 respectively.

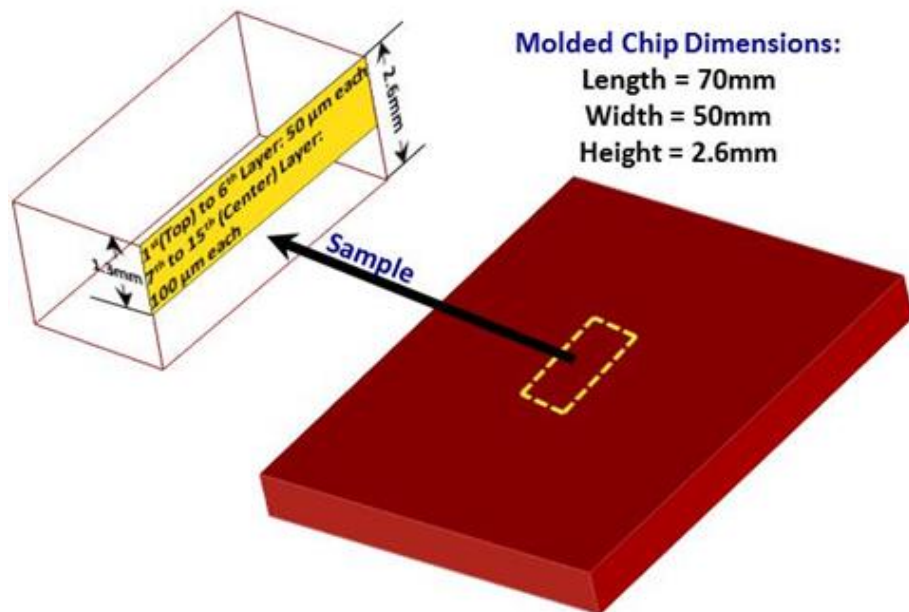


Fig. 4.1: Schematic of moulded chip and sample for thin sections

Table 4.3: Pigments Particle Size Distribution

Equivalent Circular Dia. ( $\mu\text{m}$ )	Number of Particles, %			
	Experimental Run-R7		Experimental Run-R17	
	Top Layer	Centre Layer	Top Layer	Centre Layer
$d \leq 0.2$	47.44	61.15	62.91	61.45
$0.2 < d \leq 0.25$	20.65	21.40	13.35	17.59
$0.25 < d \leq 0.3$	12.68	7.73	8.51	8.36
$0.3 < d \leq 0.4$	14.83	7.64	8.51	8.58
$0.4 < d \leq 0.5$	3.58	1.71	4.06	3.58
$d > 0.5$	0.82	0.36	2.67	0.43

Table 4.4: Inter-Particle Distance Distribution

Nearest Neighbour Distance - NND ( $\mu\text{m}$ )	Number of Particles, %			
	Experimental Run-R7		Experimental Run-R17	
	Top Layer	Centre Layer	Top Layer	Centre Layer
$d \leq 1$	22.95	18.62	51.89	37.79
$1 < d \leq 2$	40.19	26.80	24.15	28.66
$2 < d \leq 3$	21.81	24.10	13.09	16.50
$3 < d \leq 4$	11.01	16.91	5.82	9.45
$4 < d \leq 5$	2.91	8.00	2.33	5.65
$5 < d \leq 6$	0.62	3.87	2.04	1.41
$6 < d \leq 7$	0.52	0.72	0.39	0.43
$7 < d \leq 8$	0.00	0.63	0.10	0.11
$8 < d \leq 9$	0.00	0.00	0.19	0.00

### 4.3 Results and Discussions

In order to establish how the variation in process variables impacts the pigments dispersion in polymer matrix, and hence on the output colour of compounded plastics, image data provided in Table 4.3 and Table 4.4 were analysed and results are discussed here.

ESEM micrographs of top and centre layers (for brevity only) of the two experimental runs are presented in Figs 4.2 and 4.3. The bright spots (high grey value) in these micrographs represent dispersion of white pigments ( $\text{TiO}_2$ ), which is the dominant inorganic pigment of the colour formulation used. This was also verified by EDX results (not shown here). The dark background (low grey value) of micrographs, however, corresponds to polymer resin blended with solvent red and other fillers.

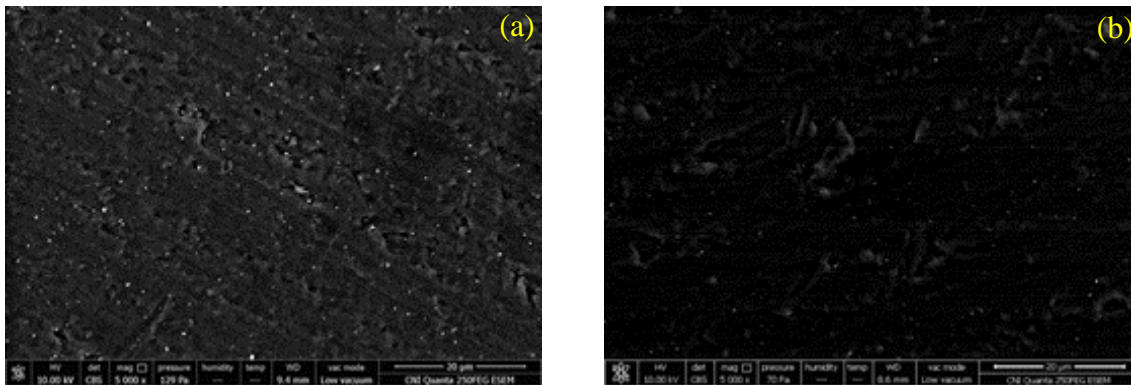


Fig. 4.2. ESEM image@ 5000x - Run 7 Sample Chip: Top layer (a); Centre layer (b)

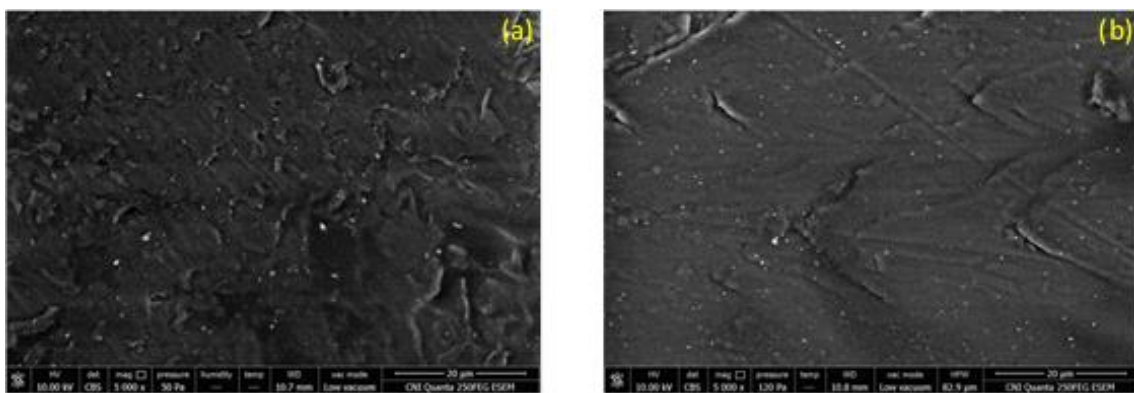


Fig. 4.3: ESEM image @ 5000x - Run 17 Sample Chip: Top layer (a); Centre layer (b)

The characterization data obtained through processing of micrographs as given in Table 4.3 and Table 4.4 were analysed to distinguish oversized particles i.e. agglomerates that cause a reduction in the scattering power of particles resulting into a lower  $L^*$  value of output colour [59, 66]. Distribution graphs comparing two experimental runs are presented in Figs 4.4 & 4.5 for pigments particle size and in Figs 4.6 & 4.7 for inter-particle distance. Particle size distribution graphs reveal that for R17, percentage of particles exceeding 0.5 micron diameter is high, whereas that of particles with optimal diameter i.e. 0.2 ~ 0.35 micron, is comparatively less than R7. This clearly indicates that the processing conditions (high temperature end) employed in R17 have produced more agglomerates resulting into a loss of pigments' scattering power leading to a lower  $L^*$  value of the output colour. This reveals a good agreement with statistical analysis results of same plastic grade discussed in chapter 4, where a negative effect was observed on  $L^*$  by increasing the temperature.



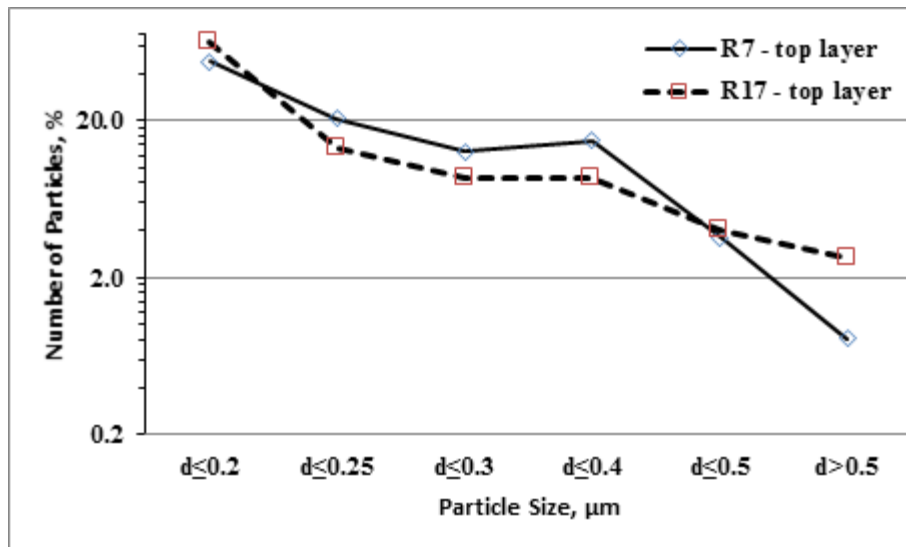


Fig. 4.4: Particle size distribution graph - top layers

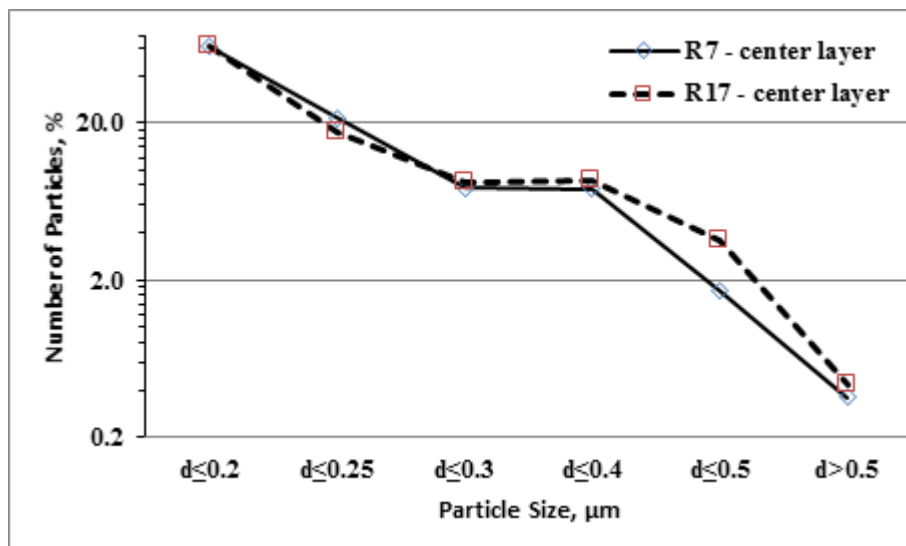


Fig. 4.5: Particle size distribution graph - centre layers

Similarly spatial distribution graphs shown in Figs 4.6 & 4.7 reveal that R7 compared with R17 have more evenly distributed particles along abscissa representing nearest neighbour distance (NND). Moreover, for R7 the weighted average of NND values as stamped in respective Figs for top and centre layers comes out to be higher than R17. This gives another indication that R7 particles are more adequately distributed compared with R17. These graphs further indicate that percent particles in R17, separated by a  $\text{NND} \leq 1\mu\text{m}$ , seem to be almost twice than that in R7. This clearly points towards concentration of the particles in localized regions opposing randomness of the inter-particle distance, and causing inadequate spatial distribution of pigments [20]. The inadequacy of pigments spatial distribution in R17, reduces their scattering power leading to a lower  $L^*$  value [66].

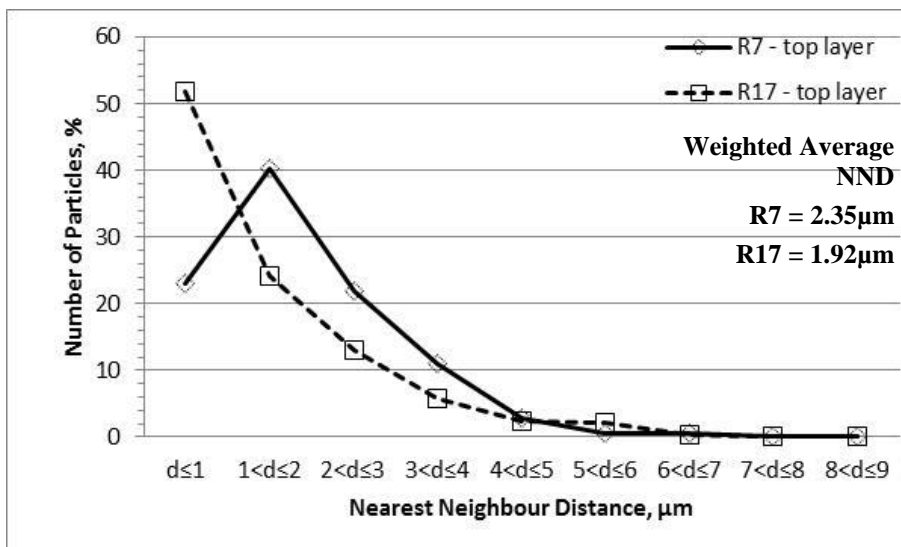


Fig. 4.6: Nearest Neighbour Distance graph - top layers

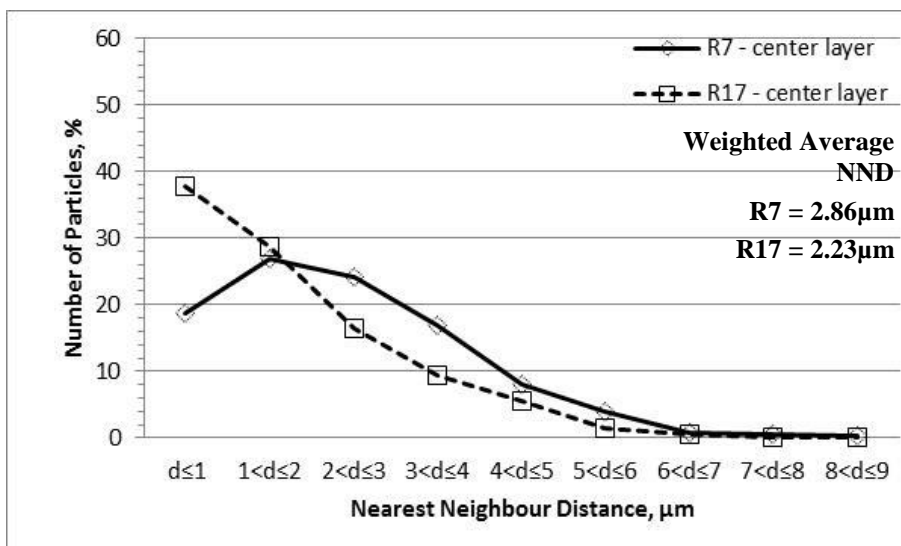


Fig. 4.7: Nearest Neighbour Distance graph - centre layers

Presented below in Fig. 4.8 and Fig. 4.9 are the colour data both in coordinates of CIE Lab colour space, and in delta values i.e. deviation of samples from reference. The colour difference between the samples is caused in increasing order by  $L^*$ ,  $b^*$  and  $a^*$  values. However with respect to the reference colour, the colour difference is mostly caused by  $L^*$  value in Run 7 and that in Run 17 by both  $L^*$  and  $C^*$ . It is obvious that Run 7 has shown significant reduction in colour difference in approaching towards the colour of the selected standard reference. The reduction in  $L^*$  can be attributed to better dispersion and distribution of white pigments, whereas that in chroma to better mixing of solvent red in polymer matrix.

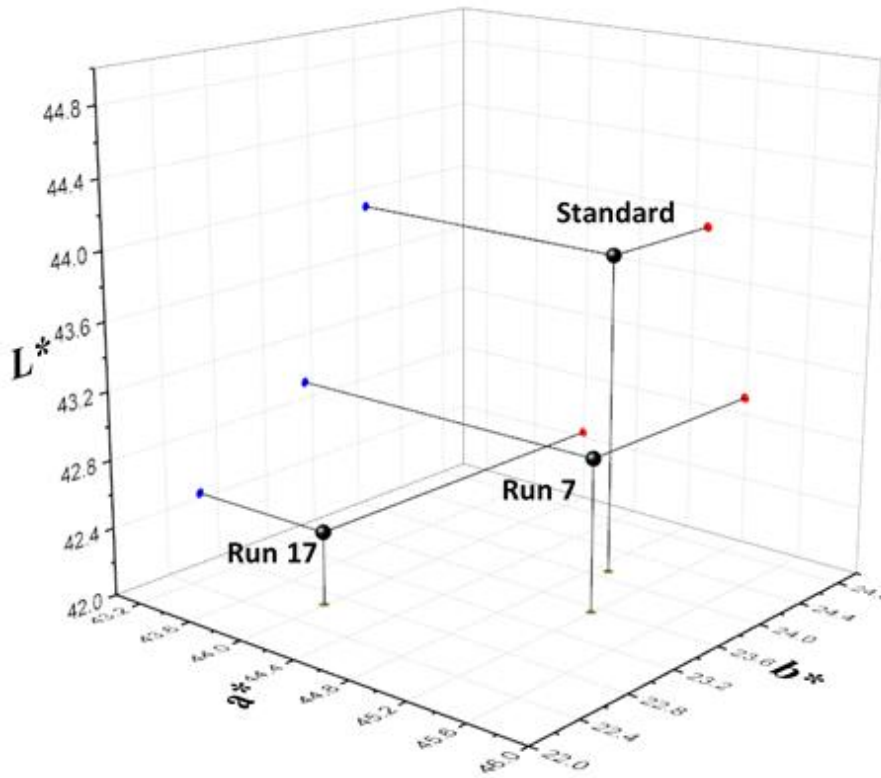


Fig. 4.8: Colour data of samples and the standard reference – CIE Lab colour space

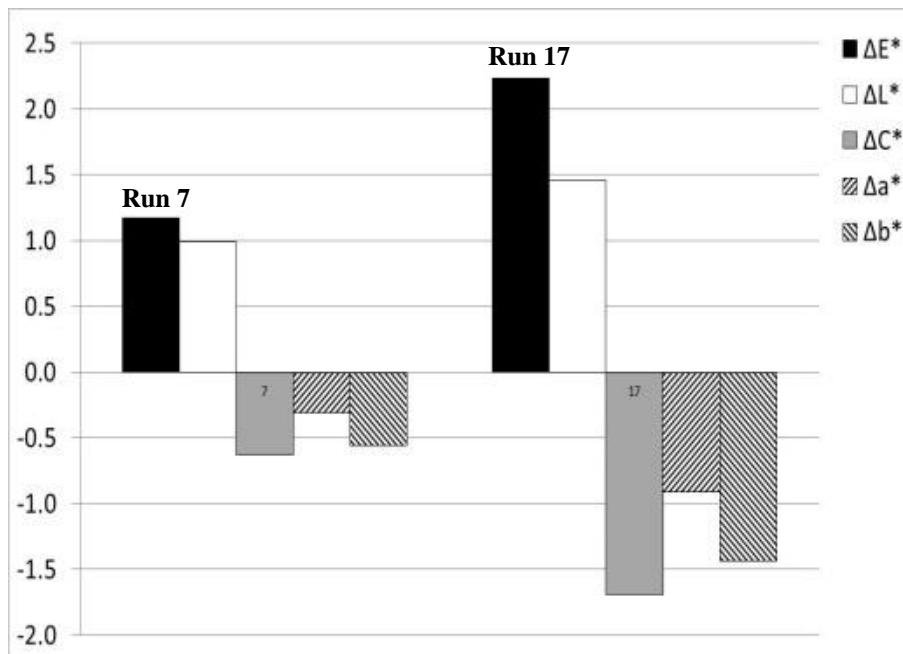


Fig. 4.9: Colour difference between samples and the standard reference

Spectral curves of the two experimental runs are shown in Fig. 4.10. Horizontal axis represents the entire wavelength range of visible light, whereas, the vertical axis shows the reflected

intensity against each wavelength. Increased intensity at around 600 nm and distinctness of the shape of the curve clearly illustrates hue and saturation of sample's colour - a vibrant red. However, the reflectance intensity level for Run 7 at the wavelength range: 650 nm to 700 nm (Fig. 10b), is higher than that of Run 17, which can be associated with more effective light scattering due to higher degree of pigments dispersion in Run 7.

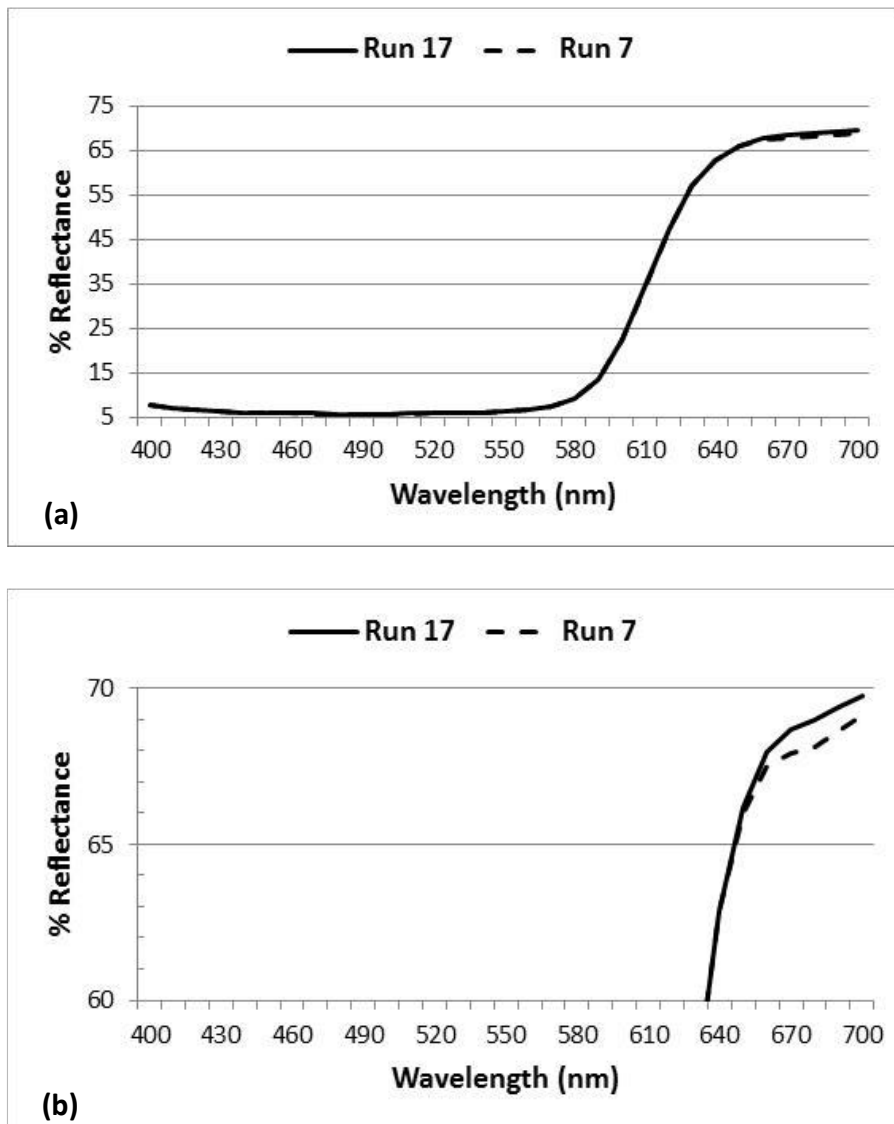


Fig. 4.10: Spectral Curves: reflectance intensity @ full spectrum (a); @ red spectrum (b)

#### 4.4 Conclusions

The characterization of a polycarbonate compounded plastic grade using ESEM and image analysis technique has revealed that dispersion of white pigments such as TiO<sub>2</sub> in a polycarbonate matrix is directly influenced by input process variables such as temperature, employed during extrusion. This study quantifies pigments dispersion level and correlates it

with processing conditions. The implemented technique is proved to be useful in detection of small differences in pigments particle size and spatial distribution and relating them to small variation in colour coordinates such as  $L^*$ . It further reveals the negative effect that a rise in temperature can impose on  $L^*$ . A similar effect was identified by statistical analysis explained in chapter 4. This study offers plastics compounders a powerful tool in quantifying pigments dispersion level in polycarbonate compounded plastics under varying processing conditions, and help them to discover an optimal set of process variables ensuring consistency in desired colour during compounding.

#### **4.5 Summary**

In this part of study, three input variables to the extrusion process - temperature, screw speed, and feed rate, are investigated for their impact on colour pigments dispersion vis-à-vis plastics coloration. Pigments dispersion is quantified using scanning electron micrography and image analysis. A correlation between processing conditions and distribution graphs for pigments particle size and inter-particle distance is discussed and compared with colorimetric data. The results obtained through these investigations are quite promising and could help plastics compounders achieve consistency in plastics coloration.

## Chapter 5

### Numerical Analysis of Mixing Efficiency under Varying Process Conditions in Intermeshing Co-rotating Twin Screw Extruder

#### 5.1 Introduction

Mixing is a key process in plastics industry, where a variety of additives, such as colour pigments, stabilizers, antioxidants, fillers, lubes etc., are incorporated into basic polymer matrix, or a blend of two or more polymers. To carry out mixing process, both batch type (e.g. Banbury mixer) and continuous type mixer (extruders) are used. Among continuous mixers, twin screw extruders are widely used in compounding operations for their high throughput, product uniformity and being economical in energy consumption. Co-rotating, intermeshing twin-screw extruders are preferred over other extrusion machines because of their self-wiping feature that provides advantages, such as a complete elimination of any stagnant zone. Kneading discs are the dominant elements in a modular machine that determine dispersive mixing efficiency. For a high Chroma opaque compounded polycarbonate grade, 3-D isothermal flow pattern is simulated in the kneading discs region of a Coperion ZSK-26 co-rotating twin-screw extruder. A quasi-steady state finite element method was implemented to avoid time dependent moving boundaries. Mixing parameter  $\lambda$ -lamda, is determined to quantify dispersive mixing efficiency of the kneading block zone under different processing conditions. Simulation results are correlated with input process variables, and compared with experimental colorimetric data.

##### 5.1.1 Twin screw extruders (TSE)

Extruders are widely used not only in plastics industry, but also petrochemical and food industries for melting, mixing, blending, reacting, devolatilizing and numerous other tasks. Based on number of screws they are classified in two types: single screw and twin screw extruders. In single screw extruders, extrusion process and conveying mechanism are highly dependent on frictional and viscous properties of material. In TSEs however, these properties play a lesser role on conveying behaviour.

TSEs can be designed in various configurations, however main classification is made if the screws are intermeshing or non-intermeshing, and whether co-rotating or counter-rotating. The non-intermeshing TSEs do not have the benefit of positive conveying characteristics as no protrusion exists between the flights of one screw and the channels of the

other screw. In intermeshing TSEs, flights of one screw protrude into the channels of other screw and their positive conveying characteristics depends upon the degree of intermeshing that ranges from fully intermeshing to partially intermeshing (in some cases near to non-intermeshing).

As regards classification due to direction of screw rotation, in counter-rotating extruders, material is sheared and pressurized in a mechanism quite similar to calendaring where a material is effectively squeezed between two counter rotating rolls [11], and are preferred for shear sensitive materials. In co-rotating screws, material transfer from one screw to other screw takes place in a Fig.-of-eight pattern and are preferred for temperature sensitive materials as the material is conveyed through the extruder quickly with little possibility of entrapment. The intermeshing co-rotating extruders can further be classified as low and high speed machines. The low speed extruders have high degree of positive conveying characteristics because of closely fitting flight and channel profile, and are preferred in profile extrusion applications. The high speed machines are characterized by their self-wiping feature. Because of the openness of the channels, material transfer takes place easily from one screw to another. They are primarily used in compounding operations [12].

### **5.1.2 Methods for modelling twin screw extrusion**

Modelling techniques that have been presented by various authors include: analytical modelling; flow analysis network (FAN); quasi steady state approximation; moving reference frame (MRF) method; mesh superimposition technique. Each approach has its own pros and cons as discussed below.

Analytical modelling provides the simplest way to understand the pumping behaviour of extruders, however is valid only for Newtonian fluids, furthermore mere throughput behaviour would not suffice to understand the flow mechanism in extruders, but rather shear stress and velocity distributions are more important to know for an insight of the flow behaviour, which require numerical solution of the problem.

The most common simplified numerical approach is FAN method, which works based on dividing flow region into control volumes and then carrying out flux balance on each volume. However because of geometric and information limitations restrict its use to simple geometries only.

Quasi-steady state approximation was introduced by Lee and Castro [51]. They mentioned that the transient part in the continuum equation could be considered negligible if the Reynolds number was very small as usually the case in polymer processing. With this

approximation, the resulting solution is dependent only on instantaneous material properties and boundary conditions, and screws relative positions within the barrel i.e. sequential geometries at defined angles of rotor position, can be selected and simulated under a steady state condition. Each screws relative position however, requires new meshes to be generated for a solution to run, results are then compiled together for those relative positions to understand the flow behaviour over a complete rotation cycle. Transient nature and complexity of flow geometry in twin screw extruders do not allow to reach a truly steady state condition. Many researchers therefore have successfully employed quasi-steady state approximation in simulating dispersive mixing behaviour of twin screw extruders.

Yang and Manas-Zloczower [52, 53] implemented this technique to simulate dispersive mixing behaviour of a Banbury mixer and for an intermeshing co-rotating twin screw extruder (ICRTSE). Bravo [54] employed same approximation for obtaining flowfield solution in kneading discs region of an ICRTSE. Recently, using same approximation, Sobhani et al [55] characterized mixing flow behaviour in co-rotating twin screw extruder, and Goger [56] analysed dispersive mixing behaviour in conveying elements of a counter rotating twin screw extruder. Disadvantage of this technique is that it involves lot of meshing work, and neglecting transient term in energy equation is not justified.

Moving reference frame (MRF) provides an alternate to quasi-steady state approximation, however Ortiz-Rodriquez [48] stated its limitation in predicting flow behaviour of double flighted screw as two different radial vectors were defined. Another disadvantage he mentioned was its restricted capability in describing distributive mixing behaviour in twin screw extruders.

Mesh superimposition technique [57] is pretty close to quasi-steady state in nature and even more sensitive to transient effects, however geometric complexities involved in twin screw extrusion restrict it to relatively course mesh patterns causing error to the results. Keeping in view these pros and cons, quasi-steady state approximation approach has been adopted for simulation of extrusion process in present study.

### **5.1.3 Objectives**

Main objectives of this study are outlined below:

- 1). Undertake analysis of dispersive mixing behaviour in the kneading discs (staggered at 45° zone) of Coperion ZSK26 co-rotating twin-screw extruder, under varying processing



conditions following a design of experiments (DoE), which was executed for compounding of a high Chroma opaque polycarbonate grade at SABIC IP Cobourg Plant.

2). Correlate the kneading block mixing efficiency with change in processing conditions employed, and then compare with experimental colorimetric data of the plastic grade leading to conclusions.

## 5.2 Geometry, Material and Process Considerations

Three main considerations that have direct influence on mixing efficiency of a co-rotating intermeshing twin screw extruder are: 1) Kneading discs geometry, 2) material rheological properties, and 3) processing conditions is the key geometric parameter that affects the mixing efficiency. As mentioned in the introduction section, the extruder we simulated is a Coperion ZSK26 co-rotating intermeshing twin screw extruder. The technical data of this extruder is provided below in Table 5.1. Kneading discs were staggered at 45° with forward (right handed) configuration as shown below in Fig. 5.1.

Table 5.1 Technical Data ZSK26 Twin Screw Extruder

Specification	Size
Shaft centreline distance	21.1 mm
Screw outside diameter	25.5 mm
Flight depth	4.55 mm
Barrel diameter	26.5 mm
Forward Kneading discs Zone	KB45/5/18

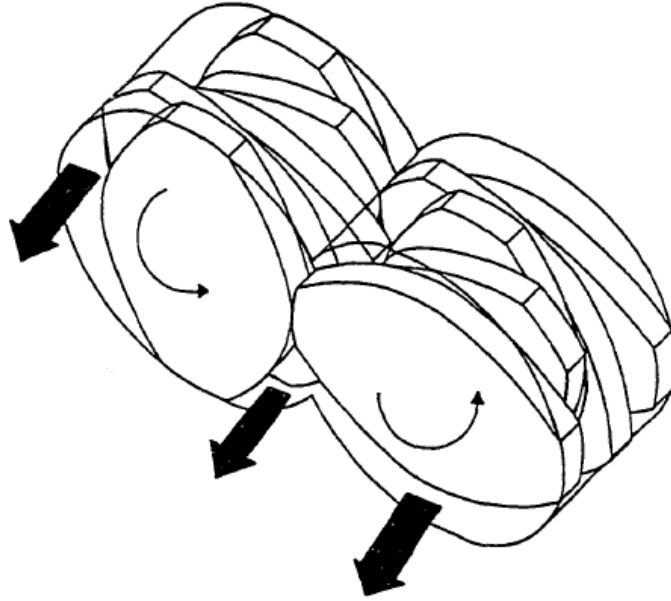


Fig. 5.1: Kneading Discs staggered at 45° in forward (right handed) configuration

Material tested in simulation is a high Chroma opaque polycarbonate based compounded plastic - a blend of bisphenol A. polycarbonate resin (LEXAN), five colour pigments including Titanium dioxide, and two fillers. Resin grade used in the blend has a melt flow index (MFI) of 6.5g/10min at 300°C/1.2kg load and density of 1.19 g/cm<sup>3</sup>. Material samples were tested for their rheological properties on ARES rotational rheometer, and the two parameters i.e. consistency index  $m$  and power index  $n$ , defined by power law model, are presented below in Table 5.2. Consistency index represents unit shear viscosity of the material reflecting its temperature dependency, whereas power index reflects shear thinning behaviour; higher the value of  $n$  is, lower would be the shear thinning behaviour. Polycarbonate resins are more sensitive to temperature as compared to shear rate, although their rheology still holds non-Newtonian characteristics [70] as obvious from data provided in Table 5.2. A mathematical expression of the power law viscosity model is shown in equation (5.1).

$$\bar{\tau} = m|\dot{\gamma}|^{n-1}\dot{\gamma} \quad (5.1)$$

where,  $\bar{\tau}$  is shear stress tensor,  $\dot{\gamma}$  the shear rate tensor,  $m$  the consistency index, and  $n$  the power law index. The two DoE runs i.e. R7 and R17 shown in Table 5.2 represent two different processing conditions employed during extrusion for manufacture of compounded plastics grade.

Table 5.2 Material Properties and Processing Conditions

Run #	Consistency Index $m$ ( $N.s^n/m^2$ )	Power Law Index $n$	Processing Condition		
			Temperature ( $^{\circ}C$ )	Screw Speed (rpm)	Feed Rate (kg/hr)
R7	3381.80	0.872	240	900	23
R17	379.53	0.928	300	900	23

### 5.3 Simulation with OpenFOAM®

Computational fluid dynamics (CFD) is the best available approach that provides numerical solution to complex fluid flow problems that otherwise cannot be solved analytically. Navier-Stokes equations that govern fluid flow in complex environment, are discretized into algebraic equations and are solved simultaneously using various numerical schemes. Availability of high speed computational and storage resources have made it possible to solve huge set of equations simultaneously in short period of time and store the data.

Basic steps involved in a CFD package include: 1) Pre-processing, where flowfield domain, mesh, and boundary conditions are defined; 2) Processing - a solver using a numerical scheme, solves huge set of numerical equations representing the problem defined in pre-processing step; and 3) Post-processing that help visualize the results and manipulate the data for analysis.

OpenFOAM® - Open Field Operation and Manipulation, is an open source CFD package that was developed by Open CFD Ltd and released in 2004 under General Public Licence. Basically OpenFOAM® uses libraries to create executable files, which are defined as applications and used to solve numerical equations. Two types of applications valid in the package are: 1) solvers to solve the equations; 2) utilities to manipulate the data. The package offers around 80 standard solvers to address various flow problems. Furthermore, it allows to develop a new solver as well as modify an existing one for customized cases. As regards utilities, over 200 utilities are available for different purposes. The package does allow to develop new utilities and modify existing ones to cater for customized cases.

#### 5.3.1 Mesh Design and Boundary Conditions

As mentioned in previous section, the specification of kneading discs zone used in this study are taken from technology line at SABIC IP Cobourg plant. The kneading discs geometry

was modelled in Solidworks®, a tetrahedral mesh was then generated with the help of GAMBIT® - a mesh generation software, and the meshed file was converted into OpenFOAM® file format so it could be opened in OpenFOAM® and used for numerical analysis.

A 3D mesh view of the flow domain is shown below in Fig. 5.2. The mesh comprises 4196078 cells with no negative volume. Tetrahedral mesh elements were selected because many researchers [55, 71, 72] found them appropriate and accurate for complex fluid domains such as in TSEs. A mesh sensitivity analysis was carried out (results not shown here) to ensure mesh independency of simulation results.

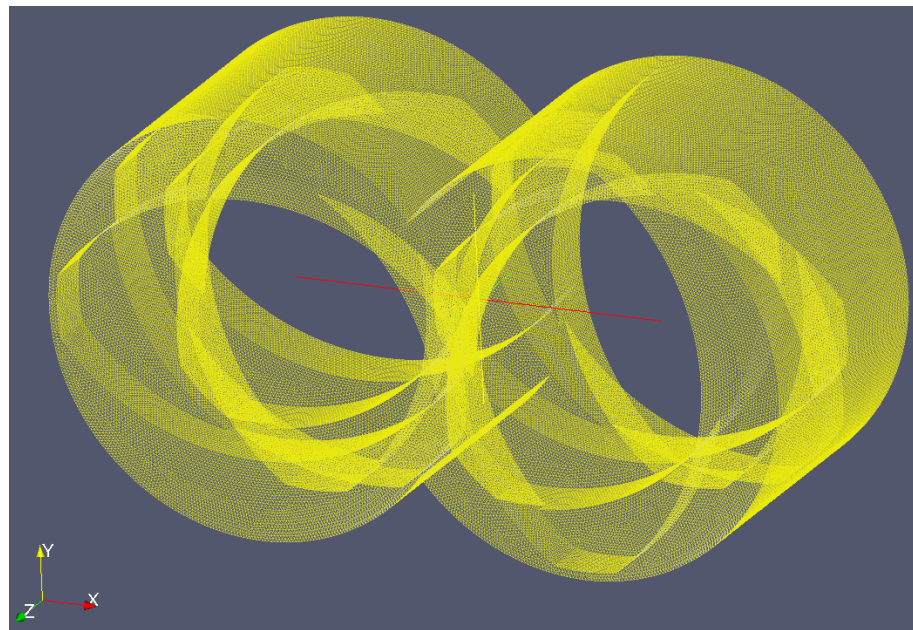


Fig. 5.2: Mesh View in z-direction with ParaFoam®

Boundary conditions employed are reflected below in Table 5.3. No-slip boundary condition was employed for both the barrel wall and walls of rotating screws, which means fluid elements are stationary on barrel wall and on screws surface they move with an angular velocity equivalent to rotating wall velocity (rpm) of the screws. As regards boundary conditions at entrance and exit planes of the kneading discs, a zero velocity gradient was set, however due to practical difficulties in calculating exact velocity profiles at these planes, a nominal value for the normal stress difference (pressure plus viscous stress) in axial direction was assigned between the two planes.

Table 5.3 Boundary Conditions for Velocity and Pressure

Boundary	Barrel	Screws	Inlet	Outlet
Velocity (U)	No-slip	Rotating Wall Velocity	Zero Gradient	Zero Gradient
Pressure (P)	Zero Gradient	Zero Gradient	Fixed Value	Fixed Value

### 5.3.2 Solver and Algorithm

The OpenFOAM® solver chosen for the numerical solution was incompressible laminar fluid flow under steady and isothermal conditions. The solver used SIMPLE algorithm to solve mass and momentum equations (5.2) and (5.3) as shown below respectively. SIMPLE algorithm that stands for Semi Implicit Methods Pressure Linked Equations, starts with determination of an initial guess for the flowfield, then using that initial guess calculates velocity field in momentum equations. The momentum equation is solved under relaxation with the aim to reduce non-linearity effect. As the momentum equation is not satisfied by the resulting velocity, therefore pressure equations are solved to obtain new pressure field. This process continues to repeat unless solution is converged.

$$\nabla \cdot \bar{V} = 0 \quad (5.2)$$

$$-\nabla P + \nabla \cdot \bar{\tau} = 0 \quad (5.3)$$

where,  $\bar{V}$  denotes the velocity vector,  $P$  is the pressure,  $\bar{\tau}$  represents stress tensor

A modification in the solver was also incorporated for obtaining other parameters such as shear stress, shear rate and vorticity tensors. The shear rate and vorticity tensors were then used to calculate dispersive mixing parameter  $\lambda$ . A mathematical expression of mixing parameter as defined by Manas-Zloczower [52, 73] is presented in equation (5.4), whereas expression for shear rate tensor, vorticity tensor and their respective magnitudes, are reflected in equations (5.5) to (5.8). In order for the solution to converge, the residuals for both velocity and pressure were set at  $5 \times 10^{-5}$ , which means the solver will stop simulation when the difference between two consecutive iterations reached below specified residual values. Simulation was run on a standalone Dell Machine (T3400) and for each solution to converge it took about 4000 iterations spanning over 172,800 seconds. Finally the results were visualized and examined with the help of ParaView® - an open source scientific visualization software.

$$\lambda = \frac{|\dot{\gamma}|}{|\dot{\gamma}| + |\omega|} \quad (5.4)$$

$$\bar{\dot{\gamma}} = \nabla \bar{V} + (\nabla \bar{V})^T \quad (5.5)$$

$$\bar{\omega} = \nabla \bar{V} - (\nabla \bar{V})^T \quad (5.6)$$

$$|\dot{\gamma}| = \sqrt{\frac{1}{2}|\dot{\gamma}:\dot{\gamma}|} \quad (5.7)$$

$$|\omega| = \sqrt{\frac{1}{2}|\omega:\omega|} \quad (5.8)$$

As mentioned in a previous section, quasi-steady state approach was implemented, which involves use of sequential geometries to cater for a complete mixing cycle. For a screw speed of 900 rpm, the time step  $\Delta t = 0.00278$  sec will lead to have sequential geometries as shown below in Fig. 5.3. We begin with the geometry at  $\alpha = 90^\circ$  for time  $t = t_0$ , where  $\alpha$  represents angle between left screw tip and the x-axis for the first disc. Next geometry for time step  $t_1 = t_0 + \Delta t$  would be located at  $\alpha = 105^\circ$ . The procedure is repeated until the screws return to their initial position i.e.  $t = t_0$  at  $\alpha = 90^\circ$ . However having two identical tips of the kneading disc, quarter of a revolution is considered to be sufficient to model a complete rotation cycle [53, 54].

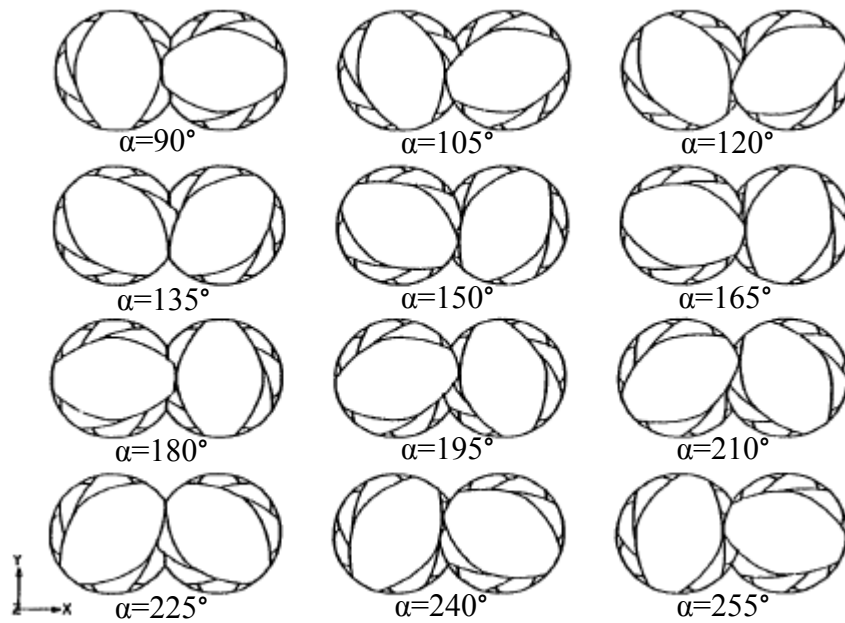


Fig. 5.3: Sequential geometries for a complete rotation of kneading discs staggered at  $45^\circ$

#### 5.4 Results and Discussion

Average values over volume and distribution range of the dispersive mixing parameter  $\lambda$  were obtained using ParaFoam® for the two cases simulated with OpenFOAM®. These values are listed below in Table 5.4. Average values were obtained by weighing  $\lambda$  value of each element over its volume for the entire flow domain. A 3D view of mixing parameter distribution

for the two cases is also presented in Fig. 5.4 and Fig. 5.5. Legends reflecting shear rate distribution are also highlighted in these views.

Table 5.4 Mixing parameter values for simulated cases

DoE Run #	Mixing Parameter $\lambda$		Shear Rate $\dot{\gamma}$ ( $s^{-1}$ )
	Average	Distribution	Distribution
R7	0.8666	0.430 ~ 0.994	1.77 ~ 22473.2
R17	0.8645	0.364 ~ 0.995	2.99 ~ 22367.6

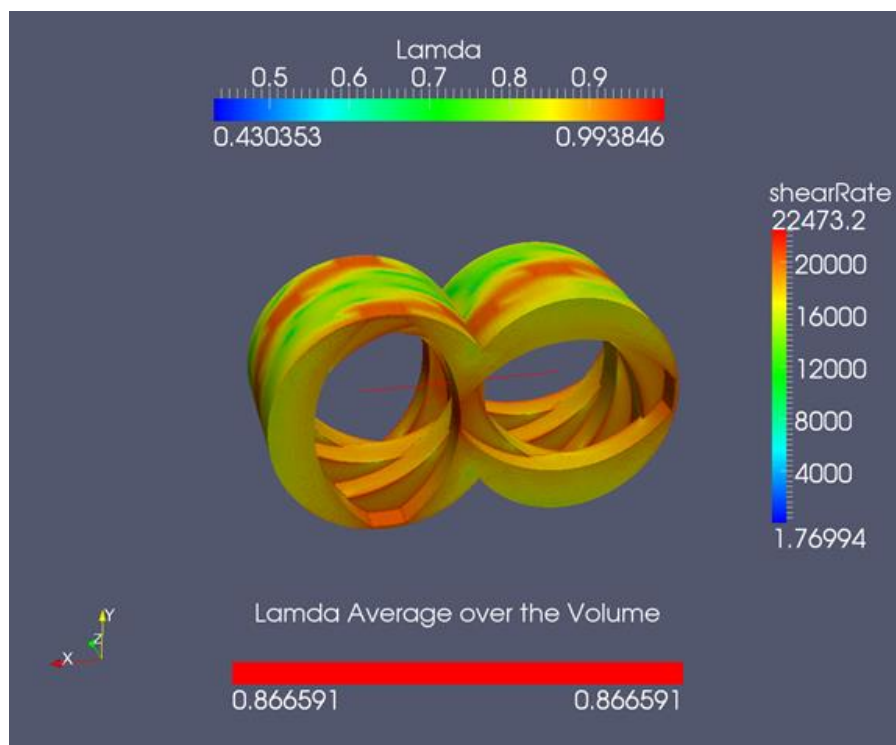


Fig. 5.4: 3D Distribution graph of mixing parameter  $\lambda$  – R7

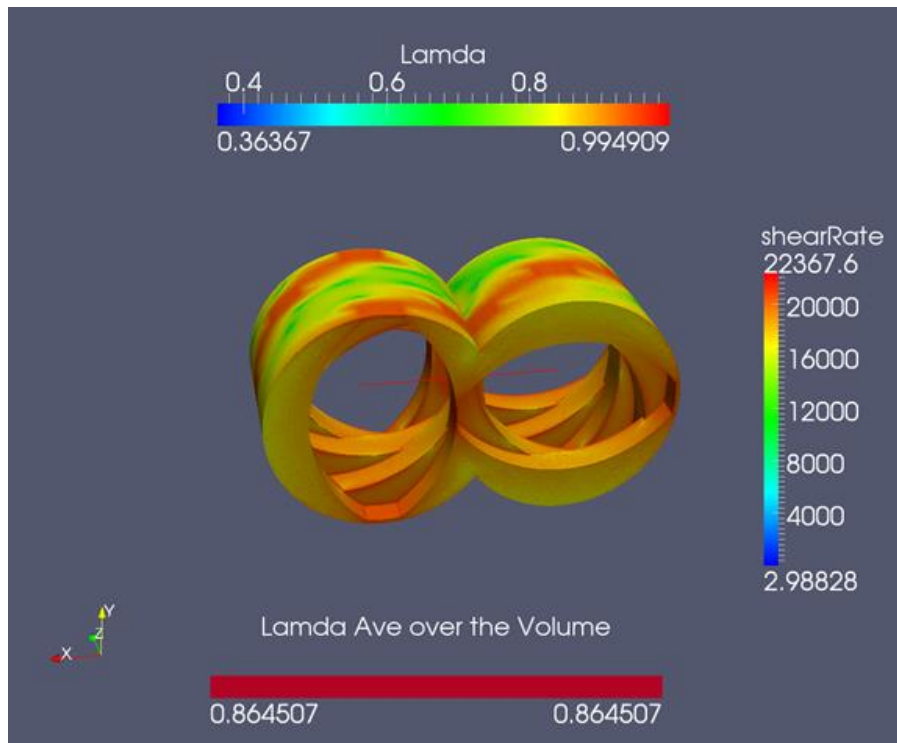


Fig. 5.5: 3D Distribution graph of mixing parameter  $\lambda$  – R17

Average  $\lambda$  values of both simulated runs are quite close to 1, which indicates the dominant flow in both cases is elongational. This confirms the overall mixing efficiency of kneading discs zone in ZSK26 extruder is extremely good. However a comparatively higher (0.24%) average  $\lambda$  value in R7 indicates that mixing efficiency is even better in R7 compared with R17. This little improvement in mixing efficiency can be associated with the processing conditions employed to R7, where the temperature was kept at 240°C. As we know dispersive mixing during compounding aims at breaking of agglomerates into primary particle size, so it would be justified to say R7 has better particle size distribution of colour pigments such as titanium dioxide. The titanium dioxide being a dominant colour pigment in the formulation used, is responsible for both the opacity and lightness (i.e.  $L^*$  value) of the output colour. As discussed in chapter 8, both opacity and lightness are directly influenced by particle size distribution of titanium dioxide, therefore it can be concluded that processing conditions employed in R7 correspond to a better mixing in kneading discs zone compared with those of R17, resulting into a higher lightness value, which was quite close to the target as shown below in Table 5.5. This seems to be in complete compliance with our findings of statistical and image analysis carried out for the same polycarbonate grade.



Table 5.5 Mixing parameter values vs measured colour coordinates

DoE Run #	Mixing Parameter $\lambda$	Colour Coordinates		
	Average	L*	a*	b*
R7	0.8666	42.27	45.19	23.54
R17	0.8645	41.8	43.99	22.66

Keeping in view quite a small difference in average  $\lambda$  values that was reported by various researchers, simulation runs for sequential geometries shown above in Fig. 5.3 were postponed. Yang [53] simulated sequential geometries for kneading discs zone of a co-rotating intermeshing twin screw extruder (Werner & Pflenderer ZSK-30) while the kneading discs were staggered at 45° in a forward configuration, and obtained average  $\lambda$  values ranged from 0.5556 to 0.5574 (a difference of 0.0018), similarly Bravo [54] simulated a total of 7 sequential geometries and average  $\lambda$  values obtained varied from 0.5702 ~ 0.5722 (a difference of 0.002). Goger [56] also reported quite a small difference in average  $\lambda$  values of 4 sequential geometries that were simulated under various screw pitch lengths for conveying screw elements of a counter-rotating twin screw extruder.

## 5.5 Conclusions

Dispersive mixing parameter  $\lambda$  provides an insight of the flow behaviour in kneading discs region of ZSK26 twin screw extruder. Average  $\lambda$  values obtained through simulation of the kneading discs zone under processing conditions represented by R7 and R17, reveal that the simulation under R7 process (a low temperature) condition, yields better dispersive mixing of titanium dioxide pigments used in the formulation. This has resulted into a better output colour of the compounded plastic grade. However to further investigate the effect of process conditions on the output colour of the plastic grade studied, other runs listed in DoE Table 3.2, may also be simulated.

## 5.6 Summary

Co-rotating, intermeshing twin-screw extruders are widely used in plastics industry for polymer compounding and blending. They are preferred over other extrusion machines because of their self-wiping feature that provides advantages, such as a complete elimination of any stagnant zone. Kneading discs are the dominant elements in a modular machine that determine dispersive mixing efficiency. For a high Chroma opaque compounded polycarbonate grade, 3-D isothermal flow pattern is simulated in the kneading discs region of a Coperion ZSK-26 co-rotating twin-screw extruder. A quasi-steady state finite element method was implemented to

avoid time dependent moving boundaries. Mixing parameter  $\lambda$ -lamda, is determined to quantify dispersive mixing efficiency of the kneading block zone under different processing conditions. Simulation results are correlated with input process variables, and compared with experimental colorimetric data.

## Chapter 6

### Contribution and Recommendations

#### 6.1 Contribution

As stated in Chapter 1 of this thesis, colour of compounded plastics is directly influenced by varying processing conditions, pigments type and concentration level in colour formulation. Furthermore, mixing efficiency of kneading discs zone in a twin screw extruder can be evaluated by quantifying the pigments dispersion level in polymer blend. Producing a compounded plastic in correct colour without making adjustments in colour formulation or processing conditions has been challenging for plastics compounder. The research work presented in this thesis contributes to understanding the influence of process variables to the extrusion process, especially of temperature, screw speed and feed rate, on the output colour of polycarbonate resin grades. Among the major accomplishments of this thesis are:

- Identification of pigments type and adjustment levels in pigments formulation needed during production, to deal with colour variation in polycarbonate compounded plastic grades, PC1 and PC2. The predictive model equations presented can help a colour expert to make precise decision regarding minute adjustments needed in reference colour formulation during production, and thus improve quality and productivity. The optimization results suggest a colour formulation slightly different from initial reference, of white, black and yellow pigments for the two plastic grades examined.
- Identification of process variables that significantly influence output colour of three PC grades: 1) a low Chroma translucent grade G1; 2) a high Chroma opaque grade G2; 3) a high luminous opaque Grade G3. The predictive model equations presented can be used as a tool to predict output colour by changing processing conditions within the tested range. The optimization results suggest process conditions that can be employed with greater confidence to achieve consistency in output colour while restricting POEs at minimum and the overall colour variation ( $\Delta E^*$ ) within a stipulated threshold of 1.0. The study further reveals usefulness of the POE technique for making the compounding process a robust while implementing process optimization.
- Introduction of a novel technique that evaluates pigments dispersion level in polymeric matrix. This technique involves use of ESEM and image analysis tool, and investigates a high Chroma opaque polycarbonate grade G2, by quantifying pigments particle size and spatial distribution within the polymeric base. The implemented technique is proved to be useful in detection of small differences in pigments particle size and spatial distribution

and relating these differences to small variation in colour coordinates such as  $L^*$ . It further reveals a negative effect on  $L^*$  due to rise in temperature. A similar effect was identified by statistical analysis explained in Chapter 3. This study offers to plastics compounders, a powerful tool for quantifying pigments dispersion level in polycarbonate resin(s) under varying processing conditions, and thus helps them optimize process conditions for consistency in desired output colour during compounding.

- Determination of dispersive mixing parameter  $\lambda$  under varying processing conditions using OpenFOAM® software. The dispersive mixing parameter provides insight of the flow behavior in kneading discs zone of ZSK26 co-rotating intermeshing twin screw extruder. Two different processing conditions representing experimental runs R7 and R17 taken from a DoE executed for statistical study explained in Chapter 3, were simulated to determine the mixing parameter  $\lambda$ . The  $\lambda$  values obtained in this study reveal that the simulation run representing R7 - a low temperature process condition, yields better dispersive mixing of the titanium dioxide pigments used in the formulation. This resulted into a better output colour of the polycarbonate grade G2 – a high Chroma opaque compounded plastic. The simulation results are in good agreement with findings of our study where a novel technique used to quantify pigments dispersion level

## 6.2 Recommendations

Various assumptions were made during the entire research study. For example in numerical analysis of the kneading disc zone of twin screw extruder, isothermal condition and power law viscosity model fitting were used. Similarly in evaluating pigments dispersion level, only 15 thin slices were assumed to represent the entire molded rectangular plaque. All these assumptions where reveal the limitations of resources and time, also indicate the potential improvements that can be introduced. Therefore following is recommended for future work.

- Numerical analysis can be extended to a complete DoE executed for statistical study explained in Chapter 3 so the mixing parameter  $\lambda$  values obtained for each experimental run can be correlated with respective colour coordinates, and optimal processing conditions further be explored.
- In present numerical study, we assumed isothermal condition and used power law coefficients to describe polycarbonate rheological properties. The numerical study can be extended by considering a non-isothermal condition and applying Carreau viscosity model fitting to viscosity curves of the polycarbonate grades examined. Polycarbonates as mentioned in Chapter 4 are more sensitive to temperature than shear rate while maintaining

their non-Newtonian nature, therefore it would be worthwhile to include thermal effects in the numerical study.

- Application of the novel technique introduced in Chapter 4 can be extended to samples representing all experimental runs of the DoE executed for statistical study explained in Chapter 3. This would certainly help investigate the effect of other process variables such as screw speed and feed rate on pigments dispersion level and consequently on output colour.

## Bibliography

1. Canadian Plastics Industry Association – CPIA, Industry Profile, June 2015.  
<http://www.plastics.ca/IndustryProfile/index.php>,
2. J. Markarian, North American compounders seek growth in innovation, *Plastics Additives & Compounding*, 8(3), pp. 42–44, 2006.
3. W. Spook, Lean compounding – key to survival, *Plastics Additives & Compounding*, 10(4), pp. 26–29, 2008.
4. J. Markarian, US compounding industry faces challenging times, *Plastics Additives & Compounding*, 10(6), pp. 38–41, 2008.
5. G. M. Rizvi, Fundamental studies into causes of colour mismatch, Research Proposal sponsored by SABIC IP and NSERC, 2009.
6. G. E. P. Box, and D. W. Behnken, Some new three-level designs for the study of quantitative variables, *Technometrics*, 2, pp. 455–475, 1960.
7. N. P. Cheremisinoff, *Polymer mixing and extrusion technology*, Marcel Dekker Inc., 1987.
8. A. Dreiblatt, Sabic Innovative Plastics twin screw extrusion training, Century Extrusion, 2008.
9. K. Kohlgrüber, *Co-rotating twin-screw extruders - fundamentals, technology, and applications*, Carl Hanser Publishers, Munich, and Hanser Gardner Publications, Inc. Cincinnati, 2008.
10. C. Rauwendaal, *Polymer mixing, a self-study guide*, Hanser Publishers, Munich 1998.
11. R. J. Crawford, *Plastics engineering*, Elsevier Science, Oxford 1999.
12. Chris J. Rauwendaal, Analysis and experimental evaluation of twin screw extruders, *Polym. Eng. Sci.*, 21, pp. 1092 – 1100 (1981)
13. A. Muller, *Coloring of plastics: fundamentals – colorants – preparations*, 1st Ed, Hanser Publishers, Munich, 2003.
14. C. Rauwendaal, *Polymer extrusion*, 4th Ed, Hanser Publishers, Munich 2003.
15. C. Rauwendaal, *Understanding extrusion*, 2nd Ed, Hanser Publishers, Munich 2010.
16. J. Markarian, Back to basics - adding colour to plastics, *Plastics Additives and Compounding*, 11(4), pp. 12–15, 2009.
17. J. Murphy, *The compounders guide to colour - pigments dyes and special effects*, *Plastics Additives and Compounding*, 1(6), pp. 10–17, 1999.
18. C. Rauwendaal, New developments in mixing and screw design, *Plastics Additives & Compounding*, 10(6), pp. 32–36, 2008.

19. L. Eidson and M. Steeves, Fundamentals of color and appearance book, Online X-rite Seminar, 2012. [http://www.xrite.com/product\\_overview.aspx?ID=934](http://www.xrite.com/product_overview.aspx?ID=934)
20. B. M. Mulholland, Effect of additives on the color & appearance of plastics, ANTEC-Conference Proceedings, pp. 1340–1346, 2007.
21. T. Belcher and K. Harvey, The influence of color, ANTEC-Conference Proceedings, pp. 1296–1307, 2007.
22. X-rite Inc., The color guide and glossary, Online 2012.  
[www.xrite.com/documents/literature/.../L11-029\\_color\\_guide\\_en.pdf](http://www.xrite.com/documents/literature/.../L11-029_color_guide_en.pdf)
23. CIED65. Colorimetry-Part 4: CIE 1976 L\* a\* b\* colour space. CIE DS 014-4.3/E. Vienna, Austria: CIE Central Bureau, 2007.
24. ASTM D 2244-93, Standard test method for calculation of color differences from instrumentally measured colour coordinates, pp. 222-215, 1993.
25. M. C. Yu, M. A. Bisell, and R. S. Whitehouse, The effect of carbon black dispersion on polymer performance. ANTEC-Conference Proceedings, pp. 3246-3250, 1995.
26. D. I. Meade, Introduction to colorant selection and application technology in coloring of plastics: fundamentals, 2nd Ed., edited by Robert Charvat 2004.
27. K. Effertz, Understanding the effects of a compounding process on the production of co-extruded vinyl sheet through the utilization of design of experiments (part II), ANTEC-Conference Proceedings, 2004.
28. T. M. Bender, Characterization of apparent viscosity with respect to a PVC-Wood fiber extrusion process, ANTEC-Conference Proceedings, 2002.
29. E. Dawkins, P. Engelmann, K. Horton, and M. Monfore, Color and gloss – the connection to process conditions, Journal of Injection Molding Technology, 2(1), pp. 1–7, 1998.
30. D. C. Montgomery, Design and analysis of experiments, 6th Ed., John Wiley and Sons, New York 2005.
31. M. J. Anderson, and P. J. Whitcomb, RSM simplified, optimizing processes using response surface methods for design of experiments, Productivity Press, New York, NY, 2005.
32. C. N. Borrer, D. C. Montgomery, and R. H. Myers, Evaluation of statistical designs for experiments involving noise variables, Journal of Quality Technology, 34(1), pp. 54-70, 2002.
33. G. Taguchi, System of experimental design: engineering methods to optimize quality and minimize cost, Quality Resources, White Plains, NJ 1987.
34. G. Derringer and R. Suich, Simultaneous optimization of several response variables. Journal of Quality Technology, 12(4), pp. 214-219, 1980.

35. M. Kosarzycki and L. Klebanov, A technique comparison for the quantification of color concentrate in a Polyacetal component, ANTEC-Conference Proceedings, pp. 1185–1187, 2008.
36. I. Groves, T. Lever, and N. Hawkins, Determination of carbon black pigment in nylon 66 by TGA. Thermal Analysis Application Brief Number TA-122, TA Instruments Ltd UK. <http://www.tainstruments.com>.
37. D. Grewell, G. Srinivasan, M.R. Kessler, and N. Kieffer, Case study of color variation of thermal formed automotive body components, ANTEC-Conference Proceedings, pp. 1763–1767, 2008.
38. D. Colquhoun et al, Improved dispersion of yellow metal azo pigment in polyethylene film, ANTEC-Conference Proceedings, pp. 2827-2831, 2005.
39. S. P. Rwei, Distributive mixing in a single-screw extruder – evaluation in the flow direction, Polymer Engineering and Science, 41, pp. 1665-1673, 2001.
40. W. D. Callister, Jr. and D. J. Rethwisch, Materials science and engineering - An Introduction, 6th Ed., John Wiley & Sons: New York, 2011.
41. ImageJ, Image processing and analysis in Java, research services branch, NIH 2014. <http://rsb.info.nih.gov/ij/>
42. E. L. Canedo, Computer simulation of plastics compounding operations in twin-screw extruders, ANTEC-Conference Proceedings, pp. 310–316, 1999.
43. J. Markarian, Compounders look to simulation software for savings in time and costs, Plastics Additives & Compounding, 7(2), pp. 34–37, 2005.
44. K. Alemaskin, I. Manas-Zloczower and M. Kaufman, Color mixing in the metering zone of a single screw: numerical simulations and experimental validation, Polymer Engineering and Science, 45(7), pp. 1011–1020, 2005.
45. R. K. Connelly and J. L. Kokini, Examination of the mixing ability of single and twin screw mixers using 2D finite element method simulation with particle tracking, Journal of Food Engineering, 79(3), pp. 956–969, 2007.
46. C. David, R. Valette, B. Vergnes and T. Coupez, A direct 3D numerical simulation code for extrusion and mixing processes, ANTEC-Conference Proceedings, pp. 1825–1828, 2008.
47. C. David, A. Durin, R. Valette, B. Vergnes and T. Coupez, A full 3D simulation for twin screw extrusion based on an immersion domain method: application to mixing elements, ANTEC-Conference Proceedings, pp. 2356–2360, 2009.



48. E. Ortiz-Rodriguez and C. Tzoganakis, 3D simulations of a reactive flow in screw elements of closely intermeshing twin screw extruders: a scale-up analysis, ANTEC-Conference Proceedings, pp. 171–175, 2009.
49. E. Ortiz-Rodriguez and C. Tzoganakis, 3D simulations of a reactive flow in screw elements of closely intermeshing twin screw extruders: conventional and variable speed extruders, ANTEC-Conference Proceedings, pp. 447–451, 2010.
50. C. Wang, M. Bussmann and C. B. Park, Numerical investigation of the effect of screw geometry on the mixing of a viscous polymer melt, *Journal of Applied Polymer Science*, 117(2), pp. 775–784, 2010.
51. C. C. Lee, and J. M. Castro, Model Simplification, in Chapter 3 from Charles Tucker III, *Computer Modelling for Polymer Processing*, Hanser 1989.
52. H. H. Yang, and I. Manas-Zloczower, *Int. Polym. Proc.*, VII, pp. 195-203, 1992.
53. H.-H. Yang, Flow field analysis of batch and continuous mixing equipment, PhD Thesis, Case Western Reserve University, 1993.
54. V. L. Bravo, Finite element simulation of flow in twin screw extruder mixing elements, PhD Thesis, McMaster University, 1998.
55. H. Sobhani, M. R. Nouri, and M. H. R. Ghoreishy, *Iran. Polym. J.*, 19, pp. 143-154, 2010.
56. Ali Goger, Modelling of counter rotating twin screw extrusion, Masters Thesis, McMaster University, 2013.
57. A. D. Gotsis, Z. Ji, and D.M. Kalyon, ANTEC-Conference Proceedings, pp. 139-142, 1990.
58. M. O. Zink, The value of transparent and opaque pigments in plastics coloration, CAD RETEC-Conference Proceedings, pp. 319-328, 2004.
59. DuPont™ Ti-Pure®, Titanium Dioxide for coatings, 2007. <http://www2.dupont.com>
60. P. J. Whitcomb and M. J. Anderson, Robust design-reducing transmitted variation: finding the plateaus via response surface methods, annual quality congress, pp. 642-651, 1996.
61. M. J. Anderson, and P. J. Whitcomb, Response surface methods (RSM) for peak process performance at the most robust operating conditions, Proceeding from International SEMATECH Manufacturing Initiative (ISMI) Symposium on Manufacturing Effectiveness, 2007.
62. W. Adams, S. L. Kraber, and P. J. Whitcomb, *Handbook for experimenters*, version 08.1., Minneapolis, MN: Stat-Ease Inc., 2009.
63. J. W. Ess and P.R. Hornsby, Characterization of distributive mixing in thermoplastics compositions, *Polymer Testing*, 6, pp. 205-218, 1986.

64. E. C. Achilleos et al, Role of processing aids in the extrusion of molten polymers, *Journal of Vinyl & Additive Technology*, 8(1), pp. 7-24, 2002.
65. R. M. Christie, Pigments, dyes and fluorescent brightening agents for plastics: an overview, *Polymer International*, 34, pp. 351-361, 1994.
66. R. Levinson et al, Solar spectral optical properties of pigments—Part II: survey of common colorants. *Solar Energy Materials & Solar Cells*, 89, pp. 351-389, 2005.
67. B. R. Palmer, P. Stamatakis, C. G. Bohren and G. C. Salzman, *J. Coat. Technol.*, 61, pp. 41-47, 1989.
68. E.S. Thiele, R.H. French, *Adv. Mater.* 10, 1271-1276, 1998.
69. M. K. Gunde, M. Kunaver, M. Mozetic, and A. Hrovat, Method for the evaluation of degree of pigment dispersion in powder coatings, *Powder Technol.* 148, pp. 64-66, 2004.
70. J. M. Margolis, *Engineering plastics handbook*, The McGraw-Hill Companies Inc., 2006.
71. A. Shah, and M. Gupta, Comparison of the flow in co-rotating and counter-rotating twin-screw extruders, *ANTEC-Conference Proceedings*, pp. 443-447 2004.
72. F. Ilinca, J. -F. Hetu, Three-dimensional finite element solution of the flow in single and twin-screw extruders, *Int. Polym. Proc.*, XXV, pp. 275-286, 2010.
73. I. Manas-Zloczower, and D. L. Feke, Analysis of agglomerate rupture in linear flow fields, *Int. Polym. Proc.*, IV, pp. 3-8, 1989.